DACITE BLOCK AND ASH AVALANCHE HAZARDS
IN MOUNTAINOUS TERRAIN:
2360 YR. BP ERUPTION OF MOUNT MEAGER, BRITISH COLUMBIA

by

MARTIN L. STEWART

B.Sc., (Honours), Carleton University, 1998

A THESIS SUBMITTED IN PARTIAL FULFILLMENT OF
THE REQUIREMENTS FOR THE DEGREE OF

MASTER OF SCIENCE

in

THE FACULTY OF GRADUATE STUDIES

DEPARTMENT OF EARTH AND OCEAN SCIENCES

We accept this thesis as conforming
to the required standard

THE UNIVERSITY OF BRITISH COLUMBIA

December 2002

In presenting this thesis in partial fulfilment of the requirements for an advanced degree at the University of British Columbia, I agree that the Library shall make it freely available for reference and study. I further agree that permission for extensive copying of this thesis for scholarly purposes may be granted by the head of my department or by his or her representatives. It is understood that copying or publication of this thesis for financial gain shall not be allowed without my written permission.

Department of _Earth + Ocean Sciences_

The University of British Columbia
Vancouver, Canada

Date _December 18th, 2002_

Abstract

The Mount Meager volcanic complex hosts deposits from the youngest known explosive volcanic eruption in Canada (2360 yr. BP). These deposits reflect the consequences of erupting dacite magmas into a region of extreme topographic relief. Regions of this kind represent one of the most hazardous and, potentially, high risk natural environments on the planet. Mapping of the Pebble Creek Formation deposits has elucidated a unique distribution of hazardous events of varying intensity, timing, and frequency associated with the 2360 yr. BP eruption event.

For example, lavas erupted onto the steep slopes of the volcano failed under gravitational stresses producing hot block and ash avalanches. During the later stages of this extrusive activity, cold rock avalanches were produced on the oversteepened slopes of the volcano, in one case mixing with a hot block and ash avalanche. Both volcanic and rock avalanches were highly mobile, travelling down the slopes of the volcano, filling the valley and running up the opposite valley wall. Deposits from these events preserve features that are diagnostic of their hot volcanic or cold mass wasting origins and allow these two deposit types to be distinguished in the field. Discrimination is essential because these deposits are superficially very similar in appearance and may be complexly interlayered, but they have different hazard implications.

The steep narrow valleys surrounding the Mount Meager volcano provide an efficient catchment for volcanic and rock avalanches. During the 2360 yr. BP eruption cycle thick block and ash avalanche deposits formed a natural dam against the flow of the Lillooet River, a major drainage system. Volume estimates and flow rates of the current Lillooet River suggests there was an ongoing competition between building of the

pyroclastic dam and filling of the lake. Gradual buildup of the dam was periodically interrupted by overtopping and catastrophic failure of the dam by the encroaching lake. This catastrophic failure released high volumes of water, flooding the Lillooet valley as far as Pemberton, B.C. and produced highly destructive debris flows.

Properly assessing the distribution and nature of volcanic and associated hazards in mountainous regions features is requisite for formulating a risk model for areas such as Mount Meager. Mapping of the deposits elucidates the distribution, and frequency of past hazardous events. The detailed stratigraphic analysis presented in this study demonstrates the destructive potential of these events based on the intensity and time of onset for analogous modern events.

Table of Contents

List of Figures

List of Tables

Insert

DATA CD:

Files Include:

1. Data – Geochemical data files (.xls format)

2. MeagerGIS – GIS mapping data files (ARCView format)

3. PCFmap – Digital outcrop map and field station map (.pdf format)

4. Thesis – Thesis (.pdf format)

5. Thesis_cdr – Draft: thesis figures (.cdr format)

6. Thesis_doc – Draft: thesis text (.doc format)

Acknowledgments

Chapter 1

Introduction

The margins of convergent plates commonly have landscapes that feature large volcanic edifices (in particular, stratovolcanoes) situated in regions of extreme topographic relief (Wood and Kienle, 1990; Perfit and Davidson, 2000). They represent one of the most hazardous and, potentially, high risk natural environments on the planet. Volcanic eruptions represent an obvious hazard. In many instances, the nature or magnitude of volcanic hazards can be substantially modified or amplified by mountainous terrain (Hickson, 1994). Lavas erupted onto steep slopes can be transformed into pyroclastic avalanches (e.g. Rose et al., 1976; Bardintzeff, 1984; Melloer et al., 1988; Elizarraras et al., 1991; Sato et al., 1992; Calder et al., 1999). These pyroclastic avalanches fill the narrow, deep valleys surrounding the volcano, and can interact with surrounding lakes and rivers. In addition, volcanic edifices (i.e. stratovolcanoes) constitute high relief, unstable landmasses that serve as ideal sources for rock avalanches (Ui, 1983; Voight et al., 1983; Siebert, 1984; Siebert et al., 1995; Richards and Villeneuve, 2001). Deposits in the Lillooet River valley below Mount Meager preserve evidence for the occurrence of such events during an eruption 2360 years ago.

In the following chapters, I elucidate the characteristics of volcanic and volcanic-related events that affected this region 2360 years ago. While each chapter deals with independent issues associated with these events, they collectively illustrate the natural hazards such events pose to infrastructure and people that utilize such regions.

Chapter 2 sets the stage for hazards assessment by describing the physical and geologic context of the region hosting the 2360 yr. BP eruption cycle. Mapping and stratigraphic analysis

of deposits must be relied upon to reconstruct the eruption cycle because historical records or accounts are unavailable. In chapter 2 I introduce the events within this eruption cycle through detailed descriptions of their respective deposits. These descriptions include: a revised, outcrop scale, map in preparation for publication as a Geological Survey of Canada (GSC) Open File Report (Stewart et al., in prep); revised stratigraphic sections for volcanic and non-volcanic deposits; and a review of the eruption cycle. Several new deposits have been mapped (e.g. mixed block and ash avalanche, intervolcanic avalanche and lake associated deposits) and observations of previously recognized deposits have been expanded (Stewart et al., 2002).

Chapter 3 illustrates criteria used to discriminate hot volcanic and cold rock avalanche deposits. Field observations demonstrate that many of the deposits are superficially similar in appearance, although they represent very distinct hazardous events. Specifically, block and ash avalanche deposits represent volcanic events, whereas rock avalanche deposits represent mass wasting events. The potential exists to misinterpret these deposits and their relationships because of these similarities. The ability to distinguish between these deposits provides a more accurate assessment of hazards existing in environments similar to the Mount Meager area. Discriminating criteria are based on field descriptions of avalanche units that are published in a GSC Current Research paper (Stewart et al., 2001; Stewart et al., in review).

Chapters 4 and 5 of this thesis uses observations presented in chapter 2 and 3 and additional spatial and volume data to examine the origins and mechanisms of the 2360 yr. BP block and ash avalanche events and related outburst flood events. The production of unique block and ash avalanches at Mount Meager coincides with effusion of lava flows onto steep north facing slopes of the volcano (Stasiuk et al., 1996 and Hickson et al., 1999). Chapter 4 explores the duration, source and failure mechanisms of the block and ash avalanche events

whose deposits fill the Lillooet river valley.

The Lillooet River valley is relatively steep sided and narrow, and thus, acted as a catchment for block and ash avalanches during the 2360 yr. BP eruption event (Stasiuk et al., 1996 and Hickson et al., 1999). Chapter 5 describes development of a lake behind these deposits and subsequent failure and outburst flooding events. Possible failure mechanisms and the nature of the failed materials are also explored in this chapter. Models of the lake filling event provide estimates of the timescales involved in the formation and failure of these deposits.

Mapping of the deposits in the Lillooet River valley below Mount Meager has elucidated a unique set of hazards deriving from intermediate volcanism within mountainous terrain. The hazards can be quantified according to characteristics including the area affected, intensity, time of onset, duration and probability of occurrence of the hazardous event. Chapter 6 examines how field observations, measurements and models presented in chapters 2-5 provide insights into these characteristics and discusses probability distributions applied to hazardous volcanic events. Understanding these characteristics is requisite for constructing a volcanic risk model for the Lillooet River valley, below Mount Meager.

Publications based on thesis work:

Stewart, M.L., Russell, J.K. and Hickson, C.J. 2001. Discrimination of hot versus cold avalanche deposits: implications for hazards assessment at Mount Meager, British Columbia. Geological Survey of Canada, Current Research 2001-A18, 15p.

Stewart, M.L., Russell, J.K. and Hickson, C.J. 2002. Revised stratigraphy of the Pebble Creek Formation, British Columbia: evidence for interplay between volcanism and mountainous terrain. Geological Survey of Canada, Current Research 2002-E3, 7p.

Stewart, M.L. and Pearce, T.H. (in press). Sieve textured plagioclase in dacitic melts: interference imaging results. American Mineralogist, 14p.

Stewart, M.L., Russell, J.K. and Hickson, C.J. (in review). Discrimination of hot versus cold avalanche deposits: implications for hazards assessment at Mount Meager, British Columbia. Natural Hazards and Earth Systems Science.

Stewart, M.L. and others, (in prep). Geology of the Pebble Creek Formation. Geological Survey of Canada, Open File Report.

Chapter 2

The Pebble Creek Formation

2.1 Introduction

The following chapter summarizes field observations of the deposits related to the 2360 yr. BP

eruption event at Mount Meager. The observations of volcanic deposits described here parallel

those that have been previously documented by Stasiuk and Russell (1989, 1990), Stasiuk et al.

(1996) and Hickson et al. (1999). In addition, I present new observations on known deposits and

introduce one new block and ash avalanche deposit type in the volcanic stratigraphy (cf. section

2.3.4). I also include descriptions of an intervolcanic avalanche, reworked pumice fallout, and

alluvial sedimentary deposits into the revised non-volcanic stratigraphy associated with the

eruption event. Section 2.5 reviews the eruption sequence based on Stasiuk et al. (1996),

Hickson et al. (1999) and new observations presented in this chapter.

2.2 Geological Setting

The Mount Meager volcanic complex (MMVC) is the most recently active volcano on the

Canadian side of the Cascade magmatic arc within the Coast Mountains of southwestern British

Columbia. This complex (Figure. 1) is a composite stratovolcano lying at the northern end of

the Garibaldi volcanic belt (Mathews, 1958; Green et al., 1988). This belt consists of a series of

Quaternary stratovolcano complexes including MMVC, Mount Cayley volcanic complex and

Mount Garibaldi volcanic complex.

   The MMVC preserves a number of deeply eroded volcanic centres that have been active

during the past 2.2 myr (Read, 1978, 1990) (Table 1). The geology of the MMVC is well-
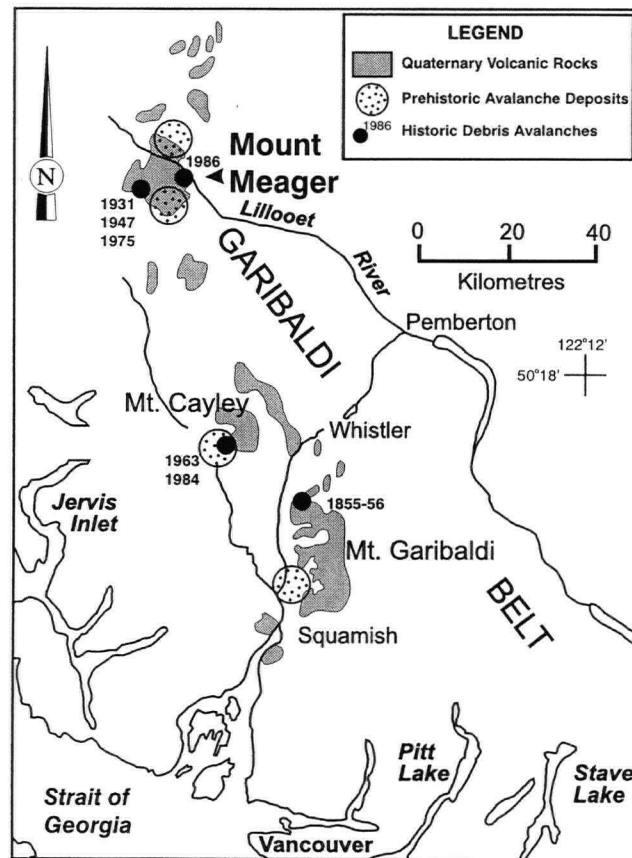
Figure 1. Location of Mount Meager volcanic complex is shown with respect to the distribution of other Quaternary volcanic edifices in the Garibaldi belt of southwest British Columbia (after Hickson, 1994). Locations of prehistoric and historic rock avalanche deposits associated with major volcanic edifices are also shown (after Evans, 1992).

EVENT		AGE (years)	GEOLOGIC UNITS	FLOW EVENTS
x?	*Recent Events* - regular seasonal occurrences of rockfall activity, debris flows and minor avalanches.	<10		undoc.
x5	*Major Historic Events* - recorded avalanche events resulting in the loss of life, infrastructure damage or flooding.	<70		5
	Devastation assemblage - major avalanche event deriving from Devastator Peak. Deposits fill Devastation Creek.	2170		1
	Plinth Assemblage - large syn- to post-volcanic avalanche derived from Plinth Peak.	<2360		1
	Pebble Creek Formation - thick (>100m) accumulations of volcanic avalanche (pyroclastic flow) deposits from the Pebble Creek eruption event. *Plinth Assemblage* - syn-eruptive avalanche deposits deriving from Plinth Peak.	2360	5	>>9
	Plinth Assemblage - small exposure of Plinth derived avalanche directly underlying Pebble Creek volcanic deposits.	>2360		1
	Pylon Assemblage - large undated avalanche from Pylon Peak.			1
	Plinth Assemblage - large landslide deriving from the south flank of Mount Meager.	4000		1
	Fraser Glaciation - peak ice advance at 15,000 yr., essentially ending at 10,000 yr.	10,000		
	Plinth Assemblage and Capricorn Assemblage - major edifice building eruption episodes. Deposits are eroded down to sub-volcanic intrusive roots of the volcanoes.	90,000 - 10,000	7	?
x3	*Pylon Assemblage* - major edifice-building eruptive center. Appears to be extremely long-lived.	500,000 - 1,000,000	4	?
	Devastator Assemblage - age unknown.		7	?
	Unsubdivided Pliocene Assemblages - remnants of early deposits of the embryonic Mount Meager volcanic complex.	1,900,000		

Table 1. Summary of avalanche events, volcanic cycles and related events from historical records (Read, 1978; 1990; Clague, 1998; Hickson et al, 1999). Included are the number of deposits mapped in the Mount Meager volcanic complex, and the number of individual events recognized from these deposits. History records a large number of major rock avalanche events in the Mount Meager volcanic complex (MMVC), but deposits from similar prehistoric events are poorly preserved in the geologic record. No rock avalanche deposits are recognizable prior to the end of the Fraser glaciation (10,000 yr. BP). Deposits of large volume volcanic cycles prior to the glaciation have been mapped throughout the complex. Major volcanic cycles occur approximately every 250,000 to 300,000 years. The Pebble Creek Formation is young enough to have escaped significant erosion from glaciation, and thus preserves a nearly complete record of events within that eruption cycle. Note the close association in time between the Pebble Creek volcanic cycle and production of avalanches on the north slope of the MMVC which hosted that eruption.

described by Read (1977, 1978, 1990), Anderson (1975), Stasiuk and Russell (1989, 1990), Stasiuk et al. (1996) and Hickson et al. (1999). The MMVC produced the most recent eruption in the belt and the most recent known eruption event in Canada, which is dated at 2360 yr. BP (Lowden and Blake, 1968; Rutherford et al. 1975; Lowden and Blake, 1978; Mathews and Westgate, 1980; Evans, 1992; Clague et al., 1995; Leonard, 1995). These volcanic deposits are defined as the Pebble Creek Formation (PCF). A revised distribution of these deposits is presented as an attachment to this thesis (CDRom) and is summarized in Figure 2. The PCF volcanic deposits are dacitic in composition (Read 1978, 1990; Stasiuk & Russell, 1990; Stasiuk et al., 1994; Hickson et al., 1999) with trace amounts of andesite (Figure. 3). These deposits overlie basement rocks of the southern Coast Belt including Triassic metamorphic supracrustal rocks of the Cadwallader Formation, and Tertiary monzonite intrusions of the Coast Plutonic Complex (Read, 1978; Gabrielse et al., 1992). The Plinth assemblage is the next oldest volcanic assemblage dating to between 90,000 to 100,000 yr. BP (Read, 1978). These deposits form a large portion of the north section of the MMVC and directly host the 2360 yr. BP eruption vent.

This region of the Coast Mountains has been characterized by rapid rates of uplift over the past 4 myr (Farley et al., 2001) which has led to relatively high rates of erosion. Thus, the Mount Meager volcanic complex is highly dissected and is presently perched above 1100-1200 m elevation (Figure. 2), well above the present day erosion surface marked by the Lillooet River (400-500 m elevation). The three most prominent peaks of the volcanic edifice, Meager, Capricorn and Plinth, rise to elevations of 2650 m, 2551 m, and 2677 m, respectively, to the south of the Lillooet River.
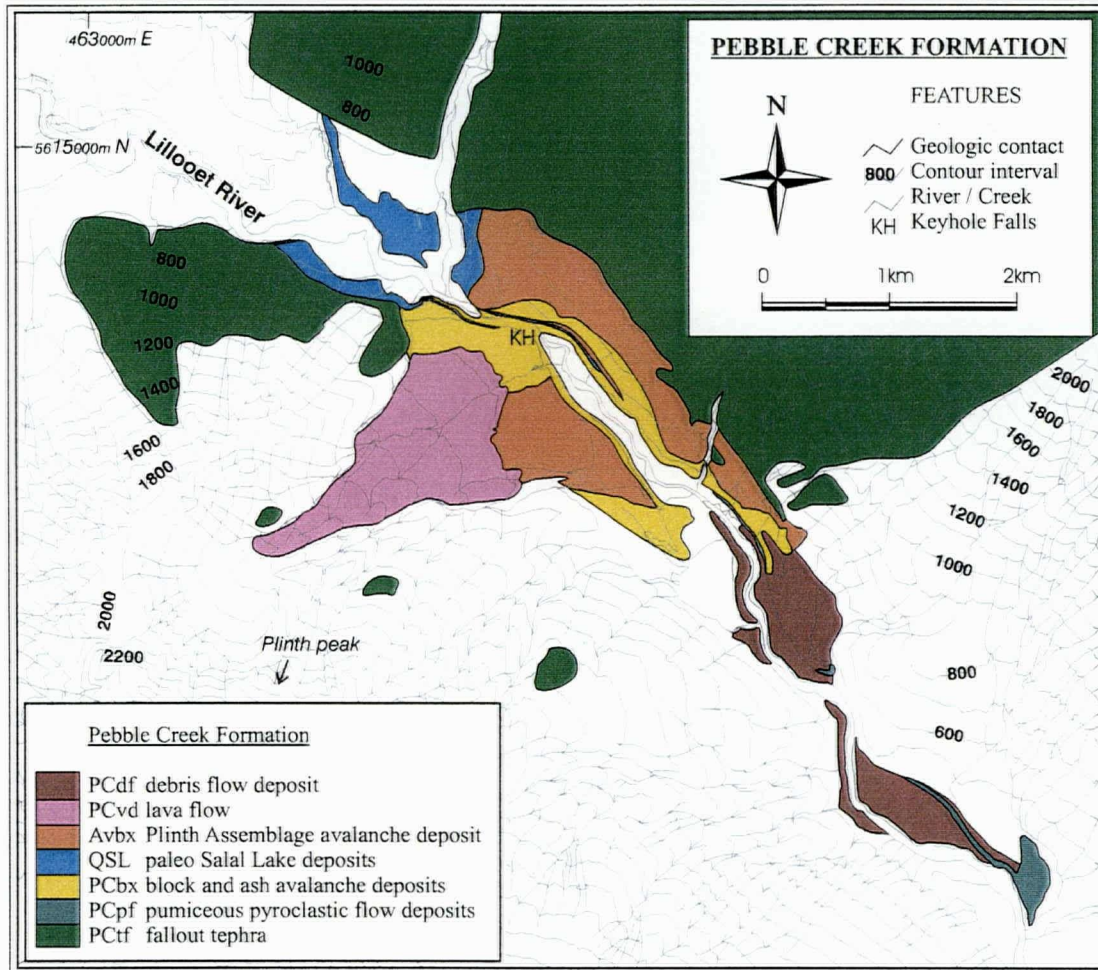
Figure 2. Geological map for the area situated north of Mount Meager and along the Lillooet River. Includes volcanic and rock avalanche deposits within the Pebble Creek Formation (PCF), as defined by Hickson et al. (1999) and Stewart et al. (2001 and 2002). This map is based on earlier work by Read (1978), Stasiuk and Russell (1990), Stasiuk et al. (1996), Hickson et al. (1999) and Stewart et al. (2001). Revisions are based on field work carried out through the University of British Columbia and the Geological Survey of Canada during the 2000 and 2001 field seasons. This figure is based on oversize map included with his thesis.
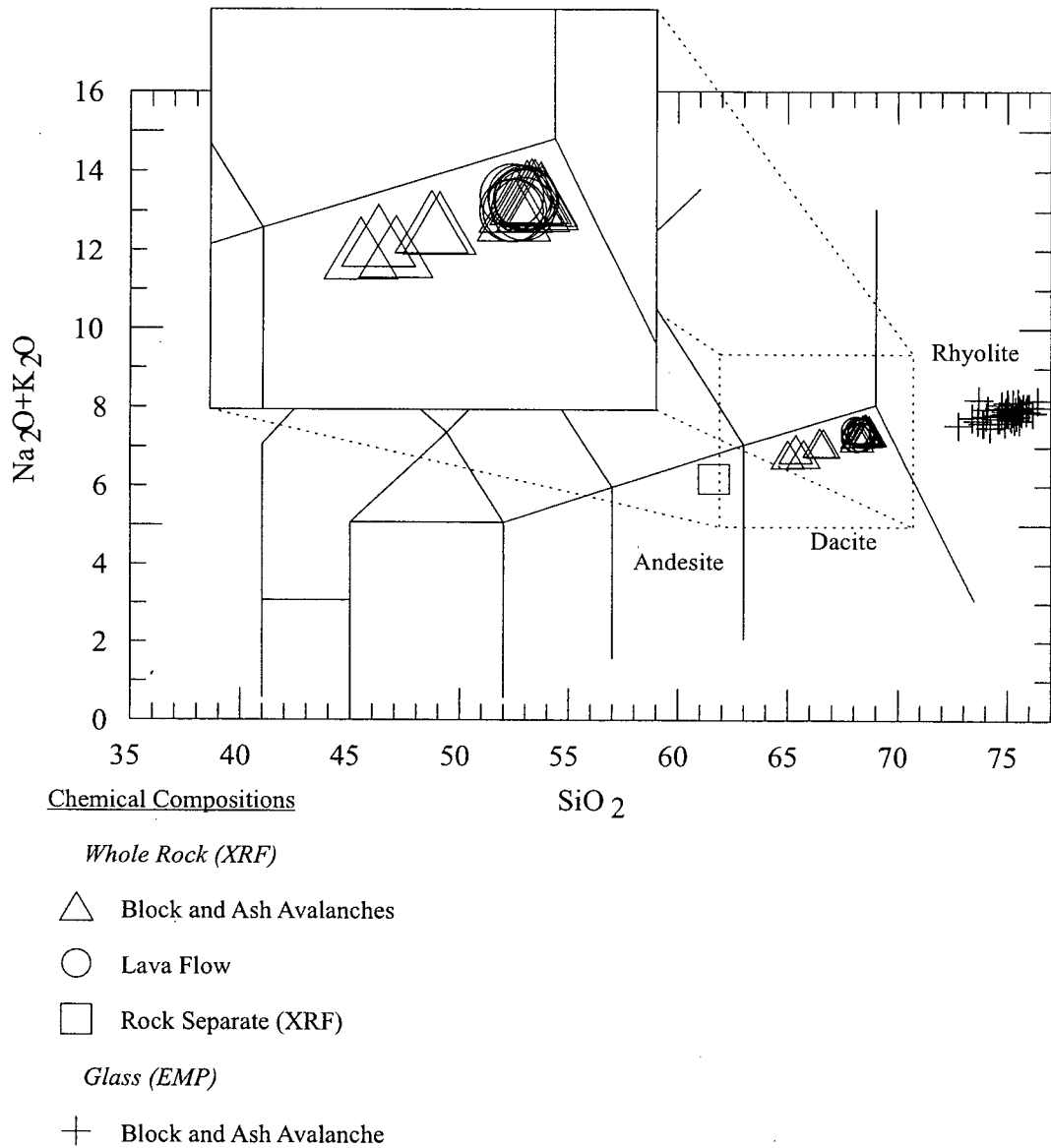
Figure 3. Total alkali's - silica discrimination plot (LeBas et al., 1986) for samples from the 2360 yr. BP Pebble Creek eruption event. Whole rock compositions determined by X-ray fluorescence (XRF) techniques range from rhyodacite to andesite. These compositions may represent various proportions of mixing between a rhyodacite (e.g. lava flow compositions) and an andesite end-member (rock separate). Glass compositions determined from electron microprobe analysis (EMP) indicate that latest liquids are rhyolite. (see Appendix I for data and analytical techniques)

2.3 Volcanic Deposits

2.3.1 Pyroclastic Fallout Deposit (PCtf)

Pyroclastic fallout blankets South-facing slopes opposite Mount Meager and the north slopes of Plinth peak (Figure. 2). Distal equivalents of this deposit have been traced as far east as Alberta (Stevenson, 1947; Nasmith et al., 1967; Westgate and Dreimanis, 1967). This deposit consists primarily of well-sorted white to light grey pumice clasts in an open framework (Figure. 4). Primary deposits are characterized by massive bedding, angular, rough clast surfaces and the presence of sintered and deeply oxidized gas-escape pipes in proximal deposits. Large tree trunks can be found enclosed in fallout tephra, still rooted in paleosols (Figure. 5: column F).

The pumice clasts are highly vesicular to fibrous and show breadcrusted surface textures. Maximum clast sizes range from ash size fragments in distal deposits (Stevenson, 1947; Nasmith et al., 1967; Westgate and Dreimanis, 1967) up to 80 cm on the North slopes of the volcano. Lower portions of the fallout deposit are remarkably homogeneous containing 97-98 wt% white pumice. Upper portions of the deposit contain accessory clasts including up to 44 wt% grey and grey mixed pumice, and 3 wt% fragments of welded pumice breccia (Figure. 6). The welded pumice breccia clasts contain flattened grey pumice fragments and granitic inclusions. The matrix ranges from pink to purple with abundant crystal fragments. Rare clasts show textures of three fragmentation and two welding events.

Grey pumice clasts contain friable subrounded inclusions (< 2cm) of granitic clasts. Accidental clasts include Plinth assemblage fragments comprising up to 13 wt% and granitic clasts comprising up to 4 wt% of the fallout deposit clasts. Cores of large white pumice blocks commonly show oxidation haloes ranging from light grey through orange and red zones to a white exterior. Blocks weather light yellow or, in water saturated deposits, to dark brown.
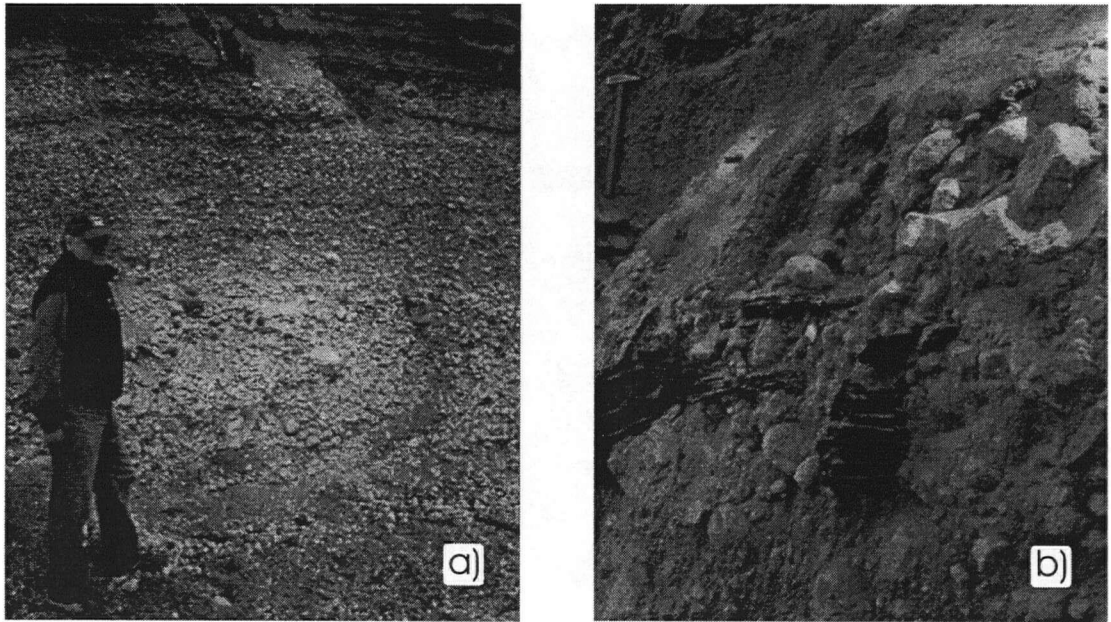
Figure 4. Field photographs of deposits from the explosive pyroclastic units of the Pebble Creek Formation. a) Pyroclastic fall deposits are massive beds of well sorted pumice blocks and lapilli. Well bedded layers shown at the top of the exposure are from reworking on the steep slopes. b) Blocks within pumiceous pyroclastic flow deposits can reach up to 1.8 m in diameter. This exposure contains large blocks and charred tree trunks floated to the top as the pyroclastic material was transported down the Lillooet valley before coming to rest here, more than 6 km away from the source vent. Hammer is 60 cm in length.
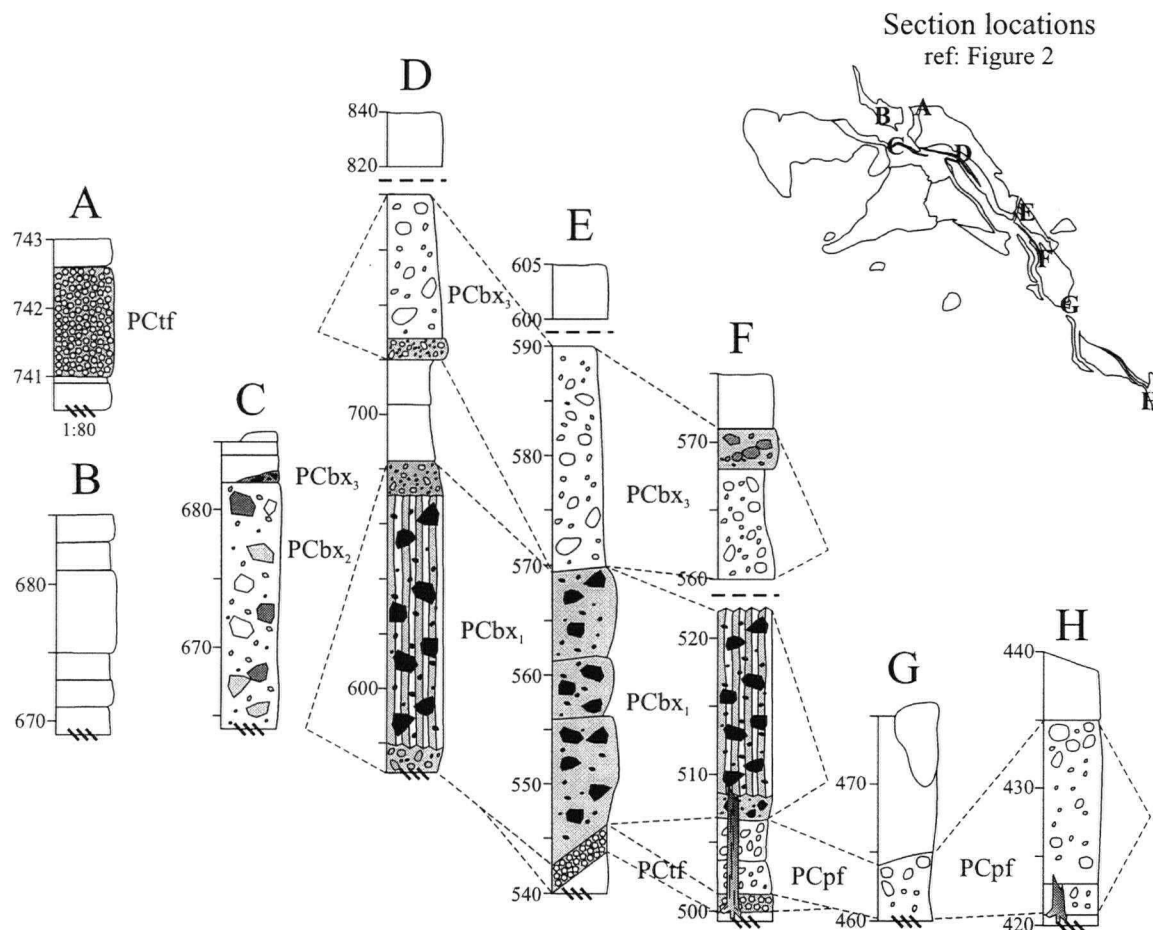
Figure 5. Stratigraphic sections of the Pebble Creek Formation deposits shown on map (Figure 2). Elevations are given in meters to the left of each section. Units outlined include pyroclastic fall (PCtf), pumiceous pyroclastic flow (PCpf), mixed block and ash avalanche (PCbx2), welded (PCbx1) and unwelded (PCbx3) block and ash avalanche deposits.

Weight Proportion of Clasts in Pyroclastic Fallout
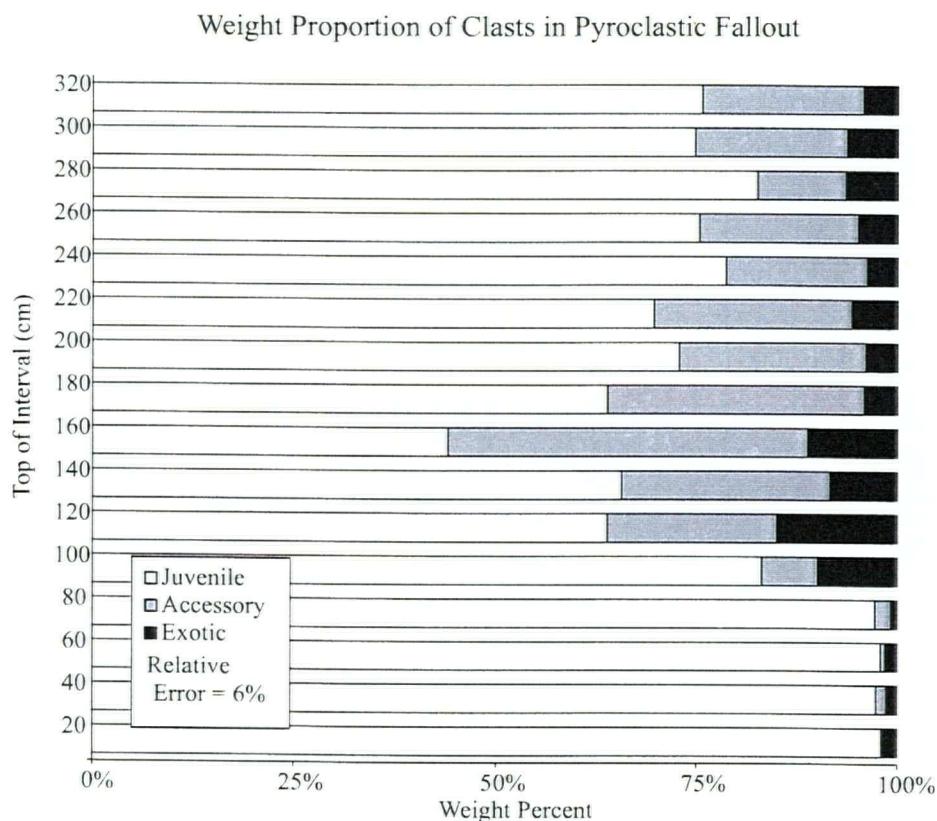
Figure 6. Clast type abundances (wt%) in pyroclastic fall section based on clasts greater than 1cm in diameter. Juvenile clasts are white to grey homogeneous pumice; accessory clasts include flow banded grey, grey and white and welded fragmental clasts; exotic clasts include Plinth Assemblage volcanic dacite and granite clasts excavated from the conduit walls. Stratigraphy derives from the gradual buildup of material raining out of an eruption column. While primary pyroclastic fall sections appear homogeneous and structureless, clast abundances demonstrate that a distinct cryptostratigraphy exists. This stratigraphy may represent changes in the dynamics of magma flow due to cooling and flow zonation in the subvolcanic conduit during the Plinian eruption event. Relative error derives from replicate samples taken from the same interval in the pyroclastic fall stratigraphy. The photograph shows an example of an accessory clast of welded fragmental pumice clasts. Inset is a detail of a welded fragment within the welded block indicating portions of this material experienced three fragmentation and two welding events.

2.3.2 Pumiceous Pyroclastic Flow Deposits (PCpf)

Two distinguishable pumiceous pyroclastic flow deposits occupy the Lillooet River valley. These deposits are characterized by a predominance of pumice clasts. The earliest flow deposit lies directly on pyroclastic fallout in proximal deposits and overlies till and orange oxidized reworked pumice in distal deposits (Figure 5: column H). This oxidized pumice can be found incorporated into lower portions of the pyroclastic flow. The upper subhorizontal surface of this deposit contains angular, fines-depleted and deeply oxidized pumice fragments in a wavy, pitted surface.

The upper pumiceous pyroclastic flow deposit is similar in character to the lower deposit. This deposit overlies the scoured upper surface of the earlier pyroclastic flow. Blocks are denser than in the underlying pyroclastic flow and occasionally contain a subvitreous tan-coloured glass. The upper contact of the deposit is moderately welded and grades into overlying densely welded block and ash avalanche deposits (Figure 5: column F).

Pumiceous pyroclastic flow deposits are massive and poorly sorted to crudely reverse graded (Figure 4b). They range from 3m (Figure 5: column F) to greater than 10m (Figure 5: column H) in thickness. Distal deposits are exposed as far as 5.5km downstream of Keyhole Falls (Figure 5: column H). Breadcrusted clasts as large as 1.8m and large carbonized tree trunks lie in the upper portions of this deposit. Proximal deposits envelope charred trees still rooted in paleosols with large (~25cm) clasts imbricated on the upriver side of the trunks.

The pumiceous pyroclastic flow deposits consist of subrounded clasts of pumice which are similar in appearance to fallout pumice. Based on weighing sorted clasts, less than 1% of the clasts derive from distinctly mingled magmas. Sharp banding in these mixed samples is comprised of equal proportions of light white dacite and a dark brown plagioclase-phyric

andesite magma (Figure 3). Mixed grey and white pumice are present as well, and occasionally contain angular inclusions of grey pumice. These are compositionally indistinguishable from white pumice.

2.3.3 Welded Facies Block and Ash Avalanche Deposit (PCbx$_1$)

Below the eruptive vent a large apron of block and ash avalanche deposits extends into and along the Lillooet River valley (Figure 7). It attains thicknesses of greater than 100m along its axis near Keyhole Falls (Figure 5: column D). Most of this apron is composed of poorly sorted, welded ash to block size vitrophyric breccia. A large canyon cuts through much of the eastern limb of the pyroclastic apron. This deposit thins to less than 15m at the eastern limit (Figure 5: column F). Nearly ubiquitous, meter scale, columnar joints cut vertically through its entire height (Figure 8a). Above Keyhole Falls and at the eastern limit of the deposit the joints are oriented radially or horizontally with respect to exposed cliff faces. At column E (Figure 5) the joints disappear and the deposit becomes slightly less welded. Here individual avalanche units ranging from 5-15m thick can be seen lapping directly onto pyroclastic fall (TF) and bedrock. In denser welded and jointed sections the individual avalanche units are virtually indistinguishable. Weak reverse grading, imbrication of clasts, and discontinuous horizontal layering suggest that these sections may also be composed of numerous individual avalanches.

The principle component of this deposit is dense, black, glassy, porphyritic lava breccia. Clasts are angular and up to 1.5m in diameter. These clasts can be equant and randomly oriented or flattened and aligned parallel to bedding. Other clast types include flow banded and mixed lava blocks, dense grey pumice and white granodiorite and accidental clasts of grey Plinth Assemblage material.
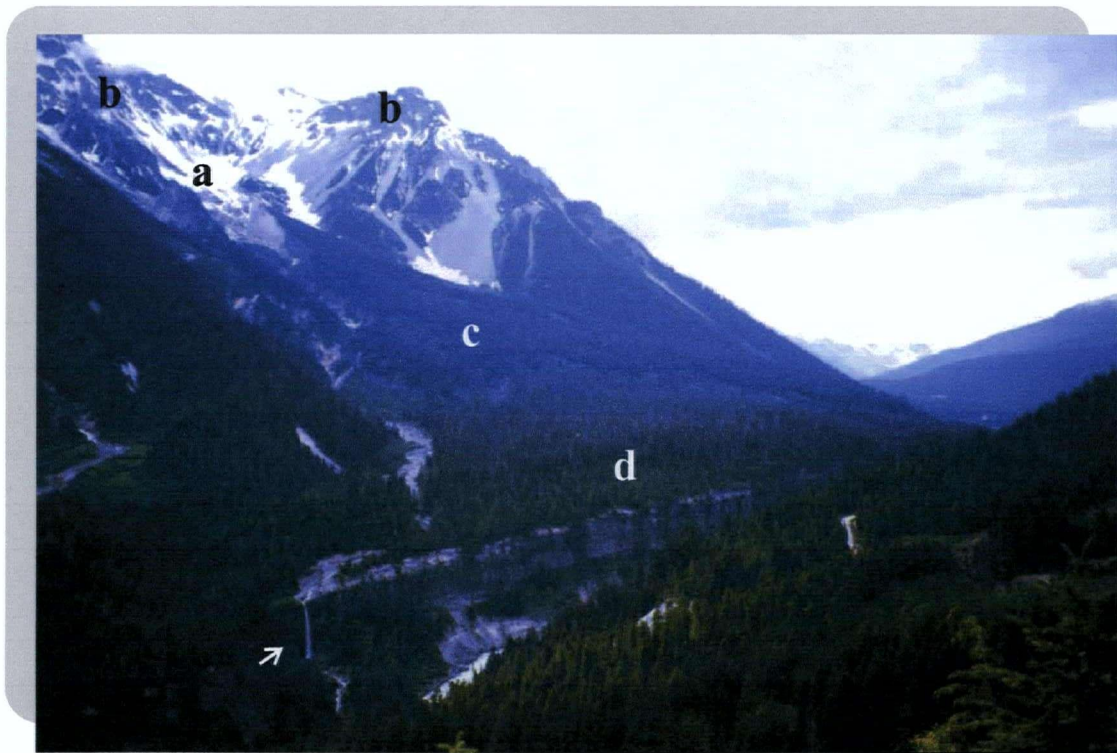
Figure 7. Westward viewing photograph, taken from the Southeast region of the map area, shows the major topographic features of the northern slopes of Mount Meager and the Lillooet River valley. The main elements include: a) the location of the vent to the 2360 yr. BP eruption responsible for the Pebble Creek volcanic deposits, b) massive outcrops of Plinth assemblage volcanic rocks situated immediately above the vent area (Plinth Peak is above the left hand corner of photo), c) an apron of Pebble Creek lava flow extending from the vent into the present-day Lillooet River valley, and d) outcroppings of densely welded block and ash flow deposits of the Pebble Creek formation in the Lillooet River valley. The waterfall (arrow) is approximately 40m in height.
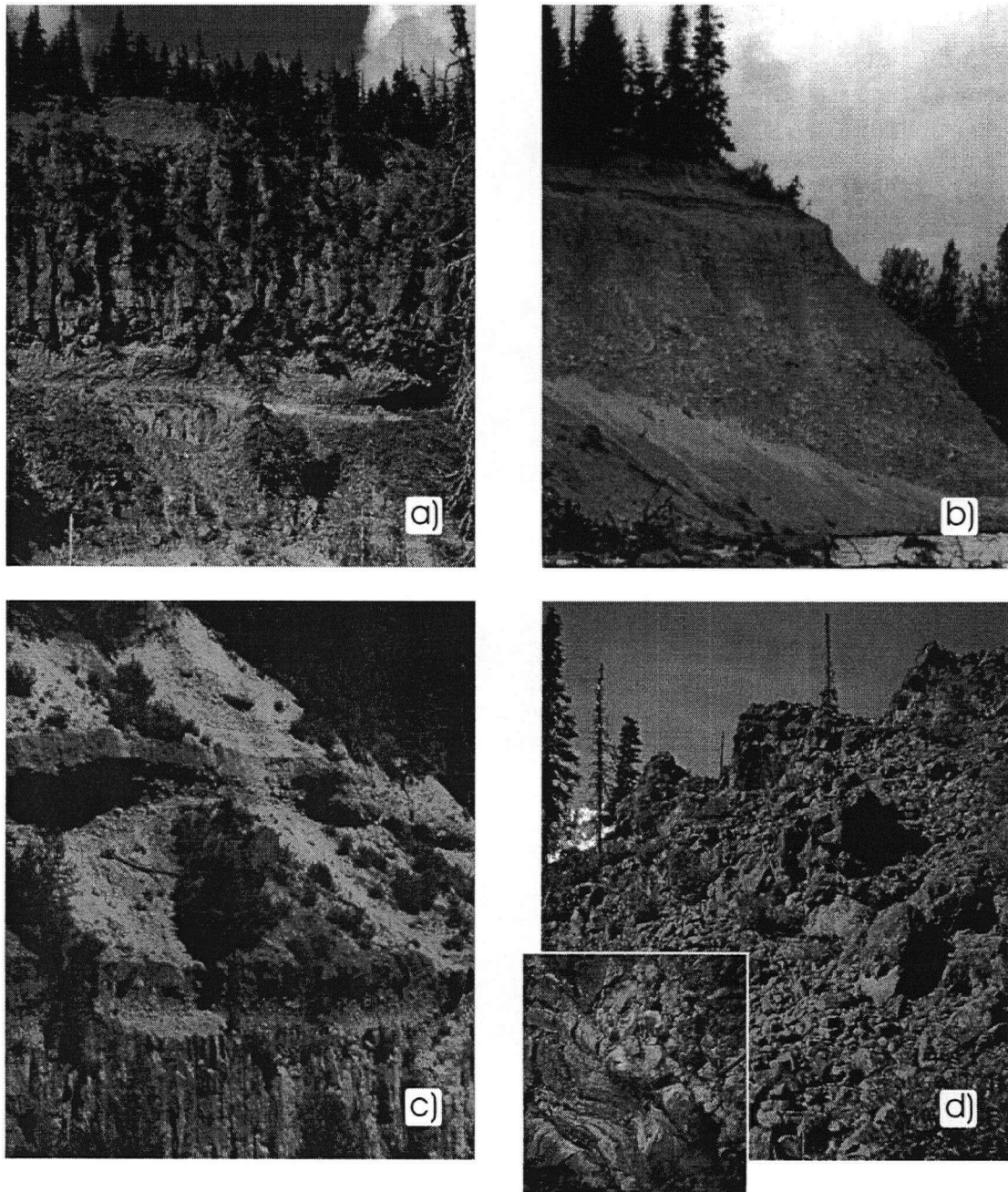
Figure 8. Field photographs of the products of quiescent extrusion of lavas that followed the explosive phase of the 2360 yr. BP eruption. These lavas failed on the steep slopes of the volcano producing block and ash avalanches (a) that formed densely welded deposits filling the base of the valley (cliff is approximately 60m in height). Overlying deposits include a mixed block and ash avalanche deposit (b), comprising Pebble Creek Formation blocks (deposited hot) and Plinth Assemblage clasts (deposited cold), and moderately to non-welded block and ash avalanche deposits (c). The uppermost unit in the PCF is a viscous, plagioclase-phyric, dacite lava flow. The front of this flow is characterized by a well developed flow-top breccia as pictured here and basal breccia (inset). The three large spines in the background are 3-4m in height. Exposures in images a to c result from erosion of these deposits by outburst flooding events.

The top of this unit is variably preserved. At section D (Figure 5) there is an abrupt break in deposit style. Unconsolidated block and ash avalanche deposits and intercalated debris flow and avalanche deposits overlie a sharp upper surface of the strongly welded block and ash avalanche deposits. These debris flow and avalanche deposits are not present further downstream (e.g. column E, Figure 5). The transition from densely welded to poorly welded or unwelded block and ash avalanche deposits remains, although the boundary is more gradational.

2.3.4 Mixed Block and Ash Avalanche Deposit (PCbx$_2$)

Within the block and ash avalanche stratigraphy is a previously unrecognized deposit type. This deposit is massive, poorly sorted and comprises approximately equal proportions of Plinth Assemblage clasts and Pebble Creek Formation clasts. Based on the bimodal composition of clasts, this unit is designated as a "mixed block and ash avalanche deposit". Plinth assemblage fragments are subangular and have both weathered and fresh fracture surfaces. Pebble Creek fragments include glassy blocks, flow banded blocks, dense pumice and dense mixed pumice up to 1.5m in diameter. Pebble Creek Formation clasts show breadcrusted surfaces and occasionally internal prismatic joints. This deposit is matrix supported but in places becomes nearly clast supported.

2.3.5 Poorly Welded to Unconsolidated Facies Block and Ash Avalanche Deposit (PCbx$_3$)

The uppermost pyroclastic unit in the Pebble Creek stratigraphy is a poorly sorted, moderately welded to unwelded facies, monolithologic block and ash avalanche deposit. This unit overlies welded facies block and ash avalanche deposits and an avalanche deposit on the northern banks of the Lillooet River (Figure 8c). It attains a maximum thickness of approximately 60m over

Keyhole Falls (Figure 5: column D). The block and ash avalanche deposit thins to a fine 1m ash and lapilli rich layer overlying the mixed block and ash avalanche to the west. To the east it lies directly on cliffs of welded facies block and ash avalanche deposits. It is massive and commonly structureless. In places it appears some clasts may be imbricated.

The primary components are grey to red dense pumiceous and glassy blocks. Pumiceous blocks up to 1.8m in diameter are breadcrusted or subrounded. In poorly welded regions the clasts are vesicular but dense in comparison to pumiceous blocks and are angular. Pumiceous clasts from these deposits contain higher proportions of plagioclase, biotite and hornblende phenocrysts than pumice clasts from fallout or pumiceous pyroclastic flow deposits. The matrix is mottled grey and pink and contains abundant fine angular black glassy fragments similar in appearance to larger clasts.

2.3.6 Lava Flow (PCvd)

A large glassy lava flow forms the uppermost volcanic unit of the Pebble Creek stratigraphy. It forms a 20-30 m thick tongue that is 100 m wide at higher elevations and more than 1000 m wide at its terminus where it overlaps block and ash avalanche deposits. The lava flow is 2.5 km long and is distributed over 500 m of vertical elevation. The flow front is characterized by steep slopes of flow top breccia (Figure 8d) or vertical 20 m cliffs carved into the flow front.

Flow top breccia includes polygonally jointed and breadcrusted vesicular lava blocks, steep 4-5 m high spines (Figure. 8d) of massive lava and bands of extremely scoriaceous lava. Lavas and lava blocks are a vitreous black, red or grey colour. They are plagioclase-phyric (>10-20%) and may contain biotite and/or hornblende. A strongly welded basal breccia underlying the flow front grades from deformed fingers of lava to fractured and fragmented lava

clasts (Figure. 8d). A fine red ash sintered onto clast surfaces and fractures, partially fills voids in the breccia. Flow banding is preserved as continuous red oxidized bands of fine vesicles which parallel the slope of the lava flow. Contacts with deposits underlying the lava flow are obscured by flow breccia and talus.

2.4 Non-volcanic Deposits

2.4.1 Rock Avalanche Deposits (Avbx)

The Lillooet River valley and slopes surrounding Mount Meager host a series of poorly sorted, monolithologic rock avalanche deposits (Figure. 9a). These units are primarily composed of fragments of plagioclase-quartz-phyric dacite. They can resemble pyroclastic deposits in that they are composed almost exclusively of monolithologic volcanic fragments. However, these deposits represent reworked volcanic material that source from old volcanic stratigraphy high up on Plinth peak (Hickson et al., 1999; Stewart et al., 2001). These units are massive and form extensive avalanche aprons or small lenses within volcanic strata. They are predominantly matrix supported but can be framework supported on the margins of larger deposits or in small deposits close to the mountain. Maximum clast sizes range from 55cm to 240cm.

Within the Pebble Creek stratigraphy there are two large avalanche deposits composed of Plinth Assemblage material. A small intervolcanic avalanche overlies flood deposits in column D (Figure 10) and is itself overlain by the latest block and ash avalanche deposit. It forms a thin lense that is 15m thick and at least 500m in length.

The largest rock avalanche deposit found in the field area overlies and mimics the geometry of the block and ash avalanche deposits. This unit forms a prominent topographic hump where it intersects steep slopes above Keyhole falls opposite Mount Meager (Figure 2).
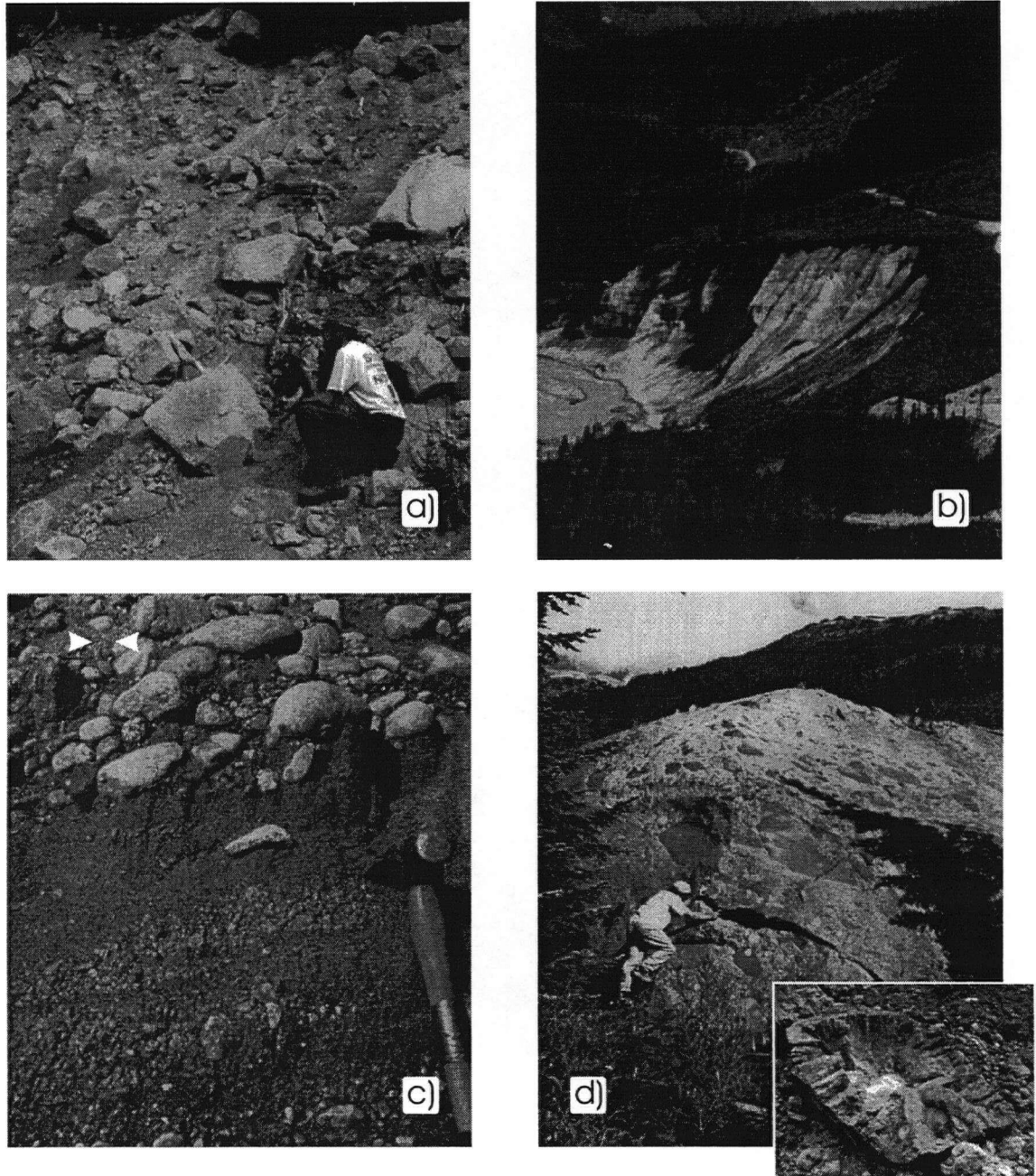
Figure 9. Outcrop photographs of non-volcanic units associated with the Pebble Creek Formation. Poorly sorted monolithologic avalanche deposits (a) composed of Plinth assemblage clasts can be found within and overlying volcanic deposits from the 2360 yr. BP eruption event. The unconsolidated accumulations of primary pyroclastic fall are subject to reworking on steep slopes. On the north slope of Mount Meager, this reworked pumice has accumulated to economically exploited volumes thicker than 80m (b) (clearing to the lower right is a pumice mine). Cobble-rich lithic sands and pumice rich sands (c) preserve evidence for a large delta having formed along the shores of a lake named paleo-Salal Lake (Stewart et al, 2002). Thin beds of similar deposits preserve a lake high-stand mark on the volcanic deposits that dammed the lake. Failure of this natural dam resulted in catastrophic outburst floods producing debris flows on at least two occasions. Boulders up to 15m wide (d) contain delicate jointing features normal to clast surfaces (inset) indicating this deposit was still hot when it formed.

This feature forms a barrier which has diverted local streams laterally along much of its width (see oversize map). It overlies most of the volcanic Pebble Creek deposits (Figure 10: columns A to F). Some large clasts within this unit feature flat, regular joint or parting surfaces that are sometimes oxidized and are inferred to be columnar joint faces. In many cases these regular joint surfaces terminate against freshly broken surfaces.

2.4.2 Reworked Pyroclastic (pumice) Fallout (Qtf)

Situated on the steep northern slopes of Plinth Peak and along the southern banks of the Lillooet River, deposits of pumice are at least 80m thick. These units are characterized by crude reversely graded beds, subrounded to rounded clasts and interspersed thin lenses of Plinth assemblage avalanche deposits. From their upper extent down to 800-900m elevation these deposits lie at critical angles (37^0) and overlap directly onto primary fall. Below this they shallow up to 22^0 in a large apron extending to the margins of the Lillooet river. Plinth assemblage avalanche deposits can be seen underlying this deposit in bluffs along the river.

2.4.3 Alluvial Deposits Related to paleo-Salal Lake (Q_{SL})

The northwest portion of the map area contains several related fluvial, debris flow, deltaic and lakeshore sedimentary deposits. Fluvial and debris flow sediments are deposited on a subhorizontal erosional surface truncating the densely welded facies block and·ash flow deposits (Figure 10: column F). These deposits grade from framework supported angular cobbles and boulders at its base to well sorted pumiceous pebbly sands at its top. They are comprised of penetratively oxidized Pebble Creek formation, Plinth assemblage pebbles and cobbles and medium to fine-grained sand matrix. This deposit extends for at least 500m
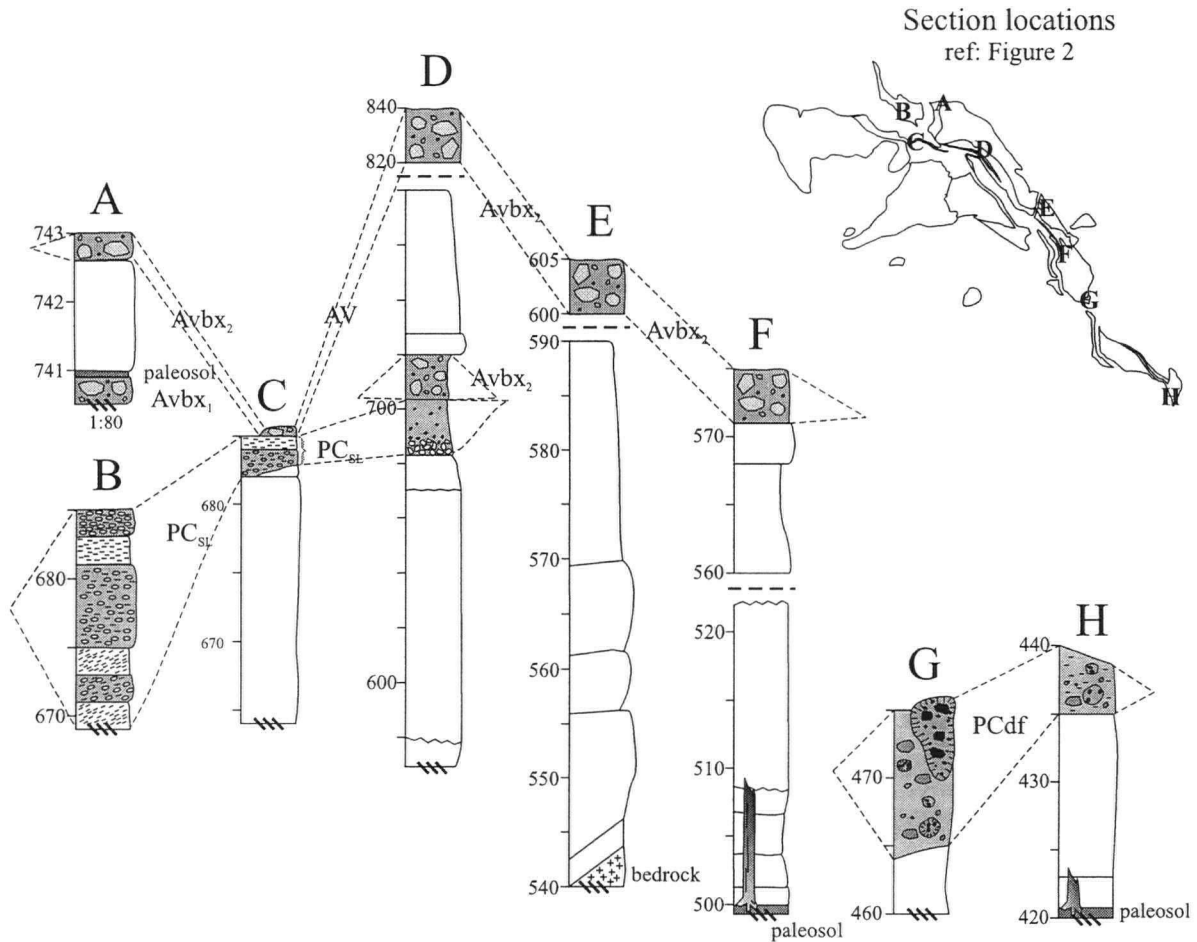
Figure 10. Stratigraphic sections of the non-volcanic Pebble Creek Formation deposits illustrated in map view in Figure 2. Elevations are given in meters to the left of each section. An avalanche deposit (Avbx) overlies pyroclastic deposits in much of the Lillooet valley. Sections A, B, C and D illustrate a consistent lake strand mark that can be observed from alluvial deposits (PCSL) associated the paleo-Salal Lake. Failure of the pyroclastic deposits resulted in a catastrophic outburst flood producing debris flows, including a hot debris flow (PCdf) containing blocks up to 15m in width.

downstream of Keyhole Falls and upstream lies contiguous with lakeshore deposits at similar elevations (Figure 2, Figure 10: columns B to D). In places it is overlain by the youngest Plinth rock avalanche deposit.

Upriver from Keyhole Falls, eroded bluffs surround the valley floor at 685m elevation for several km's along the shore (e.g. Figure. 8b and Figure. 9b). These bluffs are comprised of block and ash avalanche deposits and reworked pyroclastic fall farther upstream. Well sorted silt, sands, and pebbly to cobbley sands lie in thin, laterally continuous beds on top of these benches 15-40m above the current Lillooet River flood level. These sediments range in thickness from 6cm silt laminae to >8m very well sorted lithic sands. Pebbles and cobbles in coarser deposits are very well rounded and include pumice, granitoid, metamorphic and vesicular basalt clasts.   South and west of the current Salal Creek outlet is a gently sloping delta comprised of poorly sorted conglomerates and interbedded, well sorted sand lenses (Figure 9c). There is a distinct progression from forset beds at the base of the exposure through to flat lying topset beds on top of the exposure. Bedding fabric is defined in the conglomerates by flat-lying and imbricated oblate shaped clasts (Figure 9c). These clasts are framework supported, very well rounded cobbles and pebbles identical in composition to those found lying on the eroded benches mentioned above. These well sorted beds are normally graded coarse- to fine-grained, lithic or pumice sand with up to 15cm well rounded pumice cobbles.

2.4.4 Debris Flow Deposits (PCdf)

Filling the base of the valley east of the block and ash avalanche deposits and overlying pumiceous pyroclastic flow deposits are thick massive beds of poorly sorted, reworked Pebble Creek derived debris flow deposits. There appears to be two separate deposits of similar

composition. The earlier of the two fills the entire width of the valley while the second forms a terrace filling a wide erosional feature cutting the earlier debris flow deposits.

Embedded in these thick (>10m) deposits are boulders up to 15m in width (Figure 9d). These debris flows can be framework supported to matrix supported. Clasts are primarily reworked blocks of welded block and ash avalanche that comprise much of the pyroclastic apron upstream from this deposit, as well as up to 5% angular Plinth assemblage and rare dense pumice fragments. Welded block and ash avalanche derived clasts are subrounded and, in the earlier deposit, have prismatic jointed cores and delicate cm-scale joints normal to the clast surface. Similar deposits fill the valley farther downstream but contain only broken remnants of prismatically jointed clasts. A thin veneer of this deposit lies on top of the distal pumiceous pyroclastic flow deposits, 30m above the current elevation of the Lillooet River.

2.5 Eruption History

The 2360 yr. BP eruption event at Mount Meager began with an explosive eruption which generated a Plinian eruption column. The source to this eruption appears to be a crater seated on the slopes of Plinth peak in a large amphitheatre shaped scar. All tephra deposits lie north and east of this point, downslope from which extend pyroclastic flow and lava flow deposits. The actual vent is obscured by a resident glacier, till or scree deposits. The eruption column may have reached heights of at least 15-17 km (Hickson et al., 1999).

Hickson et al. (1999) have suggested there may have been a small explosive event prior to the Plinian eruption based on the presence of welded pumice breccia (cf. 2.3.1) incorporated into the pyroclastic fall deposits. No primary deposits matching these clasts have yet been identified. Pyroclastic fall deposits lie directly on paleosols, glacial till and minor avalanche

deposits and, based on clast measurements (Figure 6), the earliest eruption products are juvenile white pumice clasts. Based on new observations presented above, I propose that the welded pumice breccia clasts are magmas quenched in a shallow proto-conduit preceding the Plinian eruption event.

The presence of multiple fragmentation and welding episodes (Figure 6) in the welded pumice breccia and the abundance of bedrock clasts (sp. granodiorite) demonstrate that the fragmentation process was episodic and incorporated wallrock material. These clasts must have been emplaced in conduits shallow enough to allow vesiculation of the pumice fragments, while insulating the material sufficiently to reweld following multiple fragmentation events. Clasts of the welded pumice breccia remained above the glass transition (Tg) long enough to form breadcrust textures following deposition from the Plinian eruption column.

Grey pumice clasts from the 1991 eruption of Mt. Pinatubo, Philippines, are interpreted to derive from magmas flowing along the conduit walls (Polacci et al., 2001). The proximity of these magmas to the conduit wall formed steep velocity and thermal gradients resulting in shear strain features and increased crystal growth from cooling. Magmas close to the center of the conduit erupted relatively quickly forming microlite-poor, white pumice clasts. Strain features and the presence of granitoid wallrock clasts in similar grey pumice accessory clasts from Mount Meager are consistent with these clasts forming from magmas close to the conduit walls as at Mount Pinatubo.

The initial eruption phase closed with the transition from a sustained Plinian column phase to the formation of gravitationally driven pumiceous pyroclastic flows. Extremely long runout distances of these flows from the vent, in comparison to avalanche deposits deriving from high on the volcano (Figure. 2), suggest the flows comprising these deposits must

originated from higher above the volcano. That is, they are the products of a collapsing eruption column.

Pumiceous pyroclastic flow deposits deriving from these flows contain trace pyroclasts with mingled andesite and dacite magmas. Stasiuk et al. (1996) and Hickson et al. (1999) postulate that this subvolcanic mingling could have triggered the eruption. The concurrent appearance of mingled clasts and the collapse of the eruption column suggests that there may be direct links between extrusive behaviour and the composition of the erupted magmas. An increase in magma density or changing magma rheology from this mixing event may have resulted in the switch from highly explosive behaviour to less explosive styles of eruption.

The collapse of the Plinian eruption column was shortly followed by the production of block and ash avalanches. These are essentially avalanches of hot fragmented lavas similar to the Merapi-type block and ash avalanches described by Bardintzeff (1984). These avalanches derive from the failure of lava flows or domes on the steep slopes of the volcano. The resultant deposits fill the valley below the volcano to depths of greater than 100m. Chapter 4 examines in detail the formation and depositional mechanisms affecting these deposits in the Lillooet River valley.

Rock avalanche activity was interspersed within the late stages of the block and ash avalanche formation. The source of these deposits was old, cold Plinth material which comprises the volcano hosting the eruption vent. The first event to occur was a small volume intervolcanic avalanche. Deposits are preserved as a lens above Keyhole Falls which is contained within pyroclastic strata. The next recognized avalanche event was a mixed block and ash avalanche which incorporated both hot pyroclastic material and cold rock from the Plinth assemblage (cf. 2.3.4). This deposit may have formed in a similar manner to pyroclastic flows

generated at Arenal Volcano, Costa Rica, in 1993 (Alvarado and Soto, 2002). The failure of a portion of the crater wall resulted in the conjoint failure of lavas which mixed together as an avalanche that swept down the flanks of the volcano. A cold rock avalanche postdates block and ash avalanche activity as shown in figure 10 and represents a significant collapse of a large $(44x10^6$ m3) portion of the north side of the volcano. Volcanic activity ends with the production of a lava flow. This lava flow extends from the inferred crater to within 200m elevation above the Lillooet River.

The deposition of significant accumulations of pyroclastic deposits in the valley below Mount Meager resulted in the damming of the Lillooet River. Sediments and sedimentary structures consistent with delta and shoreline deposits encroach on pyroclastic deposits, upstream of Keyhole Falls. These deposits suggest that a large lake built up upstream of this natural dam. Water levels overtopped and eroded the upper portions of this dam. At least one and possibly two such events caused the dam to fail resulting in catastrophic outburst floods. A large failure event removed large portions of the dam while the pyroclastic materials were still above the glass transition temperature. These materials mixed with the flood waters forming hot debris flows. After being deposited, clasts cooled below the glass transition forming the prismatic joints. A second, smaller debris flow of similar composition may have been deposited cold during a subsequent dam failure event. Chapter 5 explores the features of the pyroclastic dam as well as timescales and mechanisms of its failure.

Chapter 3

Discriminating Hot Versus Cold Avalanches

3.1 Introduction

Block and ash avalanche and rock avalanche deposits at Mount Meager share many attributes: (a) they are poorly sorted, (b) they lack internal structure, (c) they vary from unconsolidated to indurated, (d) they are virtually monolithologic, and (e) clasts are volcanic in composition (i.e. dacite). These traits cause the rock avalanche deposits to resemble primary volcanic deposits (e.g., block and ash avalanche deposits). Despite these similarities, the avalanche deposits represent two distinct processes. Mass wasting of the Mount Meager volcanic edifice has produced cold rock avalanche deposits, whereas collapse of active lava flows and domes has produced hot block and ash avalanche deposits.

Mapping these deposits accurately at Mount Meager required that I properly discriminate the deposit types. Criteria used to identify hot volcanic deposits is well entrenched in the volcanological literature (Cas and Wright, 1988). Because the deposit types at Mount Meager are of interest to a variety of disciplines including not only volcanology, but sedimentology and avalanche studies, the need was seen to reiterate this discriminating criteria in section 3.2 using Mount Meager as a case study. In addition, section 3.3 compares recent ideas on the formation, transport and depositional mechanisms of rock and volcanic avalanches. Volcanic avalanche hazards are similar to rock avalanche hazards because they share similar mechanical properties, but include several important distinctions. Volcanic avalanches exhibit higher temperatures, increased fluidization from explosive degassing and the potential to decouple highly mobile ash-cloud surges. These features increase the intensity and area affected

by a volcanic avalanche event in relation to an equivalent size rock avalanche event.

3.2 Criteria For Distinguishing Deposits in the Field

Hot avalanche deposits are distinguished from cold rock avalanches by features indicative of high emplacement temperatures (Figure. 11). Firstly block and ash avalanche deposits may contain lava blocks with radially-oriented joint sets (Figure. 12a,b). A number of blocks may also show concentric sets of joints. Interior sets of joints are relatively coarse and comprise widely spaced joints, whereas the outer set is finer-scale and features more closely spaced joints (Figure. 12a,b). Locally, these fine joints are expressed on the surface of the blocks as fine crenulated fractures. All of these joints result from volume changes at the melt-glass transition during cooling of the clast. They are a direct indication that the clast temperatures at the time of deposition were above the glass transition temperature (e.g., $T_g >$ 550 ^{0}C). Their orientation perpendicular to the exterior of the clast indicates that the joints formed after the original fragmentation event. Indeed, the delicate nature of the radially-oriented joint sets strongly suggests that they probably formed after the avalanche came to rest and also implies that the deposit was above T_g.

Secondly, the presence of "breadcrust" textured blocks within unwelded portions of the Pebble Creek block and ash avalanche deposits (Figure. 12c) is also indicative of high emplacement temperatures. The breadcrust texture comprises an irregular set of fractures or joints that are oriented perpendicular to the clast exterior and that penetrate several centimeters into the clast. The texture results where the exterior of a block has cooled through the glass transition temperature but the interior remains hot and viscous. As the interior lava continues to exsolve a gas phase, the block expands causing the brittle exterior shell to fracture (Walker,

Physical Properties
- monolithologic
- poorly sorted
- no internal structure
- angular to subround
  clast shapes

Avalanche Deposit

Hot Features
- breadcrust textures
- radially-oriented joints
- incipient welding

Cold Features
- weathered, regular
  columnar joints
- fresh irregular joints

Block & Ash Flow Deposit

Rock Avalanche Deposit
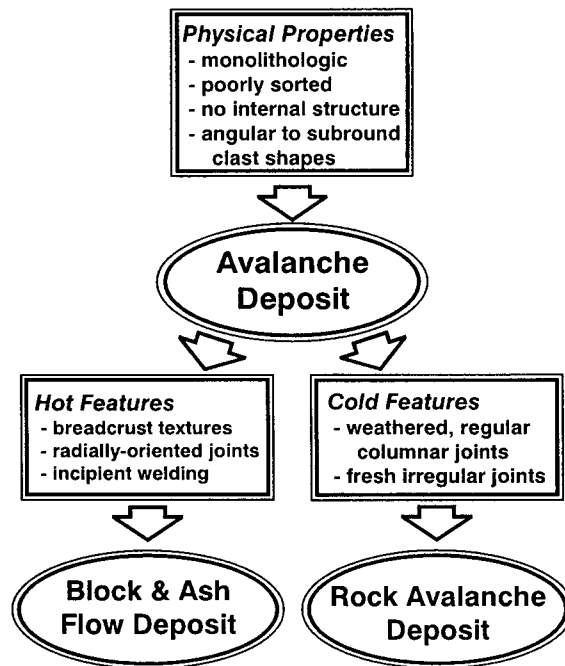
Figure 11. Flow chart showing the relationship between field characteristics (rectangles) of avalanche deposits and the inferred origins (ellipses). Rock avalanche deposits derived from volcanic edifices share many of the general traits of volcanic block and ash avalanches. However, careful and detailed mapping of these deposits can supply a number of features that rigorously discriminate avalanches that are volcanic in origin from rock avalanches.
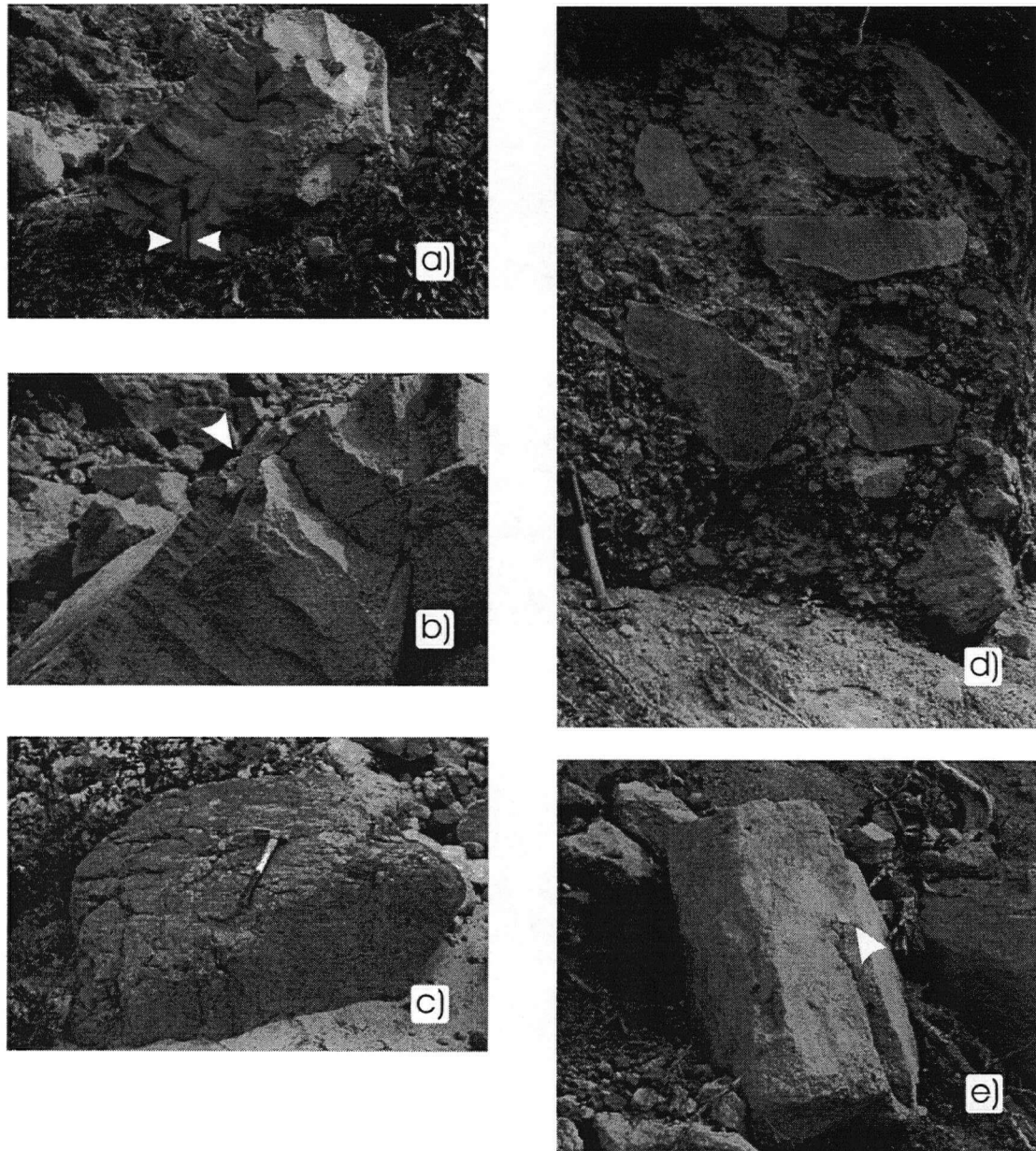
Figure 12. Field photographs of clast features used to discriminate hot (volcanic) from cold (mass wasting) deposited avalanches. These features include radially oriented joints (a) containing concentric sets of joints (b) that illustrate the direction of cooling in volcanic clasts (i.e. normal to clast surface). Breadcrust textures (c) form from fracturing of the cold brittle shell of an expanding hot, viscous lava clast deposited from a block and ash avalanche. Incipient welding (d) indicates this deposit came to rest at temperatures exceeding the glass transition (Tg) temperature, allowing the clasts and matrix to anneal forming a coherent unit. Fragmented columnar jointed volcanic rocks containing pre-fragmentation weathered surfaces and adjacent fresh fragmentation surfaces indicate clasts such (e) were deposited from a cold rock avalanche. Hammer is 45 cm long, note coin (arrow) in (b) and (e).

1969; Cas and Wright, 1988). The breadcrust texture is also a delicate feature that is unlikely to have survived transport and, therefore, is a strong indicator that the deposit came to rest at high temperatures with clast temperatures greater than Tg.

Our third criteria is the presence of incipient welding in portions of the deposit as illustrated by the Pebble Creek block and ash avalanche deposit (Figure. 8a and 12d). The glassy matrix anneals under the combined effects of lithostatic load and temperature. Essentially, if the deposit is above Tg and the load is sufficiently high, the glass particles will anneal and flow fast enough to create a cohesive deposit before cooling (Smith, 1960; Ross and Smith, 1961). Welding can be considered diagnostic of hot emplacement temperatures.

Evidence for the 'cold' origins of rock avalanches derived from volcanic edifices can be elusive at best; commonly, there is only an absence of evidence for a 'hot' origin. Many of the blocks in the Mount Meager rock avalanche deposits have faces defined by joint surfaces that are weathered or oxidized (Figure. 12e). These joints are inferred to be columnar joints formed during the original cooling of the volcanic source rock. Many of the blocks show joint surfaces that are terminated by fresh irregular broken edges formed during transport. The cooling joints and weathering surfaces predate transport which suggests that the avalanche material derives from a cold, weathered source.

Using the criteria introduced above (summarized in Table 2) we were able to recognize a deposit which contained features indicative of both a hot volcanic avalanche and a cold rock avalanche (cf. 2.3.4). Clasts in this deposit derive from two distinct sources including a hot lava dome or flow and cold volcanic bedrock. It likely formed from the conjoint failure and mixing of these source materials forming a unique type of mixed block and ash avalanche.

Characteristic	(A) Pyroclastic Block and Ash Avalanche	(B) Rock Avalanche	(C) Mixed Avalanche	Diagnostic[1] (Ranking)
Origin	Lava Collapse	Mass Wasting	as in A and B	
Source	Pebble Creek and Plinth Eruptions	Plinth Assemblage Deposits	as in A and B	
Age	2360 and 90,000 yr. BP	various	2360 yr. BP	
Lithology	Monolithologic; >90% dacite volcanic clasts	Monolithologic; >90% Plinth dacite clasts	Heterolithic; Plinth and Pebble Creek clasts	
Sorting	None	None	none	
Internal Structure	none to minor clast alignment	None	none	
Induration	Unconsolidated to indurated or strongly welded	Unconsolidated	Unconsolidated	S
Clast Shape	Angular and subrounded	Angular	as in A and B	?
Clast Surface	Smooth to rough	Rough, fractured	as in A and B	W
Clast Features	Breadcrust textured surface, radially-oriented joints	Joint bounded surfaces	as in A and B	S

Table 2. Field characteristics of deposits filling the Lillooet valley which allow for discrimination of hot (volcanic) versus cold (mass wasting) avalanche events. These features are ranked by the ability of the feature to discriminate between these two types of deposits; [1] S – strong evidence; W – weak evidence; ? – possible evidence.

3.3 Comparing Rock and Volcanic Avalanche Hazards

3.3.1 Rock Avalanches

Rock avalanches are mass wasting events affecting oversteepened portions of the volcanic edifice (e.g. Ui, 1983; Siebert, 1984). They are driven by gravitational stresses (Erismann and Abele, 2001) induced by tectonic uplift and exhumation. Once a rock or volcanic avalanche has been initiated, flow is governed by the conversion of gravitational potential energy to kinetic energy, with friction acting against flow. That kinetic energy is used to supply momentum (velocity) and further mechanical breakdown of particles.

Long runout distances (termed fahrboschung – Heim, 1932) of avalanches exceed the expected travel distances for flow governed by frictional forces alone (Heim, 1932; Scheidegger, 1973; Hsu, 1975 etc.). The size of an avalanche and its runout is positively correlated for avalanche deposits (Hsu, 1975; Ui, 1983; McEwan, 1989; Corominas, 1996). Long run-out distances can result from acoustic fluidization (Melosh, 1979; Hungr, 1990; Schneider and Fisher, 1998; Erismann and Abele, 2001) and may be assisted by a lubricating medium (Ui, 1983; Siebert, 1984; Erismann and Abele, 2001). Indeed, run-out distances in excess of 100 km have been documented in steep volcanic terranes (e.g. Stoopes and Sheridan, 1992).

Rock avalanches may have exploited a minimum vertical drop of 1400 m at Mount Meager. They were directed across the Lillooet River valley and, consequently, did not travel a significant distance down valley. However, the deposits can be found up to 180m above the paleo-Lillooet drainage on the steep opposite valley slopes, and spread out to a width of 4 km in the valley (Figures 2 and 5).

3.3.2 Volcanic (Pyroclastic) Avalanche Deposits

Block and ash avalanches commonly result from the explosive or gravitational collapse of lava flows or domes induced by high strain rates that exceed the viscous limits of the lava (Voight and Davis, 2000; Woods, 2000: selected examples include Rose et al., 1976 {Santiaguito}; Bardintzeff, 1984 {Merapi}; Mellors et al. 1988 {Mt. St. Helens}; Elizarraras et al., 1991 {Colima}; Sato et al., 1992 {Unzen}; Calder et al., 1999 {Montserrat}). At Mount Meager the transition from viscous flow to brittle failure appears to coincide with an increase in slope above the Lillooet River valley. Once movement has been initiated, transport is governed

by the same principles that drive rock avalanche motion.

Runout distances of block and ash avalanches are indistinguishable from those of similar classifications of avalanches (Hayashi and Self, 1992; Corominas, 1996). In contrast to rock avalanches deriving from coherent bedrock, rock avalanches deriving from pyroclastic deposits or volcanic sources can have longer runout distances for avalanches of similar sizes (e.g. Ui, 1983). Pyroclastic deposits tend to be hydrothermally altered, fragmented and may contain fluids which can assist in transport (Ui, 1983; Siebert, 1984). A failing lava dome or flow can be fractured, blocky and may release hot gases during failure thus assisting transport of a block and ash avalanche (Cole et al., 1999; Ui et al., 1999). Notwithstanding these differences in runout, the underlying transport mechanisms for these types of events are identical (Hayashi and Self, 1992; Corominas, 1996). The distribution of block and ash avalanche deposits and rock avalanches in the Lillooet River valley show similar extents and significant overlap (Figure. 2 and 5).

Despite the predominant similarities in transport processes between rock avalanches and block and ash avalanches, volcanic events include some important differences over and above hazards posed strictly by an avalanche. The production of ash cloud surges can affect a much wider area than its parent block and ash avalanche. In addition, block and ash avalanches are comprised of extremely hot, viscous fragmented lava blocks, ash and hot gases. Coupled with potentially explosive dissolved gases the intensity of the hazard is much greater than that of a cold rock avalanche.

During transport, highly fluidized pyroclastic avalanches can undergo flow transformations and density stratification from particle settling, gas elutriation and boundary layer processes (Fisher, 1979 and 1995; Wilson, 1980; Druitt, 1998; Calder et al., 1999). These

flow transformations can result in the formation of a density current of elutriated ash and hot gases known as an ash cloud surge or a basal surge (depending on their origin) that can decouple from the avalanche proper. These have sufficient energy and increased fluidity to travel great distances, and can surmount substantial topographic boundaries (e.g. Millar and Smith, 1977; Fisher, 1990; Branney and Kokelaar, 1997; Calder et al., 1999). The residual pyroclastic avalanche tends to flow into topographic lows and be contained by topographic barriers (Fisher, 1995; Branney and Kokelaar, 1997; Fujii and Nakada, 1999).

The deposits resulting from the elutriated ash cloud tend to be thin, erodible and rarely preserved in the geologic record (Hobblit et al., 1981; Hickson and Barnes, 1986). Pumiceous pyroclastic flows extend at least 5-7 km downstream of the vent area. It is highly probable that the pyroclastic surges traveled even greater distances, and higher up the valley walls, although no deposits have yet been recognized. Surge runouts have been known to exceed the runout of its source avalanche by as much as 10 times (Rose et al, 1976; Druitt, 1998).

Both portions of the pyroclastic avalanche are fast moving (up to 300 m/s: Fink and Kieffer, 1993; Valentine and Fisher, 1993) and feature high magmatic gas contents, and high particle concentrations. Temperatures of the avalanche proper may be nearly magmatic (e.g. 700 - 1000 ^{0}C: Valentine and Fisher, 1993; Bursik and Woods, 1996; Cole et al., 1998; Voight and Davis, 2000), and temperatures of surges can be high (e.g. 100-300 ^{0}C: Voight and Davis, 2000). On this basis, avalanches from volcanic eruptions may cause greater damage over a wider area than rock avalanches.

Chapter 4

Block and Ash Avalanche Formation

4.1 Introduction

Deposits that fill the Lillooet valley below Mount Meager are poorly sorted, matrix supported volcanic breccias. These highly fragmented, massive to bedded deposits contain all the characteristics of avalanche deposits. Features such as dense welding of the matrix and breadcrusted volcanic clasts indicate these deposits were formed from fragmentation of hot volcanic lavas. This process is inferred to be the same as modern analogues of block and ash avalanches forming from the collapse of active lava domes and lava flows. In this chapter, field data from the 2360 yr. BP eruption event is analyzed to elucidate the duration, source and failure mechanisms of the block and ash avalanche events whose deposits fill the Lillooet River valley. Finally, this chapter explores a distinct change in the rheological behaviour of the lavas erupted late in this event.

4.2 Duration of Block and Ash Avalanche Production

Volume estimates of the rock avalanche deposit and block and ash avalanche deposits have been calculated from the distribution of deposits in the field and from digital reconstruction of the paleotopography of the valley. Topography below the inferred eruption vent represents the eroded remnants of the recent deposits associated with the 2360 yr. BP eruption event. These deposits lie in a broad, glacially scoured valley. Glacial erosion has produced consistently steep, planar slopes along the valley walls and regular slope gradients along the length of the river. Volumes of the block and ash avalanche, rock avalanche and lava

flow deposits are presented in Table 3. Based on minimum and maximum reconstructions of the geometry of the lava flow, the relative error on volumes is estimated to be approximately 17%.

Calculating the expected duration of an eruption event is vital in assessing how long an area will be exposed to a particular hazard. This is difficult to measure directly in the case of the duration of an extrusive episode as the magma chambers that feed silicic eruptions cannot be seen or easily imaged. The only data available comes from mapping of deposits from previous eruptions such as the Pebble Creek Formation at Mount Meager. During the 2360 yr. BP eruption, the steep sided Lillooet valley was filled by block and ash avalanches to depths greater than 100m. The volume of material extruded during the block and ash avalanche production phase may be as much as 0.44 km^3 (Table 3). Using documented effusion rates for selected historic silicic eruptions (Table 4) an estimate of the duration of this phase of the eruption can be calculated.

Unit	Thickness (m)	Runout (km)	Drop (m)	Volume (km^3)
Volcanic Deposits				
Lava Flow	20-30	2.4	740	0.045
Block and Ash Avalanches	200	?	?	0.44
Pumiceous Pyroclastic Flow	15	>7.8	>980	?
Non-Volcanic Deposits				
Rock Avalanche	20	>3.5	>580	0.044
Eroded Debris				
inferred		>70		0.19

Table 3. Volumes and geometric parameters of major deposits that fill the Lillooet valley below Mount Meager. Volumes are calculated from reconstructions based on cross sections and computational methods illustrated in Appendix III.

Location	Magma	Max. Rate (m^3/s)	Avg. Rate (m^3/s)	Measured Period	Total Volume (km^3)
Galeras, CO[1]	andesite		0.14	long term	0.00004
Montserrat, W.I.[2]	andesite	< 10	2.1	days 1.5 yr. avg.	0.246
Mt. St. Helens, USA[3]	dacite	1 to 40	0.35	days 6 yr. avg.	
Mt. St. Helens, USA[4]	dacite	0.7 to 40.4	0.35	1-16 days average	0.074
Santiaguito, GT[4]	dacite	0.6 to 1.9	0.16 0.41	a few years 10-12 yr average	1.0
Unzen, JA[5]	dacite	3-8		a few weeks	
Unzen, JA[6]	dacite	4.6			0.21
67 Domes (various)[7]			2.9		

Table 4. Historical extrusion rates for silicic lava domes and flows. Maximum rates typically exist as short pulses lasting from days to weeks. These pulses are interspersed over long periods of relatively slow growth. Average rates are yearly time average estimates which include both high and low extrusion rates integrated over time. 1. Calvache and Williams, 1997; 2. Sparks et al., 1998; 3. Swanson and Holcomb, 1990; 4. Anderson et al., 1995; 5. Nakada, S., 1993; 6. Nakada and Motomura, 1999; 7. Newhall and Melson, 1983

Eruption cycles are normally characterized by long periods of relatively low effusion rates on the order of 10^{-1} m^3/s (Table 4). Periods of slow effusion are punctuated by short pulses (days to weeks) of extrusion rates as high as 40 m^3/s (Swanson and Holcomb, 1990; Anderson et al., 1995). These pulses commonly occur at the start of an eruption cycle (e.g. Nakada, 1993), and may recur periodically throughout the lifetime of an eruption (Swanson and Holcomb, 1990; Nakada, 1993; Anderson et al., 1995; Sparks et al., 1998). For example, the andesitic

Soufrière Hills lava dome on Montserrat experienced 3 pulses of accelerated growth from 1995 to 1997 (Sparks et al., 1998). Over periods lasting several days the dome experienced growth rates of up to 10 m^3/s. These periods were separated by months where growth rates averaged 2.1 m^3/s. In comparison, the 1980 to 1986 domes erupted at Mount St. Helens grew at rates as high as 1-40 m^3/s during 20 pulses that lasted for a only a few days. The time-averaged growth rate for this period was 0.35 m^3/s.

A sustained extrusion rate of 10 m^3/s would require 1.4 yrs. to produce the block and ash avalanche deposits at Mount Meager. This would be an exceptionally long period to sustain such high extrusion rates. A yearly time averaged eruption rate of 0.4 m^3/s may be more realistic estimate based on known historical eruptions of similar volume and composition (Table 4). At this rate it would take 53 years to produce the deposits in the Lillooet valley.

Block and ash avalanche deposits filling the Lillooet valley are densely welded. Welding in such deposits has not previously been documented, and, thus, is likely extremely rare in Nature. In the 2360 yr. BP deposits, welding is dense across flow unit boundaries and at interfaces with cold underlying bedrock. To promote this intense welding, the lavas may have been extruded at exceptionally high eruption rates leading to rapid rates of block and ash avalanche production. Invoking higher extrusion rates for these lavas provide time scales of eruption (<53 yrs.) comparable in length to historical silicic eruptions (e.g. Swanson and Holcomb, 1990; Nakada, S., 1993; Anderson et al., 1995).

4.3 Source of Block and Ash Avalanches

The exact source to the block and ash avalanche deposits in the Lillooet valley is not immediately apparent from field mapping. Data from recent avalanches consistently shows the

correlation between the volume of the material which has failed and the runout of the avalanche (cf. chapter 3.3; Hsu, 1975; Ui, 1983; McEwan, 1989; Corominas, 1996). Based on this correlation it is possible to trace the farthest runout of Lillooet valley deposits back up to their source region.

The runout of a rock avalanche can be described by the angle of reach; i.e. the slope angle expressed by a line connecting the head of an avalanche to its distal margin, along its axis of travel (Corominas, 1996). The angle of reach is most commonly expressed by its tangent. The tangent is equivalent to the ratio of an avalanches drop in elevation H to the horizontal length of runout L (H/L). Corominas (1996) demonstrates that topographic effects such as deflections, runup of steep opposing valley walls, and runout on flat plains do not affect this reach angle. Regression of data from 47 rockfall avalanche events provides a quantitative relationship between the angle of reach and volume of those avalanches. This relationship is given by the equation:

1) $\log (H / L) = -0.109 \log (V) + 0.210$

$\sigma_{error} = 0.161$

(Corominas, 1996)

Plinth assemblage material, which comprises the rock avalanches in the Pebble Creek strata, derives from deposits found at elevations not less than 1140m on the northern slopes of the volcano (cf. CDRom). Knowing the volume of this avalanche and the minimum elevation of its source provides a test of the reach angle relationship from field data. The volume of the rock

avalanche (Table 3) gives a reach angle (H/L) of 0.238 +/- 0.038 based on equation 1. The calculated source region defined by the error range of the reach angle lies between elevations of 1120m and 1500m (Figure 13). The calculated lower limit of this range corresponds with the lowest elevation of mapped Plinth Assemblage deposits. The avalanche could have derived from similar deposits which comprise the upper reaches of Mount Meager, but no lower than 1140m, the lower limit of the region defined by the reach angle.

Definable individual flow units in the welded block and ash avalanche deposits are not thicker than the major rock avalanche deposit, but have traveled a similar distance across the Lillooet valley and appear to have a similar geometry. Assuming they were of similar size and fluidity as the rock avalanches (cf. chapter 3.3.2), these block and ash avalanches derived from close to the rock avalanche source area. Thus the source of the block and ash avalanche deposits existed at an elevation of at least 1080m and possibly higher.

4.4 Failure Mechanisms of Viscous Lavas

The production of block and ash avalanches is a consequence of the catastrophic failure of viscous lavas on the steep slopes of the volcano. Recent experimental work (e.g. Webb and Dingwell, 1990, Stevenson et al., 1995; Alidibirov et al., 1997) has begun to explore the temperature dependent rheology of natural volcanic lavas. I use this experimental data to examine the reactions of a simple lava flow model to stresses exerted by gravity acting on steep slopes. Specifically, I compare gravity driven strain rates to theoretical critical strain rate limits to determine if catastrophic failure can occur in a Newtonian liquid, analogous to a lava flow failing on the slopes of the Mount Meager volcano.
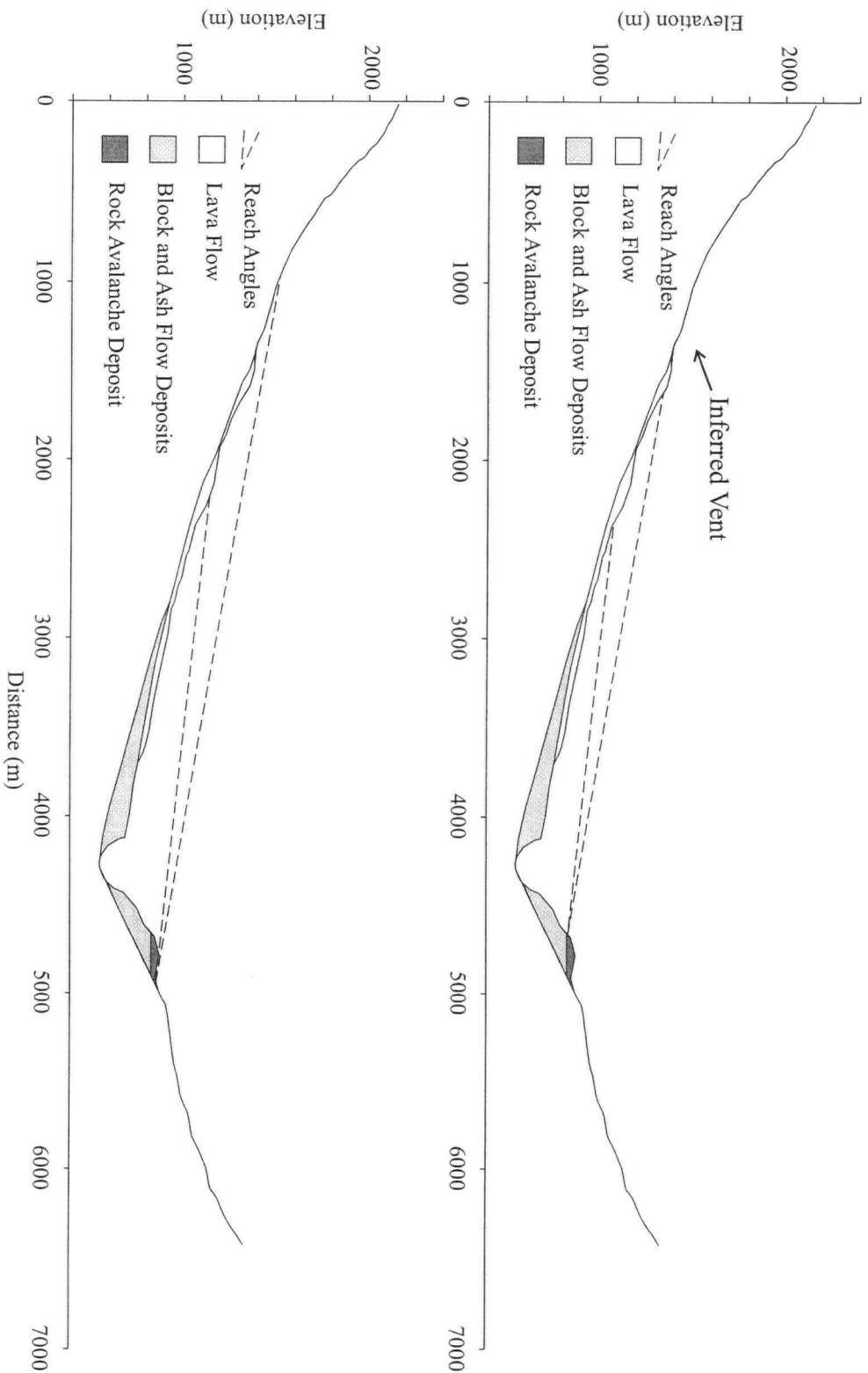
Figure 13. Projections of the angle of reach for avalanche deposits at Mount Meager based on empirical relationships relating avalanche runout to the volume of the avalanche deposit (Corominas, 1996). Cross sections are taken along the axis of travel, a line extending through the inferred vent, across the deposits normal to the valley walls. Using a range of reach angles calculated from the volumes of the valley filling deposits, and the maximum mapped runout of the avalanche events, the probable source regions for rock avalanches and block and ash flows has been shown to lie high on the slopes of the volcano, close to the inferred vent. (location: see Appendix III, section B)

Section 4.4.1 uses the analogy of a static block lying on a slope to model critically resolved shear stresses in a lava flow (Figure 14a). Strain rates from velocity gradients normal to the slope surface are calculated in section 4.4.2 using a steady-state velocity equation from Philpotts (1990) (Figure 14b). These models represent a simple analogue of the lava flow preserved at Mount Meager. Section 4.4.3 discusses the suitability of a Newtonian model to describe natural lava flows.

4.4.1 Failure of a Block Model Lava

A snapshot of a lava flow perched on steep slopes might look similar to the block model pictured in Figure 14a. Excluding any effects of flow, or internal pore pressures, the forces acting on a body derive from gravity. When this body is placed on a slope this force can be resolved into normal stresses acting to hold the body on the slope and shear stresses which drive it down that slope. Resolved stresses are a function of the gravity constant g and the weight of the overlying body of density ρ, vertical height h, lying on a slope of angle ϕ. These stresses are at a maximum at the base of the block because the base feels the weight of the entire thickness of the overlying lava flow. Thus the base is the most likely region of failure. Maximum stresses can be calculated by the following relationships deriving from the block model in Figure 14a.

2) $\sigma_n = \rho g h \cos \phi$

3) $\sigma_s = \rho g h \sin \phi$

Block Model Lava Flow

a)

ρgh

h

σ_n

$\sigma_s = \rho gh \sin \Phi$

σ_s

Φ

Steady State Velocity Profile

b)

$v = \rho g \sin \Phi / \eta * (hz - z^2/2)$

$\rho = 2300 \ kg / m^3$

$\Phi = 45^0$

$\eta = 10^8 \ Pa \ s$

Height - z (m)

Velocity (m/s)
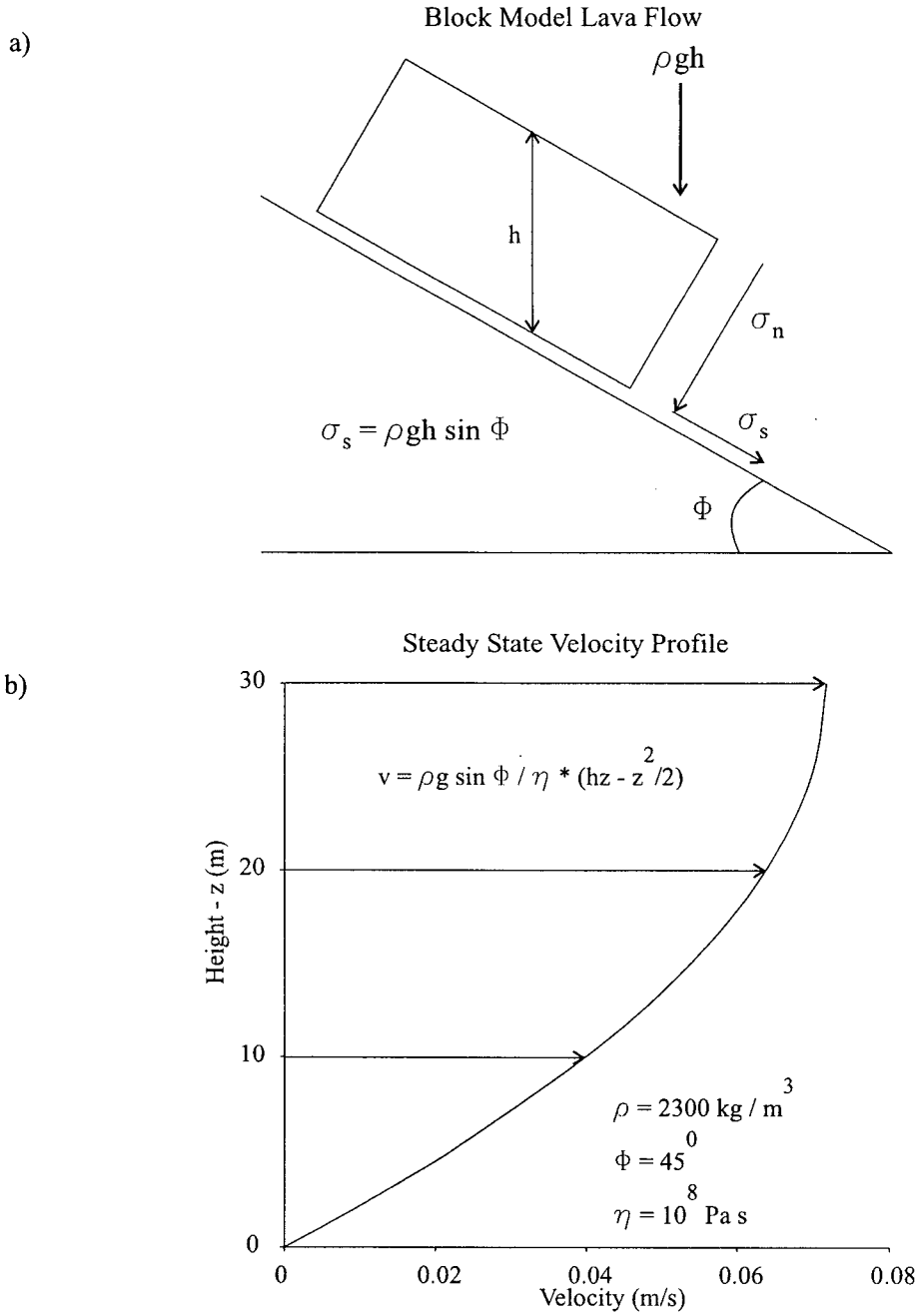
Figure 14. Two simplified lava flow models are constructed to examine the responses of a Newtonian liquid to stresses applied by gravity. Figure a) illustrates a block model used to determine the critically resolved shear stresses (σ_n: normal, σ_s: shear) acting on a static body of known vertical height (h) on a slope (Φ). Model b) uses a vertical velocity profile for a lava flow from Philpotts (1990) to examine strain rates deriving from the differential flow rates of a lava flow of a given density (ρ), and viscosity (η) on a slope (Φ).

Strain results from the reaction of a body to the applied shear stress. Dingwell and Webb (1990) show that magmatic liquids have a rheological glass transition temperature. That is, for a given relaxation time τ_R, a specific (glass transition) temperature exists at which the rheology of a magma changes from a liquid (melt) to a solid (glass) and hence the response to applied shear stress changes from viscous flow to brittle failure. This rheological glass transition can be calculated directly from the viscosity of a liquid by the following relationship from Dingwell and Webb (1990):

4) $\quad \tau_R = \eta / G$

G is the shear modulus which typically has a value of $10^{10 +/- 0.5}$ (Dingwell and Webb, 1990). The relaxation time of a liquid is the inverse of the critical (maximum) strain rate $\dot{\varepsilon}_{crit}$ that can be accommodated by the liquid at a given temperature.

5) $\quad \dot{\varepsilon}_{crit} = 1 / \tau_R$

Combining equation 2 and equation 3 we find:

6) $\quad \dot{\varepsilon}_{crit} = G / \eta$

By definition, the strain rate of a Newtonian liquid is linearly related to the applied shear stress.

7) $\sigma_s = \eta \; \dot{\varepsilon}$

Thus, for a Newtonian liquid, the maximum stress that can be applied to a liquid before it begins to react brittlely due to glassy rheology (i.e. the glass transition) is equal to the shear modulus G.

8) $\sigma_s = G$ = shear modulus

Natural data analogous to the 2360 yr BP magmas can be used to calculate whether gravitational stresses approach the critical limits of a Newtonian liquid defined above. Whole rock analysis shows the rocks to be dacitic, but microprobe analysis of matrix glass shows that the latest liquids are rhyolites (Figure 3). The erupted magmas were essentially rhyolitic liquids with suspended phenocrysts and vesicles (the addition of crystals and gases will be discussed in a subsequent section).

Recent experimental work has begun to focus on analyzing the rheological parameters of natural volcanic melts (e.g. Webb and Dingwell, 1990; Stevenson et al., 1995; Alidibirov et al., 1997). Stevenson et al. (1995) present the temperature-dependant viscosities of several natural rhyolites, and Alidibirov et al. (1997) give viscosities of reheated samples of the Mt. St. Helens dacite (Figure 15a). These viscosities are approximately Arrhenian over reasonable natural temperature ranges for silicic magmas (700-1000 ^{0}C). Linear regression curves allow temperature dependent viscosities to be calculated directly for the analogue melts (Figure 15a).

a)

Experimental Viscosity

	m	b
A	1.5987	-2.7857
B	1.9607	-7.1566
C	2.0199	-7.9209
D	2.0323	-8.5678
E	2.2179	-11.402

Viscosity (log n)

10^4 / Temperature (10^4 / K)

b)

Experimental Relaxation Time

Relaxation Time (log s)

$T_R = \eta \ / \ G$

$G = 10^{10 +/- 0.5}$

Liquid

Glass

10^4 / Temperature (10^4 / K)
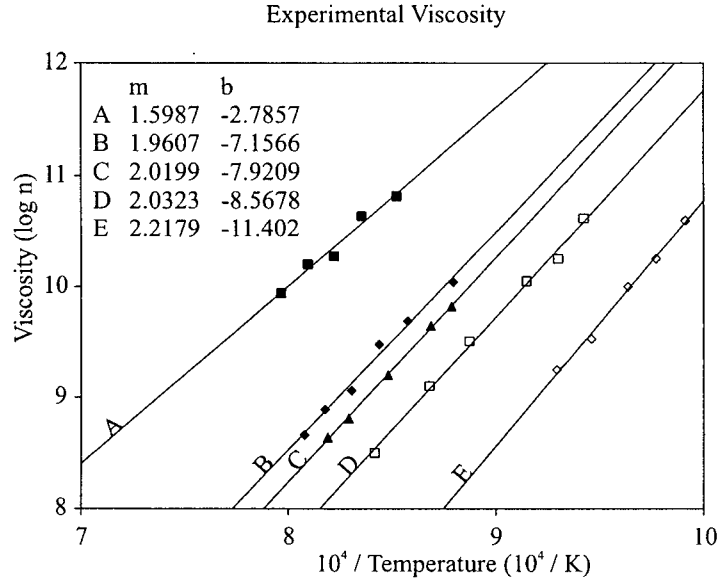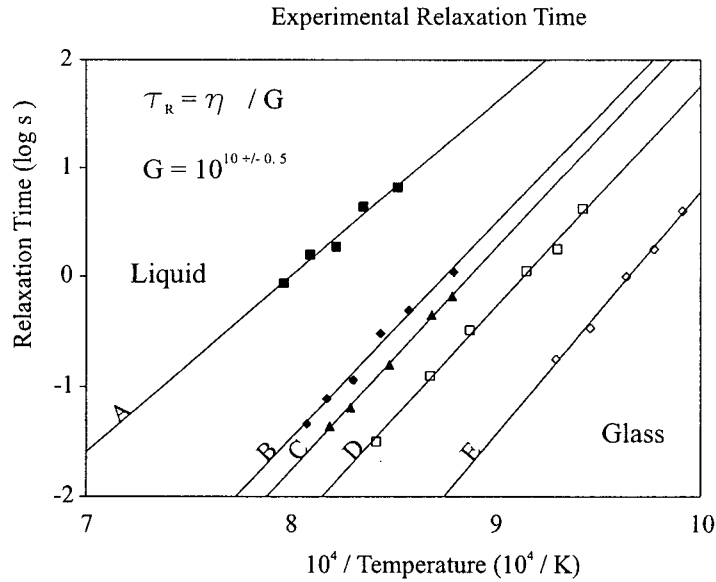
Figure 15. Experimental viscosities of natural magmas from Mount St. Helens (Alidibirov et.al, 1999: A and E) and various rhyolite localities (Stevenson et al., 1995: B to D) in Figure (a) demonstrate the extreme temperature dependence of viscosities. Over the natural temperature ranges for magmas, which are illustrated here, the magmas are essential Arrhenian, i.e. they vary linearly with temperature (inset: linear regressions of the data series). These viscosities can be used to calculate relaxation timescales (b) for Newtonian liquids using equation 4 (inset) from Dingwell and Webb (1990). The relaxation timescale (τ_R) is the inverse of the maximum strain rate which can be accommodated by a liquid before it begins to react brittlely as a glass (i.e. the rheological glass transition). The curves represent the boundary between brittle behaviour (glass) and viscous behaviour (liquid).

Figure 15b shows the glass transition curves of relaxation time versus temperature based on the viscosities shown in Figure 15a. Stress versus strain rate curves for Newtonian liquids pass through the origin and increase linearly according to equation 7 (Figure 16). This Newtonian behaviour ceases at the glass transition defined by the critical strain rates calculated from relaxation times given in Figure 15b. Stresses which exceed the strain rate limits of a viscous liquid will induce brittle behaviour and the material will fail.

I use the experimental viscosities of a typical rhyolite sample (Alidibirov et al., 1999) as an analogue to the 2360 yr. BP lava flow at Mount Meager. Stress versus strain rate curves for several temperatures are plotted in Figure 16 with the maximum critical resolved shear stresses. Critical resolved shear stresses from gravity acting on this lava body range from 10^6 to 10^7 Pa for slopes from 10^0 to 70^0 (Figure 16). This range of stresses is 3 orders of magnitude less than G, the viscous limit of a simple Newtonian liquid. In order for a lava flow to fail according to the block model presented here, it would have to be 1000 km thick. It is exceptional to find lava domes approaching 1 km in height because they tend to settle by viscous radial flow under gravitational stresses (Blake, 1990), and thus it is inconceivable to find a lava flow 1000 km thick.

4.4.2 Failure From Flow Velocity Gradient Induced Strain (VGIS)

Philpotts (1990) calculates a steady state lava flow velocity profile based on the relationship:

9) $v = (\rho g \sin \phi) / \eta * (hz - z^2 / 2)$

Stress versus Strain Rate
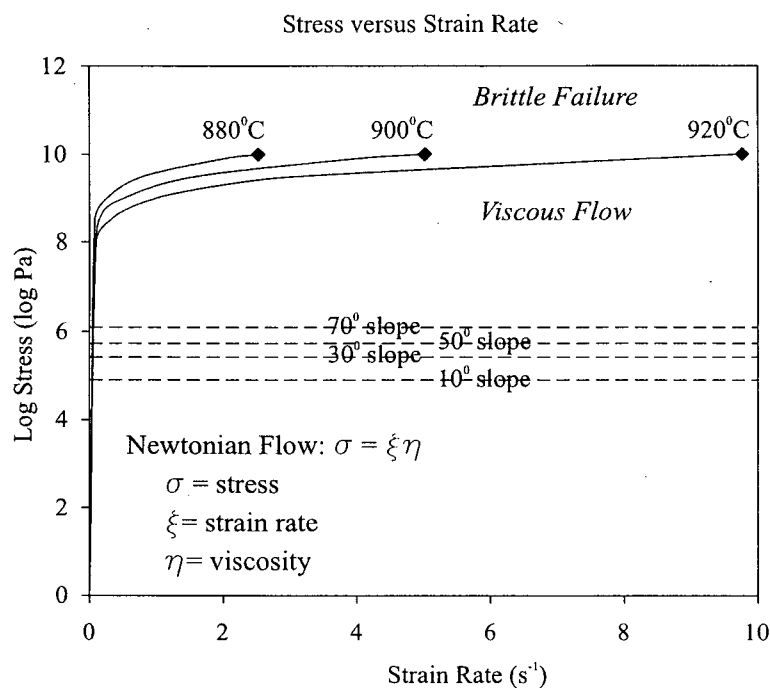
Figure 16. Example of stress and strain rate relationships for a Newtonian liquid based on the block

model lava flow (Figure 14a). Using temperature dependent viscosities from curve C (Figure 15a)

critical strain rates for the glass transition of a natural analogue rhyolite magma can be calculated.

Stress and strain rate are linearly related for Newtonian liquids (equation 7). In order to reach

critical strain rates, stresses of 10^{10}Pa must be applied to the liquid. For lavas acting like the block

model (Figure 14a), the maximum critical resolved shear stresses on slopes as steep as 70^0 are up to

10^6Pa. This is insufficient to cause brittle failure.

where z is the vertical position in a lava flow of height h. This relationship provides a velocity profile similar to that pictured in Figure 14b. By definition, strain rate is the acceleration of a body over a given distance (Munson et al., 1990).

10) $\acute{\varepsilon} = dv \,/\, dz$

Strain rates can be estimated from velocity profiles such as Figure 14b by integrating equation 10.

11) $\acute{\varepsilon} \cong v_2 - v_1 \,/\, z_2 - z_1$

From Figure 14b the greatest strain rate due to a velocity gradient exists at the base of a lava flow and thus equation 11 can be simplified by substituting $z_1 = z_0$, or $(v_1, z_1) = (0, 0)$.

12) $\acute{\varepsilon}_{crit} \cong v_2 \,/\, z_1$

Assuming the lava flow is Newtonian as in the block model (chapter 4.4.1), the critical strain rate is defined by equation 6. Substituting 6 into 12 provides the failure criteria for lava flow velocity gradient induced strain (VGIS).

13) $G \,/\, \eta = v_2 \,/\, z_2$

Substituting the velocity equation (equation 9) into this failure criteria gives:

14) $G / \eta = \{ (\rho g \sin \phi) / \eta * (hz_2 - z_2^2 / 2) \} / z_2$

solving for the height in the lava flow z:

15) $z = 2 * (\rho gh \sin \phi) - 2G$

Knowing the slope ϕ, thickness h and density ρ of the lava flow, an estimate of the length scale z across which failure can occur from VGIS can be calculated using equation 15. Table 5 gives reasonable estimates of these parameters for the 2360 yr. BP lava flow. Substituting these into equation 15 results in a negative value for z. This negative value indicates that failure cannot occur by the VGIS model for this lava flow. A lava flow on the order of 10^6 m thick would be required to approach the failure criteria. As in chapter 4.4.1, reasonable thicknesses of lava flows are insufficient to overcome the large value of G in the strain relationship (equation 15).

Density[1]	1590 kg/m^3
Height	30m
Slope	45^0
z =	-2 x 10^{10}

Table 5. Example parameters required to calculate the length scale of deformation required to cause failure in a lava flowing down a slope (equation 15). The slope and height are typical of the lava flow preserved at Mount Meager. Density is a typical value of Mount St. Helens lavas which are similar to the 2360 yr. BP lavas ([1]Alidibirov et al., 1997). In order for failure to occur (z = positive value) the lava flow must be 10^6m thick, an unreasonable value for terrestrial lavas. Thus differential strain resulting from velocity profiles (Figure 14b) in a typical lava flow will not cause a Newtonian liquid to fail brittlely.

4.4.3 Natural Lava Flows

In nature, few processes can be exactly described by simple calculational models. The extreme discrepency between parameters needed to cause the calculated Newtonian lava models to fail and realistic lava flow parameters suggests that alternative flow mechanisms must be invoked to explain the natural failure. Features of lava flows which can result in non-Newtonian behaviour which can weaken flows include suspended crystals and bubbles, and cooling and flow features such as flow top breccia.

The addition of solids (phenocrysts) or gases (vesicles) to a liquid will result in the bulk rheology of the melt to react in Bingham manner rather than a Newtonian response to applied stresses (Philpotts, 1990; Dragoni, 1993; Bagdassarov et al, 1994). Inclusions of solids and gases as well as cooling joints at the lava surfaces can act as local stress risers in the surrounding melt. An analogy taken from structural geology is that of propagation of Griffiths cracks (Griffith, 1920). These features can focus or redirect, and thus amplify, applied gravitational stresses within the melt. This uneven distribution of stress fields in a multicomponent lava may result in stresses in melt portions which exceed critically resolved

shear stresses in a purely liquid body. Further, these stresses may exceed the viscous limits described in chapter 4.4.1. Smith et al. (2001) describes how an analogous process of cavitation in fluids and metals may result in the brittle failure of lava flows.

Flow top and basal breccias may be a physical manifestation of the propagation of cooling joints into a lava flow by these processes. There may be feedback between the inward propagation of cooling joints and convective cooling of the crack surfaces. In order for a lava flow to fail completely there may be some critical point at which these cracks have developed sufficiently within a lava flow to dominate strain and thus flow behaviour of the lava. Images of lava flows which have failed show advanced breccia formation (Rose et al., 1976; Rose, 1987; Ui et al., 1999). Smith (2002) describes the "pervasive ductile shearing", "brittle failure" and "pervasive mechanical failure" of lava flows that generated block and ash avalanches at Mt. Unzen.

Lava domes may fail in a similar manner as lava flows. In addition to strain features from the radial flow of a dome, structural weaknesses may develop from periodic reintrusion and inflation processes which characterize dome growth (Blake, 1990). Endogenous growth (intrusion into a dome) provides time to develop an extensive cold brittle shell or rubbley outer carapace to a dome. It may also produce weaknesses within the dome by reintrusion. Interfaces between new and old dome lavas provide strong thermal and hence rheological gradients and planes of weakness in the lava dome.

4.5 Change in Behaviour of Erupting Lavas

The presence of block and ash avalanche deposits in the Lillooet valley indicate that lavas erupted 2360 yr. BP failed, producing avalanches of hot ash and lava blocks. The

youngest recognized event in the same eruption consists of the emplacement of a lava flow after block and ash avalanche production ceased. This lava flow does not contain strain features such as fold and thrust style deformation (Hausback, 1987; Castro and Cashman, 1999; Smith, 2002), ductile shearing, brittle fracturing (Smith, 2002), and scoriaceous fracture surfaces (Linneman and Borgia, 1993) which normally characterize lavas in a state of failure. Thus this lava flow does not appear to have produced the block and ash avalanches which preceded its emplacement.

Characteristics of these deposits indicate that erupting lavas underwent a significant change in response to gravitational stresses. A long period of brittle failure of lavas was succeeded by a period of viscous flow, without failure, until the end of the eruption cycle. The lava flow and blocks comprising the welded block and ash avalanche deposits appear identical in composition (Figure 3) and petrology. Based on these features, they should have been rheologically similar at eruption, and hence reacted similarly to applied stresses unless environmental conditions changed.

Mount Meager area is characterized by steep topography that is in a state of constant change by uplift and mass wasting processes. Late in the 2360 yr BP eruption, prior to emplacement of the lava flow, the slopes of the volcano became unstable and avalanches began to mix with the block and ash avalanches (cf. chapter 2.3.4). Eventually a major collapse occurred and a large rock avalanche was emplaced over block and ash avalanches.

The geometry of this avalanche deposit (cf. chapter 2.4.1), indicates its source lies above much of the lava flow (Figure. 13). Acoustic fluidization theory, widely believed to be the controlling mechanism of avalanche fluidization (cf. chapter 3.3.1), requires constant interaction of the moving mass flow with the underlying substrate (Melosh, 1979; Hungr, 1990;

Schneider and Fisher, 1998; Erismann and Abele, 2001). Avalanches and pyroclastic flows can be extremely erosive and commonly leave impact features on the travel surfaces (Sparks et al., 1997; Legros et al., 2000). The lava flow lies directly in the path of the rock avalanche but is not overlain by correlative avalanche deposits, displays no impact features on its surface and preserves delicate flow top breccias. In addition, the rock avalanche can be traced up to the toe of the lava flow, but no higher towards its inferred source. This evidence suggests that the rock avalanche occurred at the same time as the transition in eruption behaviour from production of black and ash avalanches to emplacement of the lava flow.

In order for a block and ash avalanche to form, two conditions must be met. Firstly, lavas must experience stresses exceeding the viscous limits of flow in order to fail brittlely (cf. chapter 4.4). Secondly, if lavas are induced to fail, they must do so on slopes sufficient to initiate movement of an avalanche. Dry unconsolidated debris can be stable on slopes up to the critical friction angle of 32^0 (Eisbacher and Clague, 1984). In order for a dry avalanche to begin to flow, failure must occur on slopes greater than this angle. Once transport begins, fluidization processes can maintain flow across shallower slopes for great distances (cf. chapter 3.3.1).

The current slopes of the lava flow do not exceed 29^0 (Figure 17) and consequently, are too shallow to initiate avalanches. The release of the rock avalanche may have significantly changed the upper slopes onto which the magmas were extruding. Prior to the rock avalanche event, the slopes may have been as steep as $40\text{-}45^0$, similar to slope angles immediately outside of the depression now filled by the lava flow (see oversize map). These slopes are commonly at or steeper than the critical friction angle. These would be sufficiently steep to result in the formation of avalanches from a failing lava flow.

Angle of Slope Along Axis of Lava Flow
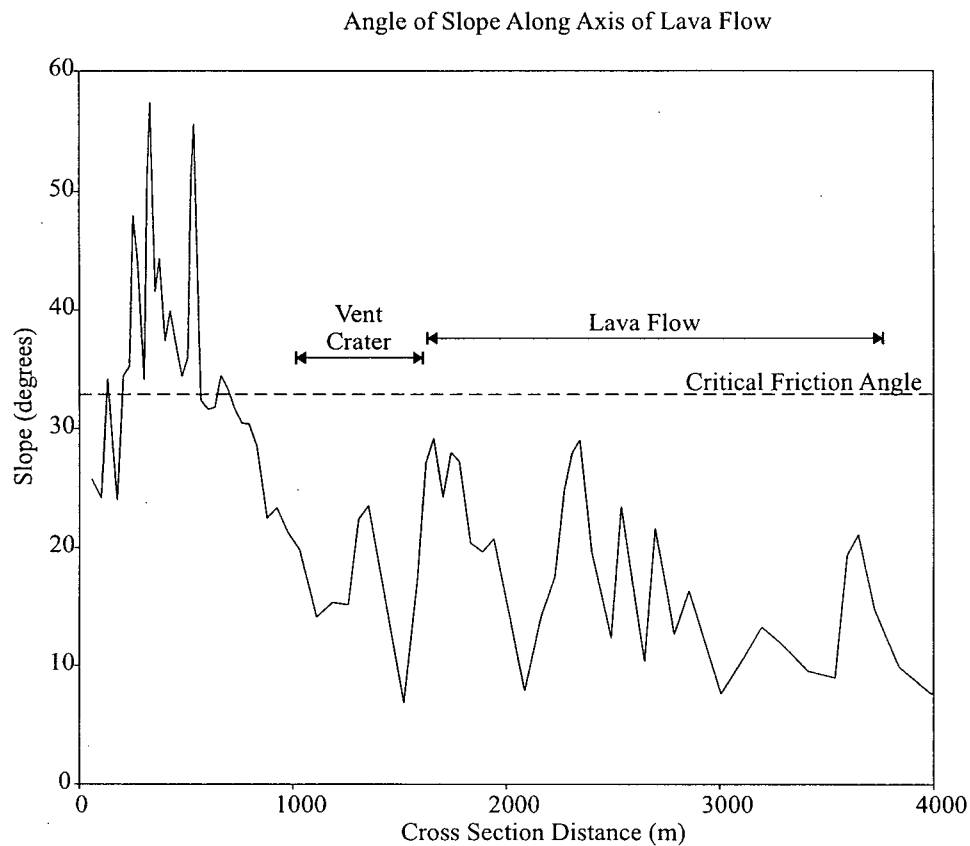
Figure 17. Average angles of slope on the north side of Mount Meager. Estimates derive from topographic cross sections based on a digital elevation model (Figure 13). Dry unconsolidated material will remain at repose on slopes up to the critical friction angle of 32^0 (Eisbacher and Clague, 1984). This critical friction angle along the axis of travel for the 2360 yr. BP avalanche events is reached only at locations above the vent crater. Thus, the current slopes below the eruption vent are unlikely to cause the formation of gravitationally driven block and ash avalanches should the extruding lavas fail brittlely.

Alternatively, lava domes may have been perched high on the volcano. Reach angles suggest the rock avalanche derived from the outer lip of the eruption crater. The material that formed the rock avalanche could have been part of a crater floor that supported and impounded extruding lava domes. The dynamics of lava dome production typically produces steep-sided features which can exceed the critical friction angle. If such a dome failed, avalanches of hot lava would fall off the oversteepened sides, traveling into the Lillooet valley below. Subsequent to the production of the rock avalanche, extruding lavas would no longer be impounded and could travel freely down the slopes of the volcano.

Chapter 5

Failure of a Pyroclastic Dam

5.1 Introduction

Mapping of volcanic deposits has shown that during the last two eruptions of Mount Meager (Table 1: 2360 and 90,000 yr. BP), block and ash avalanches filled the Lillooet valley to depths greater than 100m (cf. Chapter 2; Stewart et al, 2001). Current drainage patterns remain essentially unchanged since the Fraser glaciation 15,000 yr. BP (pers. comm., J.J. Clague) and were likely similar prior to glaciation. In this narrow steep valley it is inevitable that the block and ash avalanche events would have interacted with the flow of the river. Deposits from the most recent volcanic cycle in the valley (2360 yr. BP) suggest block and ash avalanches dammed the valley forming a lake (Hickson et al, 1999; Stewart et al., 2002). Failure of the dam produced at least two outburst floods. These floods eroded the volcanic deposits, one of which resulted in the formation of a hot debris flow.

Dams of volcanic deposits are rare in nature. The most devastating event recorded from failure of a volcanic dam occurred at the Asama volcano, Japan in 1783. A pyroclastic flow is believed to have dammed up a river close to the volcano, but within an hour it was overtopped by rising water levels. The resulting catastrophic failure produced a hot debris flow that travelled 80km down valley, leaving 1300 dead in its wake (Aramaki, 1956). Other notable occurrences include the damming of the Colorado River by an advancing lava flow (Fenton et al., 1999) and the elevating of Spirit Lake at Mount St. Helens subsequent to the May 18, 1980 eruption (Youd et al., 1981).

Other types of natural dams which can be observed in mountainous regions include: 1)

landslide dams, 2) moraine dams, 3) glacier dams and 4) snow dams (Hutchinson, 1957; Blown and Church, 1985; Clague and Evans, 1994). Of these, landslide dams present the greatest threat to people (Kershaw, 2002). The pyroclastic dam that formed during the 2360 yr. BP eruption closely resembles a landslide dam. Avalanche dams are better studied and provide a good analogy to study the mechanisms of failure and flooding of the Mount Meager dam. Manville (1999) suggests that the probability of a dam failing is controlled by: 1) material comprising the dam, 2) geometry of the dam, 3) hydrological regime of the lake and 4) a trigger event for outflow. Chapter 5.2 elucidates the structure and geometry of the deposits comprising the pyroclastic dam. The timing of filling of the lake and deposits associated with it are discussed in chapter 5.3. Failure mechanisms, erosional features and resultant debris flow mechanisms are discussed in chapter 5.4.

5.2 Pyroclastic Dam Structure

Figure 7 illustrates the large pyroclastic apron that extends down into, and fills the Lillooet valley. Deposits comprising this feature include pumiceous pyroclastic flows, welded block and ash avalanches, unwelded block and ash avalanches and rock avalanches (Figure 5 and 10). These deposits provide a varied structure and strength to the dam from the interlayering of unconsolidated debris and densely welded deposits (Figure 18).

The base and upper regions of this dam are unconsolidated, permeable and highly erodable. The core of the dam is densely welded, impermeable and strong enough to currently maintain vertical cliffs along the Lillooet River. An inherent weakness in this dam is the presence of cooling joints that cut vertically through the entire dam throughout the Lillooet canyon, except close to Keyhole Falls. These joints formed as the volcanic deposits cooled and
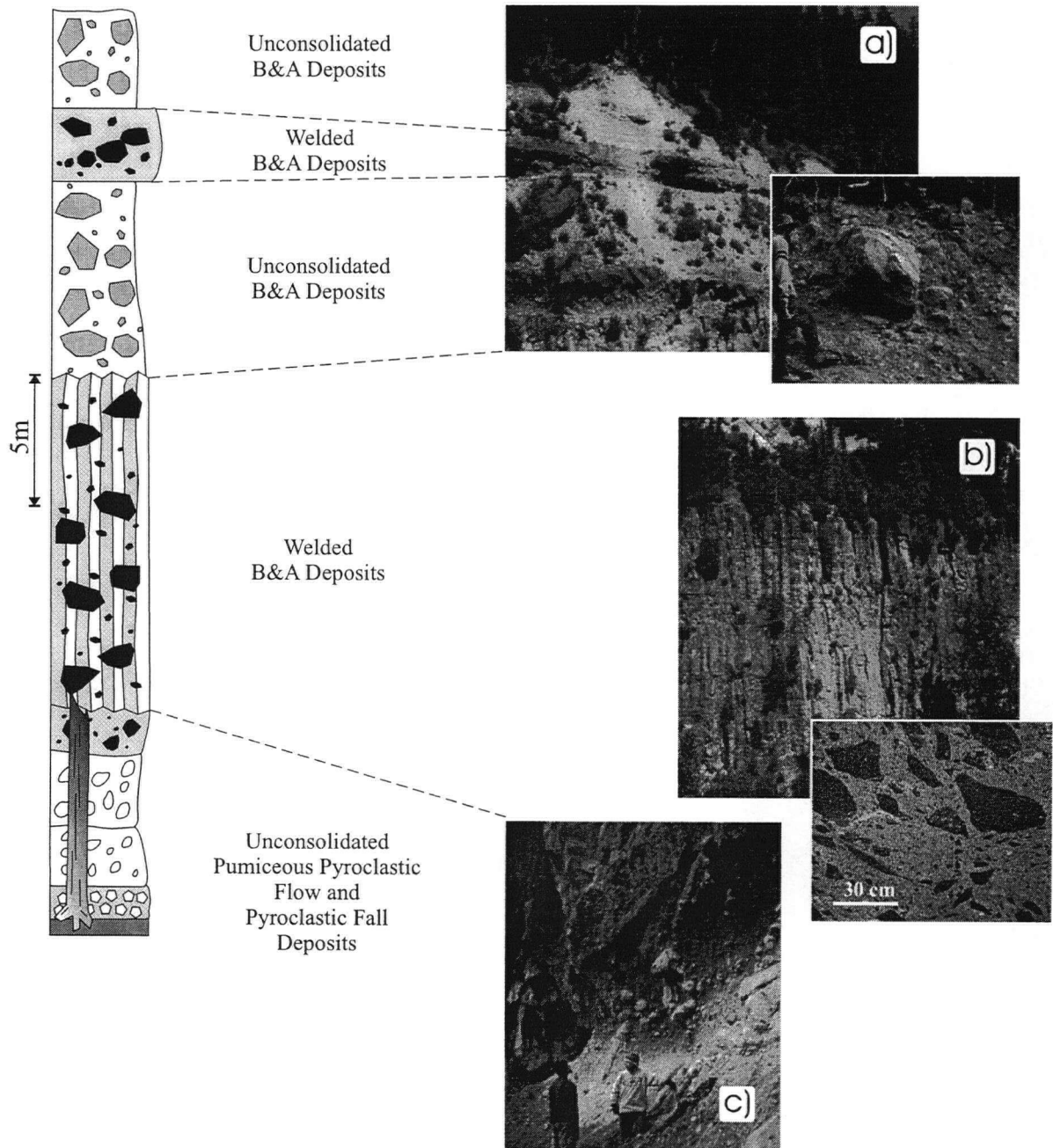
Figure 18. Idealized cross section of block and ash avalanche (B&A) and pumiceous pyroclastic flow deposits which comprised the dam that blocked the Lillooet River during the 2360 yr. BP event (cf. Figure 5). The character of the material is highly variable and includes permeable and unconsolidated block and ash avalanche deposits and pumiceous pyroclastic flow deposits interlayered with impermeable, densely welded block and ash avalanche deposits.

passed through the glass transition temperature (T_g: cf. chapter 3.2). At Keyhole Falls, the cooling joints are erratic, suggesting the cooling surface may have been irregular. The aspect ratio of this dam is typical for that of avalanche dams (Costa and Schuster, 1988). The low, wide profile and welded core (Figure 19) provides a strong and efficient dam against rising water levels.

5.3 Filling of the Paleo-Salal Lake

Sedimentary deposits and erosional features upstream of Keyhole Falls are consistent with a lake, defined as paleo-Salal lake (Stewart et al., 2002), building up behind the pyroclastic deposits. Well bedded alluvial sediments and debris flows overlie the NW limb of the pyroclastic deposits and bluffs in a broad flat valley north of the Mount Meager volcano. These deposits include subhorizontal interbedded organic rich silts and rounded pumice pebble pumice sands and thick well-sorted cobbley lithic sands. Pumice and lithic pebble sands at elevations as high as 720m on valley filling pyroclastic deposits represent the highest known elevations of alluvial deposition associated with paleo-Salal Lake. Clasts are comprised of pumice, granite, metamorphic rocks and vesicular basalt consistent with rock types found upstream of Mount Meager.

Cordy (1999) describes the presence of what appears to be a large delta at the outlet of Salal creek which lies up to an elevation of 705 m, at least 30 m above the current river levels. Deposits comprising this delta include well bedded lithic and pumiceous pebble sands. Sedimentary structures recognized by Cordy (1999) include forset and topset beds. Additional beds described by Stewart et al. (2002) contain large cobbles of primarily granite and metamorphic rock types in a lithic sand matrix. These clasts are imbricated, extremely well
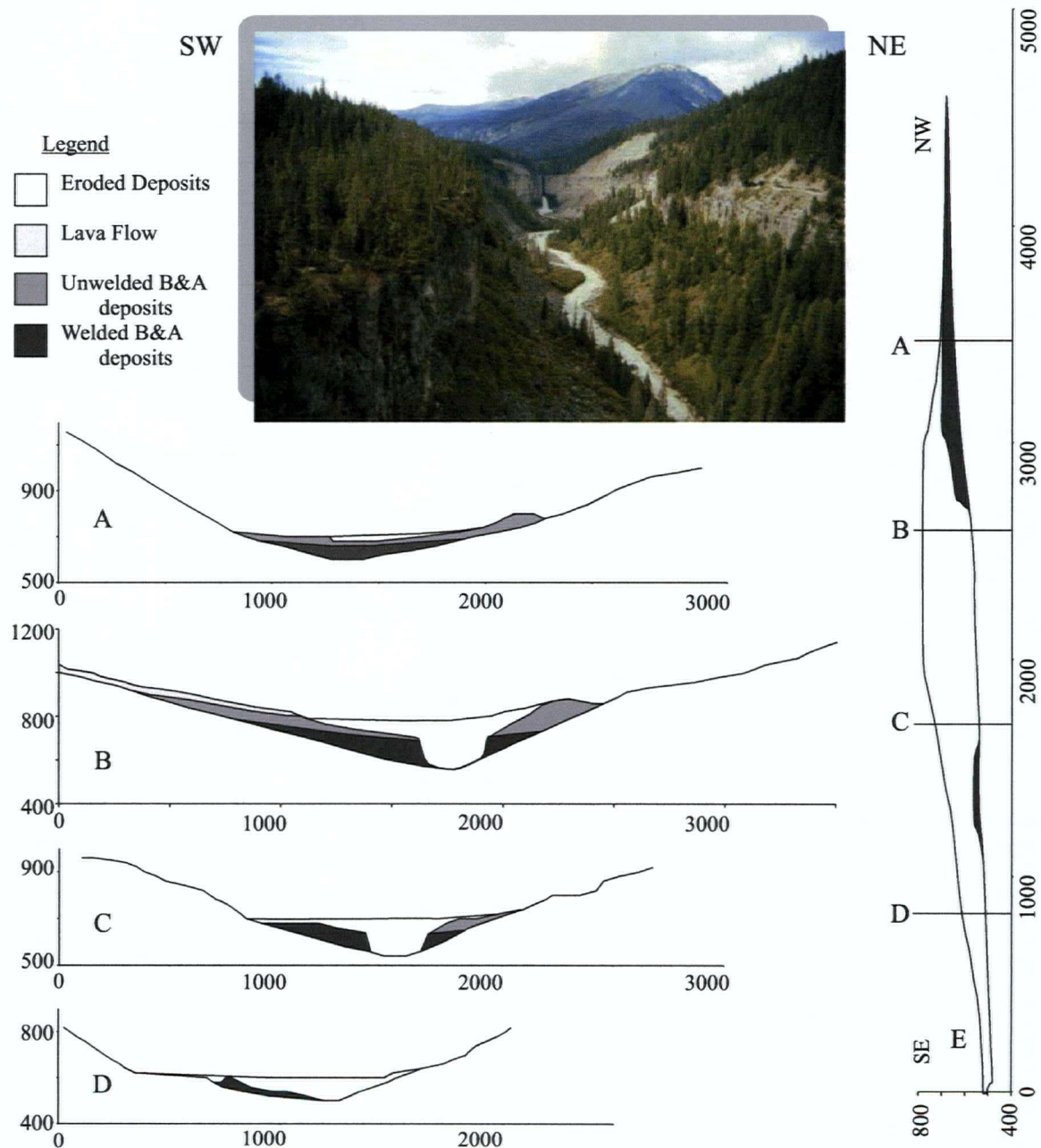
Figure 19. Cross-sections of the dam including sections normal to the Lillooet valley (A to D) and along the length of the Lillooet River (E). Looking NW, the photo illustrates the steep walls comprised of welded block and ash avalanche deposits, overlain by unwelded block and ash avalanches on the right. These deposits are exposed in a large canyon eroded by the catastrophic outburst flooding which emptied paleo-Salal Lake. Sections outline the 0.19 km^3 of material which was eroded from these deposits. The broad and low aspect dam illustrated here is typical of naturally formed avalanche dams which fill valleys in mountainous regions. Exact locations of these cross sections are illustrated in Appendix III. (photo credit: J.K. Russell).

rounded and oblate (Figure 9c). Imbrication and the shape of these clasts derive from frictional sliding (Collinson and Thompson, 1989). This process is common in alluvial systems where high energy, high volume streams meet low to non-energetic bodies of water, consistent with Salal creek emptying into paleo-Salal lake.

A prominent feature in the paleo-Salal lake basin are erosional scarps forming bluffs throughout much of its perimeter. These features result from translational slope movements in saturated unconsolidated sediments (Mate, 1997). They commonly form by removal of lateral support by wave erosion and steep shoreline aspects. These slides occur in areas affected by dominant wind and water level fluctuations. Flood deposits downstream of these features are consistent with the fluctuation of water levels during the 2360 yr. BP eruption.

Hickson et al. (1999), Cordy (1999) and Schipper (2002) provide estimates for lake volumes and time of filling of the lake from 2 days to 4 months. New mapping and more precise calculational techniques are used to recalculate these lake filling estimates (see Appendix IV for methodology). Significant elevations relating to the rise of paleo-Salal Lake include: well-bedded alluvial sediments over a wide area at 705m elevation; the highest known elevation of alluvial sediments at 720m; and, based on digital reconstructions, a maximum lake level as high as 780m (Figure 20a).

Flow regimes in the Lillooet valley are likely little changed since the end of the Fraser glaciation 10,000 yr. BP (pers. comm., J.J. Clague). The best available data of modern flow rates for the Lillooet River are from close to Pemberton, well downstream of Mount Meager (Inland Waters Directorate, 1991). There are no major tributaries emptying into the Lillooet below Meager Creek. While this data may not be accurate for the paleo-Salal Lake area it does provide a good estimate of the range of realistic flow rates for the Lillooet River, knowing from

chapter 4.2 that the eruption probably lasted through numerous seasons over as many as 53 years. Based on minimum, maximum and time-averaged flow rates measured over a 76 year period at Pemberton, B.C., it would have taken from 2 to 365 days for the lake to fill completely behind the maximum elevation of the dam (Figure 20a).

Although the range in filling times appears extreme, the maximum filling time calculated has significant implications when compared to the timescales of volcanic processes. The production rates of block and ash avalanches which produced the dam are significantly slower. Even unreasonably high extrusion rates are insufficient to keep up construction of the dam with the filling of the lake. There was likely ongoing competition between the rise in lake level and the rise in the dam height. The production of block and ash avalanches is characterized by sudden periodic catastrophic building events whereas the lake filling is a continual process driven by the steady flow of the Lillooet. Conceptually, competition between these two processes could have looked like Figure 21.

5.4 Dam Failure and Flooding

A large proportion of natural dams fail partially or wholly (Costa and Schuster, 1988). In the Canadian Cordillera almost 90% of naturally formed landslide dams fail within 50 days of formation (Clague and Evans, 1994). The 2360 yr. BP dam appears to be no exception. Erosion features and debris flows deriving from the pyroclastic dam indicate the dam failed catastrophically on at least two occasions. A distinct erosional surface overlain by debris flows and fluvial sediments on the top of the welded block and ash avalanche deposits is the earliest indication of dam erosion and flooding in the Pebble Creek stratigraphy. These features are overlain by more block and ash avalanches deposits which were eroded back by a subsequent

a)

Lake Elevation versus Filling Time

b)

Lake Elevation versus Peak Discharge
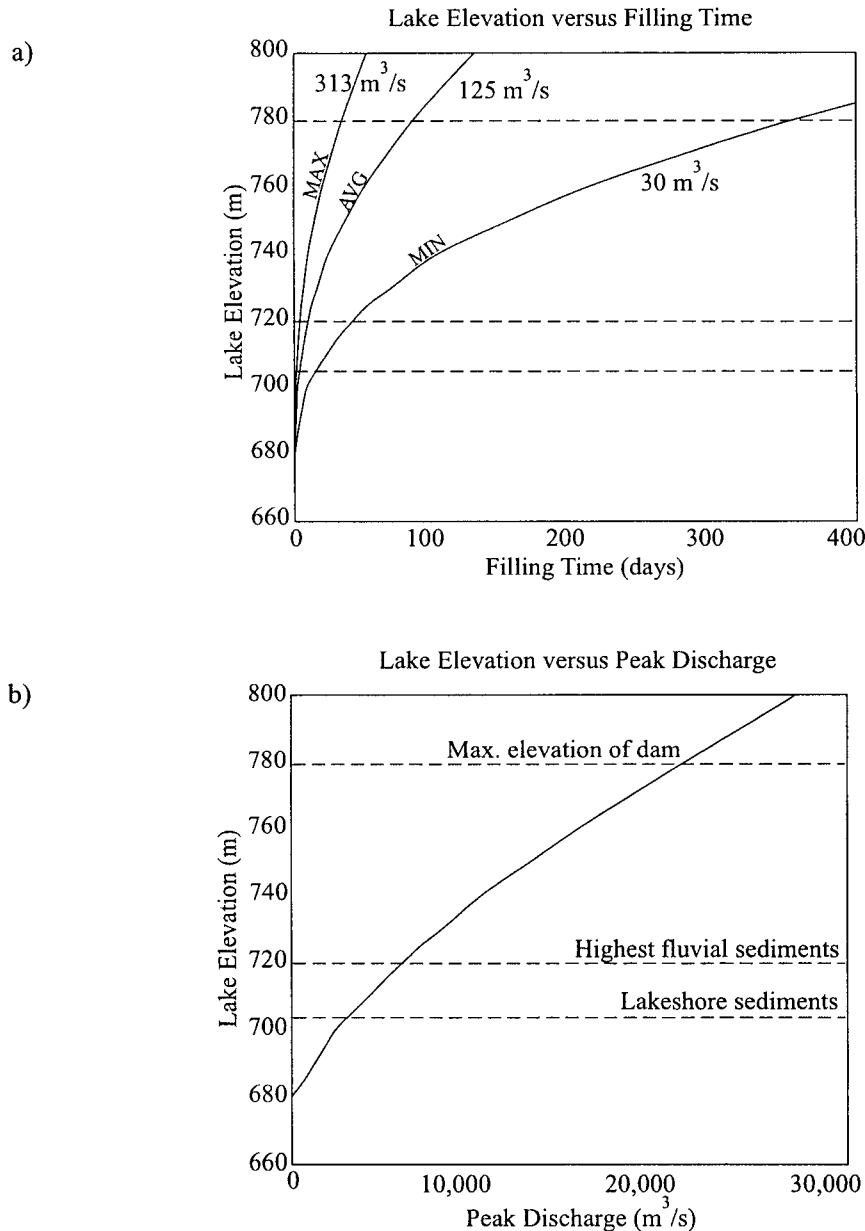
Figure 20. Historical flow rates for the Lillooet River at Pemberton B.C. (Inland Waters Directorate, 1991) provide the best approximations of the flow regime of the Lillooet River during the 2360 yr. BP eruption event at Mount Meager. Filling time curves (a) are calculated using these flow rates, and volume measurements of the paleo-Salal Lake basin upstream of the pyroclastic dam. Two lake stand elevations provided are based on occurrences of alluvial and debris flow deposits associated with the presence of the lake. The maximum lake height, and hence maximum filling time is based on the projected highest elevation of pyroclastic deposits blocking the valley. The possible range of filling times for the lake range from as little as several days up to a year until water would have overtopped the dam. Theoretical peak water discharge due to failure of this dam can be calculated based on the elevation of the dam and the volumes of water behind the dam (Costa and Schuster, 1988). Discharges greater than 20,000 m³/s could be released from failure of the dam (b). These discharges would have been highly erosive and would have had catastrophic consequences for areas downstream of the dam.
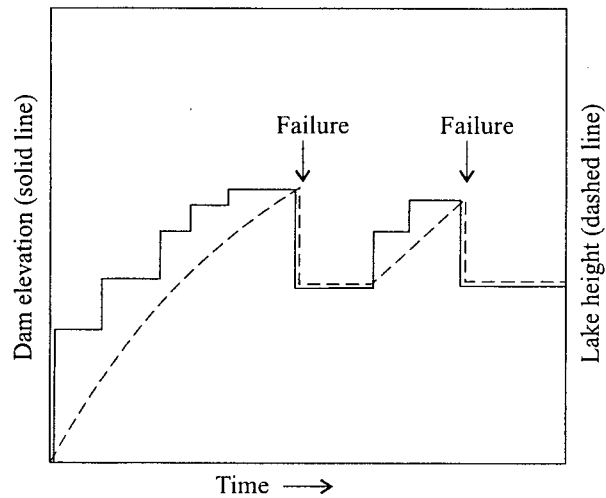
Figure 21. Conceptual time curve for production of the dam, and filling of the lake. The dam would have built incrementally as individual block and ash avalanche events built on top of previous events. While the flow of the Lillooet River would have been relatively continuous. The rate of production of block and ash avalanches was insufficient to keep up with rates of filling of the lake. On at least two occasions, lake levels exceeded the height of the dam, overtopped it, and caused the failure and emptying of the lake. At some point after the eruption stopped, the dam failed one last time leaving the canyon that is preserved in the Lillooet valley today.

failure event that cut right through underlying welded deposits down to the pre-eruption valley floor. This event left a large canyon (Figure 19) up to 200m deep and >2km long.

Failure of natural dams (Chapter 5.1) is known to occur as a result of: 1) ice avalanches, 2) rockfall and rockslides, 3) increased streamflow, 4) calving of glaciers, 5) earthquakes and 6) piping from groundwater flow (Clague and Evans, 2000). Of these, the most common mechanism for failure is from an overtopping wave generated by a mass entering the lake (e.g. rock or glacial avalanches) (Costa and Schuster, 1988; Clague and Evans, 1994 and 2000; Kershaw, 2002). There is no evidence of a direct trigger for the failure, but the short filling times of paleo-Salal Lake suggest that water levels could easily have overcome the height of the dam. In addition, the presence of a hot outburst flood deposit indicates at least one failure occurred during or shortly after the eruption. During the eruption volcanic seismicity and rock and volcanic avalanche activity in the Lillooet valley could have contributed to the instability of the dam. Hickson et al. (1999) describe erosion mechanisms which are consistent with an overtopping event initiating erosion and eventual failure of the dam.

The hazard of catastrophic failure of avalanche dams can be extreme. Outburst floods can become debris flows by eroding material in its flow path. These erosion rates are due to high volumes of output over short periods (Clague and Evans, 1994). The destructiveness of an outburst flood is a reflection of the peak discharge after the failure. Peak discharge can be calculated based on the energy of the water released, which can be reflected in 1) the geometry of the eroded channel in a dam, 2) superelevation, or runup at inflections in the flow path, 3) the size and distribution of boulders moved in the flood or 4) the potential energy of water stored behind the dam (Kershaw, 2002).

For example, Costa and Schuster (1988) predict the peak discharge from failure of a

landslide dam based on the potential energy (PE) of a confined lake. The potential energy is defined by:

16) $PE = V \times SW \times h$

knowing the volume of water in the lake (V), the standard weight of water (SW) and the height of the dam. The peak discharge (Q) can then be calculated using:

17) $Q = 0.0158 \times PE^{0.41}$

Figure 20b illustrates the effect of increased lake levels on the peak discharge of water due to failure of the pyroclastic dam in the Lillooet valley. At the maximum calculated lake levels peak discharge could potentially be greater than 21,000 m^3/s. This high rate of discharge has extreme erosive potential. Actual peak discharges can be quite variable (Clague and Evans, 2000), but must have been great enough during the outburst from paleo-Salal Lake to move boulders 15m in width. The entire discharge eroded up to 190 million m^3 of material from the pyroclastic dam (Table 3). Kershaw (2002) suggests that debris flows of this scale move as large saturated carpets as the density of the debris is too great to maintain such large boulders in suspension on the shallow decline of the valley floor. Outburst floods can become attenuated over time and distance. The Lillooet valley remains relatively confined until it debouches into the Pemberton valley, and thus the town of Pemberton could be significantly affected by outburst flooding resulting from activity at Mount Meager.

Chapter 6

Discussion: Volcanic Hazards of a Dacite Erupting in Mountainous Terrain

The Mount Meager area poses an increasing risk to people in the Lillooet valley, both near the mountain and further downstream in Pemberton, B.C.. It is essential to properly describe hazards which pose a risk to people in preparing strategies to deal with the eventuality of such an event occurring. For risk assessment a natural hazard is characterized by the area affected, intensity, speed of onset, duration and frequency of that event (Burton et al., 1978). These characteristics are inherent in a natural setting and are independent of the social environment which exists in the same area. The risk that such an event poses depends on how this hazard will affect society (cost/loss), and how society reacts to that event (mitigation). Conceptually risk might appear as the following relationship (Fournier d'Albe, 1979):

Risk = Hazard * Loss / Mitigation

The characteristics of natural hazards are measurable quantities. Evidence of volcanic hazards which exist at Mount Meager are preserved in deposits filling the Lillooet valley. Mapping of these deposits provides estimates of the limits of areas affected by the various volcanic events presented in this thesis. Detailed stratigraphic analysis has elucidated the potential for even greater hazardous areas than those defined by mapping. For example, ash-cloud surges can outrun their parent pyroclastic flows, traveling much greater distances, but are rarely preserved as mappable units (cf. chapter 3.3.2). The observation of pyroclastic flow deposits in the stratigraphy requires the assumption that ash cloud surges accompanied their

deposition and thus affected a wider area than that outlined by their mapped extents.

Pumiceous pyroclastic flow, block and ash avalanche and rock avalanche deposits are all present in the 2360 yr BP stratigraphy. Each of these hazards is localized in and fills the Lillooet valley below the eruption crater. These deposits represent extremely intense and fast moving mass flows which are highly destructive and deadly. Pyroclastic fallout and flooding events associated with the eruption are also locally intense events. They pose additional threats to infrastructure and people downwind and downstream of the volcano, though their effects may become more attenuated and less costly with increasing distance. Ash fall from the eruption has been traced as far as the Alberta-British Columbia border (Stevenson, 1947; Nasmith et al., 1967; Westgate and Dreimanis, 1967), and flood deposits have been found as far as Pemberton, B.C. (pers. comm., M.V. Stasiuk).

The duration of individual volcanic events can be short, but the time of onset prior to such events can be sufficiently long to allow some mitigation of particular hazards. For example, the catastrophic collapse of lavas forming these block and ash avalanches is a relatively rapid process, but requires a period of extrusion and buildup or flow of lavas before they can fail. Thus if lava flows are observed to be extruding onto steep slopes, stratigraphy shows that they will likely fail catastrophically and preparations can be made for such an expected event. The volume of resultant deposits in the Lillooet valley suggests the period of repeated lava extrusion and failure can last for as long as 53 years (cf. chapter 4.2). Estimates of the relative timescales of major events during this 2360 yr. BP eruption are presented in Figure 22. The final component of hazards assessment, event frequency, can be described by probability distributions.

Probability distributions for geologic events are requisite for risk assessment. Methods
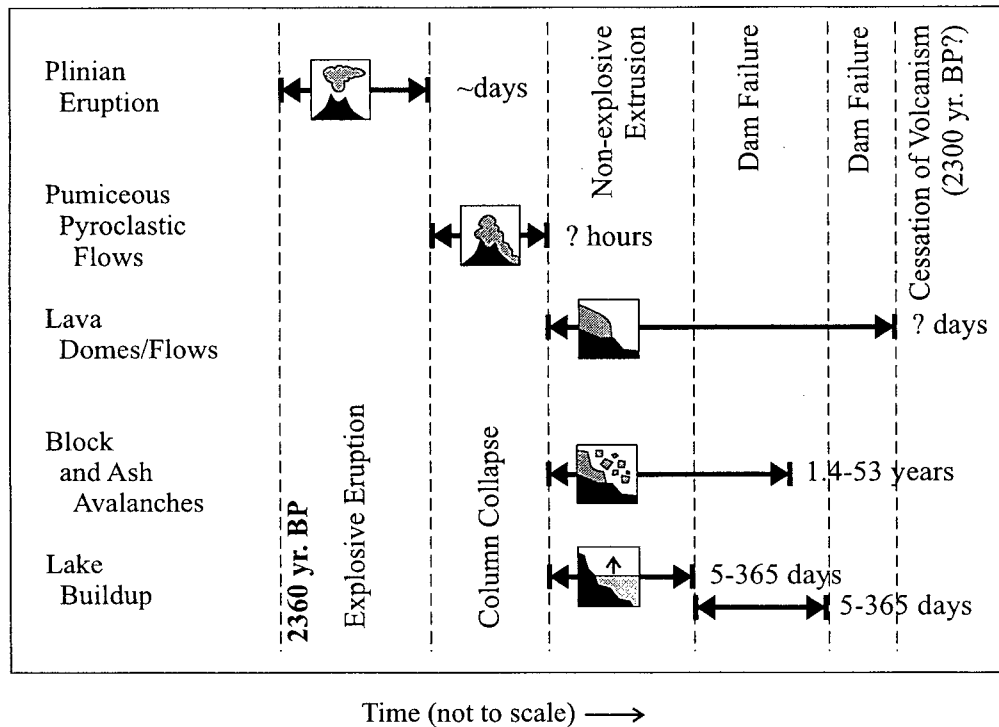
Figure 22. Comparison of timescales and the sequence of events during the 2360 yr. BP eruption cycle at Mount Meager. This cycle is comprised of an initially explosive eruption phase which may have lasted only hours, based on similar eruptions at Mount St. Helens (Christiansen and Peterson, 1981). This event was followed by a much more prolonged period of non-explosive extrusion of lavas which lasted from 1.4 to 53 years. This period was characterized by the production of block and ash avalanches which filled the Lillooet valley. The rate of production of valley filling deposits was insufficient to compete with the relatively rapid rates of filling of a lake behind the resultant dam, and consequently the dam failed on at least two occasions.

are well established in forecasting rock avalanche activity and provide a good model for determining volcanic probabilities. These methods include analysis of historic and prehistoric events and predictive forward computational models (Guzetti et al., 1999; Crovelli, 2000). Historic and prehistoric avalanche activity at Mount Meager is summarized in Table 1. Problems associated with this database include a paucity of historical data and a decreasing number of preserved deposits with increasing age. In addition, smaller events may not be recorded or are indistinguishable in the stratigraphy, limiting the database to large events.

The most common method for calculating occurrence probabilities of rock fall or avalanche events from observational data is the use of a Poisson expression (Smith and McClung, 1997; McClung, 1999; Guzzetti et al., 1999; Crovelli, 2000). The Poisson process assumes that events are discrete, independent of each other and probabilities do not change with time. Our database represents a minimum number of events unevenly distributed over time, but can provide a reasonable approximation of the probability of an avalanche event occurring in the Lillooet River valley.

Eruptive activity at stratovolcanoes is characterized by long periods of dormancy punctuated by intense and short lived eruption cycles (e.g. Cole et al., 1998; Ui et al., 1999; Thouret et al., 2000). Each cycle is comprised of numerous individual volcanic events such as the growth of a lava flow or the formation of a block and ash avalanche. Eruption forecasting is used to predict either long term periodicity of eruption cycles or short term occurrences of events within an eruption cycle. Currently the most effective means of establishing probabilities for the occurrence of volcanic cycles or events is analysis of historical records, where possible, and to map the distribution, volume and ages of deposits.

Volcanic cycles recognized in the Mount Meager stratigraphy are summarized in Table

1. This distribution is subject to the same limitations as for avalanche events including limited data due to erosion and possible errors in mapping. In addition to regular erosion from tectonic uplift, repeated glaciation (Clague et al, 1990; Clague, 1994) has affected all but the most recent volcanic deposits in the area. Most of the recognized preglacial events are major edifice building volcanic cycles (Read, 1978). Smaller eruptions similar to the Pebble Creek eruption cycle may be indistinguishable from these larger episodes. There appears to be at least one major volcanic cycle occurring every 250,000 to 300,000 years in the Mount Meager volcanic complex, and possibly as often as every 100,000 years.

During an active eruption cycle, volcanic events can be represented by a Poisson distribution because the events are discrete, independent and the probability of the next occurrence is constant. Continuous monitoring of an eruption cycle will provide a good source of data to build a probability distribution needed to forecast the next event in the cycle (e.g. Cole et al., 1998; Ui et al., 1999; Thouret et al., 2000). Mapping of volcanic deposits is essential when an eruption is just starting because historic data may not be available (e.g. Sheridan and Macias, 1995). In this case previous eruptive activity provides the best approximation of potential future activity. Block and ash avalanche deposits in the Lillooet Valley represent at least three and likely more individual volcanic avalanche events during the 2360 yr. BP eruption cycle.

The probability of flooding events occurring like the catastrophic outburst flood associated with the 2360 yr BP eruption, are entirely dependent on the occurrence of other events during an eruption cycle. If deposits fill the Lillooet valley blocking the river, a lake will inevitably back up behind the dam. Natural dams nearly always fail, commonly shortly after they develop (cf. chapter 5). Mapping has demonstrated that the previous two eruptions of

Mount Meager (2360 and 90,000 yr. BP) produced block and ash avalanches which filled and likely dammed the Lillooet Valley to depths exceeding 100m (cf. chapter 5, Stewart et al., 2001). Flood deposits associated with failure of the most recent deposits extend as far as the Pemberton valley (pers. comm. M.V. Stasiuk).

Thus, based on deposits from previous eruptions, a future eruption in the mountainous region of the Mount Meager volcanic complex will likely: 1. be dacitic in composition (Read, 1978) and hence, 2. generate block and ash flows resulting in, 3. damming and catastrophic flooding of the Lillooet valley. The exact location of the next eruption vent will likely occur in the northern sector of the volcano based on the northward-younging trend observed by Read (1978). Once the exact location of a vent has developed, the 2360 yr. BP deposits can be used as an analogy to postulate the hazardous consequences of erupting new dacitic magmas in this mountainous environment. A conceptual model of the hazards associated with volcanism at Mount Meager is illustrated in Figure 23. Mapping and detailed stratigraphic analysis is necessary to determine and quantify the hazards present in regions such as the Lillooet valley where historical records of previous activity are lacking. Once the character of the hazards is established, risk can be calculated.
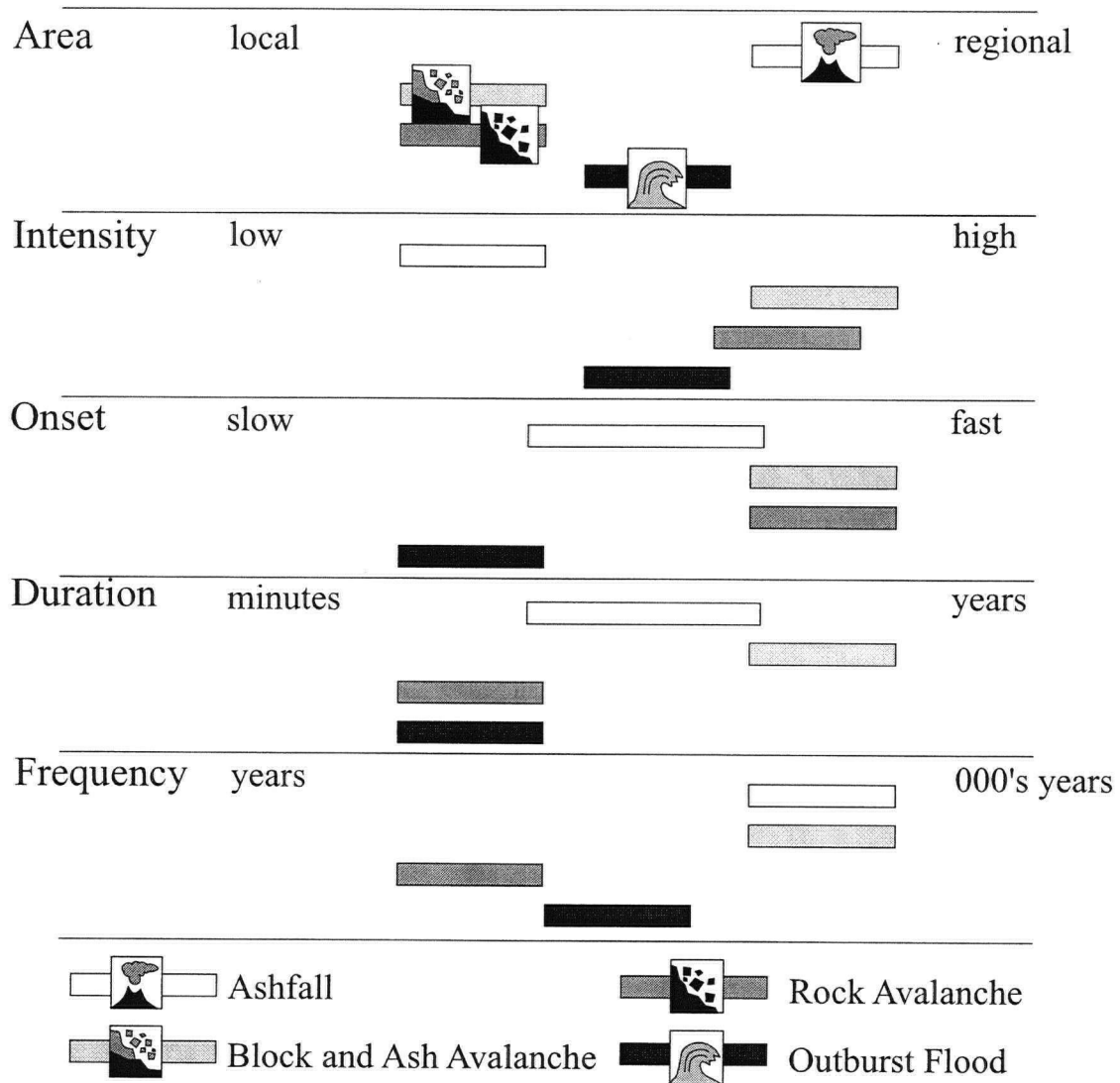
Figure 23. Conceptual diagram of the natural hazards preserved in deposits in the Lillooet valley below Mount Meager. The area affected, intensity, onset time, duration and frequency of those hazards are all measurable quantities requisite for risk assessment. Many of the volcanic events are quite rare due to the low frequency of volcanic eruptions at Mount Meager. During periods of volcanic activity these hazards can be intense, fast-moving with activity lasting from days to decades. Some events are predetermined by the presence or lack of other hazardous events. For example, outburst floods result from the damming of the Lillooet by other events (e.g. block and ash avalanches filling the valley). While the flood itself is fast moving, the observed onset of the event is extended by a period building up to failure. Properly identifying the hazards which exist in volcanic terrains in mountainous environments allow mitigation to reduce risk to the people which utilize these areas.

References

Alidibirov, M., Dingwell, D.B., Stevenson, R.J., Hess, K.H., Webb, S.L. and Zinke, J., 1997. Physical properties of the 1980 Mount St. Helens cryptodome magma. Bulletin of Volcanology, 59: 103–111.

Alvarado, G.E. and Soto, G.J., 2002. Pyroclastic flow generated by crater-wall collapse and outpouring of the lava pool of Arenal Volcano, Costa Rica. Bulletin of Volcanology, 63: 557-568.

Anderson, R.G., 1975. The geology of the volcanics in the Meager Greek map-area, southwestern British Columbia. B.Sc. thesis, Department of Geological Sciences, The University of British Columbia, 130 p.

Anderson, S.W., Fink, J.H. and Rose, W.I., 1995 Mount St. Helens and Santiaguito lava domes; the effect of short-term eruption rate on surface texture and degassing processes. Journal of Volcanology and Geothermal Research, 69:1-2 105-116.

Aramaki, S., 1956. The 1783 activity of Asama volcano, part 1. Japanese Journal of Geology and Geography, 27:2-4 189-229.

Bagdassarov, N.S., Dingwell, D.B. and Webb, S.L., 1994. Viscoelasticity of crystal- and bubble-bearing rhyolite melts. Physics of the Earth and Planetary Interiors, 83: 83-99.

Bardintzeff, J.M. 1984. Merapi Volcano (Java, Indonesia) and Merapi-type nuée ardente. Bulletin of Volcanology, 47:3 433-446.

Blake, S., 1990. Viscoplastic models of lava domes. In: J.H. Fink (ed) Lava flows and domes, vol 2. IAVCEI Proceedings in Volcanology. Springer, Berlin Heidelberg New York, 88-126.

Blown, I. and Church, M. 1985. Catastrophic lake drainage within the Homathko River basin, British Columbia. Canadian Geotechnical Journal 22, 551-563.

Bovis, M.J. and Jakob, M., 2000. The July 29, 1998, debris flow and landslide dam at Capricorn Creek, Mount Meager Volcanic Complex, southern Coast Mountains, British Columbia. Canadian Journal of Earth Sciences. 37: p. 1321-1334.

Branney, M.J. and Kokelaar, P., 1997. Giant bed from a sustained catastrophic density current flowing over topography: Acatlan ignimbrite, Mexico. Geology, 25:2 115-118.

Bursik, M.I. and Woods, A.W., 1996. The dynamics and thermodynamics of large ash flows. Bulletin of Volcanology, 58: 175-193.

Burton, I., Kates, R.W. and White, G.F., 1978. The environment as a hazard. Oxford University Press, New York.

Calder, E.S., Cole, P.D., Dade, W.B., Druitt, T.H., Hoblitt, R.P., Huppert, H.E., Ritchie, L., Sparks, R.S.J. and Young, S.R. 1999. Mobility of pyroclastic flows and surges at the Soufrière Hills Volcano, Montserrat. Geophysical Research Letters, 26:5 537-540.

Calvache, V.M.L. and Williams, S.N., 1997. Emplacement and petrological evolution of the andesitic dome of Galeras volcano, 1990-1992. Journal of Volcanology and Geothermal Research, 77:1-4 57-69.

Cas, R.A.F. and Wright, J.V., 1988. Volcanic Successions; Modern and Ancient. Chapman and Hall, London. 528p.

Christiansen, R.L. and Peterson, D.W., 1981. Chronology of the 1980 eruptive activity. in: P.W. Lipman and D.R. Mullineux (eds.), The 1980 eruptions of Mount St. Helens, Washington. USGS Professional Paper 1250, p17-51.

Clague, J.J., 1994. Quaternary stratigraphy and history of south-coastal British Columbia. Bulletin - Geological Survey of Canada, 481. 181-192.

Clague, J.J., 1998. Landslides and Engineering Geology of Southwestern British Columbia.

Technical Tour Guidebook, International Association for Engineering Geology and the Environment, 67p.

Clague, J.J. and Evans, S.G., 1994. Formation and failure of natural dams in the Canadian Cordillera. Geological Survey of Canada Bulletin 464, 35p.

Clague, J.J. and Evans, S.G. 2000. A review of catastrophic drainage of moraine-dammed lakes in British Columbia. Quaternary Science Reviews 19, 1763-1783.

Clague, J.J., Armstrong, J.E., and Mathews, W.H. 1990. Advance of the late Wisconsin Cordilleran ice sheet in southern British Columbia since 22,000 yr BP. Quaternary Research, 13: 322-326.

Clague, J.J., Evans, S.G., Rampton, V.N. and Woodsworth, G.J., 1995. Improved age estimates for the White River and Bridge River tephras, Western Canada. Canadian Journal of Earth Sciences, 32(8): 1172-1179.

Cole, P.D., Calder, E.S., Druitt, T.H., Hoblitt, R., Robertson, R.A.E., Sparks, R.S.J. and Yound, S.R., 1998. Pyroclastic flows generated by gravitational instability of the 1996-1997 lava dome of the Soufrière Hills volcano, Montserrat. Geophysical Research Letters, 25: 3425-3428.

Collinson, J.D. and Thompson, D.B., 1989. Sedimentary structures. Chapman and Hall, London, 207p.

Cordy, P., 1999. Sedimentological evidence for the damming of the Lillooet River by the 2350 B.P. eruption of Mount Meager, Southern Coast Mountains, B.C.. B.Sc. Thesis, University of British Columbia, 28p.

Corominas, J., 1996. The angle of reach as a mobility index for small and large landslides. Canadian Geotechnical Journal, 33: 260-271.

Costa, J.E. and Schuster, R.L., 1988. The formation and failure of natural dams; Geological Society of America Bulletin, v. 100, p. 1054-1068.

Crovelli, R.A., 2000. Probability models for the estimation of number and costs of landslides. USGS Open File Report 00-249.

Dingwell, D.B. and Webb, S.L., 1990. Relaxation in silicate melts. European Journal of Mineralogy, 2: 427-449.

Dragoni, M., 1993. Modelling the rheology and cooling of lava flows. In: C.R.J. Kilburn and G. Luongo, Active Lavas. UCL Press, London, p235-261.

Druitt, T.H., 1998. Pyroclastic density currents. In: Gilbert, J.S. and Sparks, R.S.J. (eds) The Physics of Explosive Volcanic Eruptions. Geological Society, London, Special Publications, 145: 145-182.

Eisbacher, G. H. and Clague, J. J. 1984. Destructive mass movements in high mountains: hazard and management. Geological Survey of Canada, Paper 84-16.

Elizarraras, S.R., Siebe, C., Komorowski, J-C., Espindola, J.M., and Saucedo, R., 1991. Field observations of pristine block- and ash-flow deposits emplaced April 16-17, 1991 at Volcan de Colima, Mexico. Journal of Volcanology and Geothermal Research, 48: 399-412.

Erismann, T.H. and Abele, G., 2001. Dynamics of Rockslides and Rockfalls. Springer, New York, 316p.

Evans, S.G., 1992. Landslide and river damming events associated with the Plinth Peak volcanic eruption, southwestern British Columbia. In: Geotechnical and Natural Hazards, BiTech Publishing, Vancouver, B.C., 405-412.

Farley, K.A., Rusmore, M.E. and Bogue, S.W., 2001. Post-10 Ma uplift and exhumation of the northern Coast Mountains, British Columbia. Geology, 29:2 99-102.

Fenton, C.R., Cerling, T.E., Webb, R.H., Poreda, R.J. and Nash, W.P., 1999. Lava dam failure and outburst-flood deposition in western Grand Canyon, Arizona. Abstracts with Programs - Geological Society of America, 31:7 p48.

Fink, J.H. and Kieffer, S.W., 1993. Estimates of flow velocities resulting from explosive decompression of lava domes. Nature, 363: 612-615.

Fisher, R.V., 1979. Models for pyroclastic surges and pyroclastic flows. Journal of Volcanology and Geothermal Research, 6: 305-318.

Fisher, R.V., 1990. Transport and deposition of a pyroclastic surge across an area of high relief: the 18 May 1980 eruption of Mount St. Helens, Washington. Geological Society of America Bulletin 102, Pages 1038-1054.

Fisher, R.V., 1995. Decoupling of pyroclastic currents; hazards assessments. Journal of Volcanology and Geothermal Research. 66, 1-4, Pages 257-263.

Fournier d'Albe, E.M., 1979. Objectives of volcanic monitoring and prediction. Journal of the Geological Society of London, 136: 321-326.

Fujii, T., and Nakada, S., 1999. The 15 September 1991 pyroclastic flows at Unzen Volcano (Japan): a flow model for associated ash-cloud surges. Journal of Volcanology and Geothermal Research, 89, p. 159-172

Gabrielse, H., Monger, J.W.H., Wheeler, J.O. and Yorath, C.J., 1992. Tectonic framework; Part A, Morphogeological belts, tectonic assemblages and terranes. In: H. Gabrielse and C.J. Yorath (Editors), Geology of the Cordilleran Orogen in Canada. Geol. Surv. Can., Ottawa, ON, Canada, pp. 15-28.

Green, N.L., Armstrong, R.L., Harakal, J.E., Souther, J.G. and Read, P.B. 1988. Eruptive history and K-Ar geochronology of the late Cenozoic Garibaldi volcanic belt, southwestern

British Columbia. Geological Society of America Bulletin, 100: 563-579.

Griffith, A.A., 1920. The phenomenon of rupture and flow in solids. Philosophical Transactions of the Royal Society of London, 221: 163-197.

Guzzetti, F., Carrara, A., Cardinali, M., and Reichenbach, P. 1999. Landslide hazard evaluation: a review of current techniques and their application in a multi-scale study, Central Italy. Geomorphology 31: 181–216.

Hausback, B.P., 1987. An extensive, hot, vapour-charged rhyodacite flow, Baja California, Mexico. In: J.H. Fink (ed), The emplacement of silicic domes and lava flows. GSA Special paper 712, p111-118.

Hayashi, J.N. and Self, S., 1992. A comparison of pyroclastic flow mobility and debris avalanche mobility. Journal of Geophysical Research, 97:B6 9063-9071.

Heim, A. 1932. Bergsturz und Menschenleben. Zurich, Fretz und Wasmuth. (english translation by N.A. Skermer. 1989. Landslides and Human Lives. BiTech Publishers, Vancouver, B.C.)

Hickson, C.J., 1994. Character of volcanism, volcanic hazards, and risk, northern end of the Cascade magmatic arc, British Columbia and Washington State. In: J.W.H. Monger (Editor), Geology and geological hazards of the Vancouver region, southwestern British Columbia. Bulletin - Geological Survey of Canada. Geological Survey of Canada, Ottawa, ON, Canada, pp. 231-250.

Hickson, C.J. and Barnes, W.C., 1986. The directed blast at Mount St. Helens, May 18, 1980; surge or flow?. In: Keller, S.A.C. (editor), Mount St. Helens; five years later. Eastern Washington University Press, Washington, 34-43.

Hickson, C.J., Russell, J.K. and Stasiuk, M.V., 1999. Volcanology of the 2350 B.P. eruption of Mount Meager Volcanic Complex, British Columbia, Canada: implications for hazards from

eruptions in topographically complex terrain. Bulletin of Volcanology, 60: 489-507.

Hoblitt, R.P., Miller, C.D. and Vallance, J.W., 1981 Origin and stratigraphy of the deposit produced by the May 18 directed blast. In Lipman, P.W. and Mullineaux, D.R. (editors), The 1980 eruptions of Mount St. Helens, Washington. USGS Professional Paper, 1250: 401-419.

Hsu, K.J., 1975. Catastrophic debris streams (sturzstroms) generated by rockfalls. Geological Society of America, Bulletin 86: 129-140.

Hungr, O., 1990. Mobility of rock avalanches. In: Report of the National Research Institute for Earth Sciences and Disaster Prevention. No. 46, p.11-20.

Hutchinson, G.E. 1957. A Treatise on Limnology, Volume 1. Wiley and Sons, New York, NY.

Inland Waters Directorate, 1991. Historical streamflow summary, B.C.. Minister of Suppky and Services Canada, Ottawa.

Kershaw, J.A., 2002 Formation and failure of moraine-dammed Queen Bess Lake, southern Coast Mountains, British Columbia. M.Sc. Thesis, Simon Fraser University, Vancouver.

Le Bas, M.J., Le Maitre, R.W., Streckeisen, A. and Zanettin, B., 1986. A chemical classification of volcanic rocks based on the total alkali-silica diagram. Journal of Petrology, 27: 745-750.

Legros, F., Cantagrel, J.M. and Devouard, B., 2000. Pseudotachylite at the base of the Arequipa volcanic landslide deposit (Peru): implications for emplacement mechanisms. The Journal of Geology, 108: 601-611.

Leonard, E.M., 1995. A varve-based calibration of the Bridge River tephra fall. Canadian Journal of Earth Sciences, 32(12): 2098-2102.

Linneman, S.R. and Borgia, A., 1993. The blocky andesite lava flows of Arenal volcano, Costa Rica. In: C.R.J. Kilburn and G. Luongo, Active Lavas. UCL Press, London, p25-72

Lowden, J.A. and Blake, W., Jr. 1968. Geological Survey of Canada radiocarbon dates VII.

Geological Survey of Canada, Paper 68-2, Part B. (Also published in Radiocarbon, 10: 207-245.)

Lowden, J.A. and Blake, W., Jr. 1978. Geological Survey of Canada radiocarbon dates XVIII. Geological Survey of Canada, Paper 78-7.

Mate, D.J., 1997. Quaternary geology, stratigraphy and geomorphology of the Ootsa Lake-Cheslatta River area, Nechako Plateau, central British Columbia. MSc Thesis, University of Victoria, Victoria.

Mathews, W.H., 1958. Geology of the Mount Garibaldi map-area, southwestern British Columbia, Canada; Part 1, Igneous and metamorphic rocks; Part 2, Geomorphology and Quaternary volcanic rocks. Geological Society of America Bulletin, 69(2): 161-198.

Mathewes, R.W. and Westgate, J.A. 1980. Bridge River tephra: revised distribution and significance for detecting old carbon errors in radiocarbon dates of limnic sediments in southern British Columbia. Canadian Journal of Earth Sciences, 12: 1454-1461.

McClung, D.M., 1999. The encounter probability for mountain slope hazards. Canadian Geotechnical Journal, 36: 1195-1196.

McEwan, A.S., 1989. Mobility of large rock avalanches: evidence from Valles Marineris, Mars. Geology, 17: 1111-1114.

Mellors, R.A., Waitt, R.B. and Swanson, D.A., 1988. Generation of pyroclastic flows and surges by hot-rock avalanches from the dome of Mount St. Helens volcano, USA. Bulletin of Volcanology, 50: 14-25.

Melosh, H.J., 1979. Acoustic fluidization: a new geologic process? Journal of Geophysical Research, 84: 7513-7520.

Miller, T.P. and Smith, R.L., 1977. Spectacular mobility of ash flows around Aniakchak and

Fisher calderas, Alaska. Geology, 5: 173-176.

Munson, B.R., Young, D.F. and Okiishi, T.H., 1990. Fundamentals of Fluid Mechanics. John Wiley and Sons, New York, 843p.

Nakada, S., 1993. Lava domes and pyroclastic flows of the 1991-1992 eruptions at Unzen Volcano, In: Unzen Volcano: the 1990-1992 eruption. Yanagi, T., Okado, H. and Ohta, T. (eds.). Nishinippon and Kyushu University Press, 56-66.

Nakada, S. and Motomura, Y., 1999. Petrology of the 1991-1995 eruption at Unzen; effective pulsation and groundmass crystallization. Journal of Volcanology and Geothermal Research, 89:1-4, 173-196.

Nasmith, H., Mathews, W.H., and Rouse, G.E., 1967. Bridge River ash and some other Recent ash beds in British Columbia. Canadian Journal of Earth Science 4:163-170

Newhall, C.G. and Melson, W.G. 1983. Explosive activity associated with the growth of volcanic domes. Journal of Volcanology and Geothermal Research, 17: 111-131.

Perfit, M.R. and Davidson, J.P., 2000. Plate tectonics and volcanism. In: H. Sigurdsson, B.F. Houghton, S.R. McNutt, H. Rymer and J. Stix (editors), Encyclopedia of Volcanoes. Academic Press, San Diego, pp. 89-113.

Philpotts, A.R., 1990. Principles of Igneous and Metamorphic Petrology. Prentice Hall, New Jersey. 498p.

Polacci, M., Papale, P. and Rosi, M., 2001 Textural heterogeneities in pumices from the climactic eruption of Mount Pinatubo, 15 June 1991, and implications for magma ascent dynamics. Bulletin of Volcanology. 63:2-3 83-97.

Read, P.B., 1977. Meager Creek volcanic complex, southwestern British Columbia. in Report of Activities, Part A. Geological Survey of Canada, Paper 77-1A, p. 277-281.

Read, P.B., 1978. Geology of Meager Creek geothermal area, British Columbia. Geological Survey of Canada, Open File 603.

Read, P.B., 1990. Mount Meager Complex, Garibaldi Belt, southwestern British Columbia. Geoscience Canada, v. 17, p. 167-174.

Richards, J.P. and Villeneuve, M., 2001. The Llullaillaco Volcano, northwest Argentina; construction by Pliestocene volcanism and destruction by sector collapse. Journal of Volcanology and Geothermal Research, 105:1-2 77-105.

Rose, W.I., 1987. Volcanic activity at Santaguito volcano, 1976-1984. In: J.H. Fink (ed), The emplacement of silicic domes and lava flows. GSA Special paper 712, p17-27.

Rose, W.I., Pearson, T., and Bonis, S., 1976. Nuée ardente eruption from the foot of a dacite lava flow, Santiaguito Volcano, Guatemala. Bulletin Volcanologique, 40(1): 23-38.

Ross, C.S. and Smith, R.L., 1961. Ash-flow tuffs; their origin, geologic relations, and identification. USGS Professional Paper, 81p.

Rutherford, A.A., Wittenberg, J. and McCallum, K.J. 1975. University of Saskatchewan radiocarbon dates VI. Radiocarbon, 17:328-353.

Sato, H., Fujii, T. and Nakada, S., 1992. Crumbling of dacite dome lava and generation of pyroclastic flows at Unzen volcano. Nature, 360:17 664-666.

Scheidegger, A., 1973. On the prediction of the reach and velocity of catastrophic landslides. Rock Mechanics, 5: 231-236.

Schipper, C.I., 2002. The catastrophic failure of a volcanic dam at Mount Meager, Southwest British Columbia, 2360 BP: an engineering approach to volcanic hazards. B.A.Sc. thesis, University of British Columbia, 57p.

Schneider, J.L. and Fisher, R.V., 1998. Transport and emplacement mechanisms of large

volcanic debris avalanches: evidence from the northwest sector of Cantal Volcano (France). Journal of Volcanology and Geothermal Research, 83: 141-165.

Sheridan, M.F. and Macias, J.L. 1995. Estimation of risk probability for gravity-driven pyroclastic flows at Volcan Colima, Mexico. Journal of Volcanology and Geothermal Research, 66: 251-256.

Siebert, L., 1984. Large volcanic debris avalanches: characteristics of source areas, deposits, and associated eruptions. Journal of Volcanology and Geothermal Research, 22: 163-197.

Siebert, L., Beget, J.E. and Glicken, H., 1995. The 1883 and late-prehistoric eruptions of Augustine Volcano, Alaska. Journal of Volcanology and Geothermal Research, 66:1-4 367-395.

Smith, J.V., 2002. Structural analysis of flow related textures in lavas. Earth Science Reviews, 57:3-4 279-297.

Smith, J.V., Miyake, Y. and Oikawa, T., 2001. Interpretation of porosity in dacite lava domes as ductile-brittle failure textures. Journal of Volcanology and Geothermal Research, 112: 25-35.

Smith, M.J. and McClung, D.M., 1997. Avalanche frequency and terraine characteristics at Rogers' Pass, British Columbia, Canada. Journal of Glacialogy, 14:143 165-171.

Smith, R.L., 1960. Zones and zonal variations in welded ash flows. USGS Professional Paper, p.149-159.

Sparks, R.S.J., Gardeweg, M.C., Calder, E.S. and Matthews, S.J., 1997. Erosion by pyroclastic flows on Lascar Volcano, Chile. Bulletin Volcanology, 58: 557-565.

Sparks, R.S.J.,Young, S.R., Barclay, J., Calder, E.S., Cole, P., Darroux, B., Davies, M.A., Druitt, T.H., Harford, C., Herd, R., James, M., Lejeune, A.M., Loughlin, S., Norton, G., Skerrit, G., Stasiuk, M.V., Stevens, N.S., Toothill, J., Wadge, G. and Watts, R., 1998.

Magma production and growth of the lava dome of the Soufrière Hills Volcano, Montserrat, West Indies: November 1995 to December 1997. Geophysical Research Letters, 25:18 3421-3424.

Stasiuk, M.V. and Russell, J.K., 1989. Petrography and chemistry of the Meager Mountain volcanic complex, southwestern British Columbia. In: Anonymous (Editor), Cordillera and Pacific margin. Paper - Geological Survey of Canada. Geological Survey of Canada, Ottawa, ON, Canada, pp. 189-196.

Stasiuk, M.V. and Russell, J.K., 1990. The Bridge River assemblage in the Meager Mountain volcanic complex, southwestern British Columbia. in Current Research, Part E. Geological Survey of Canada, Paper 90-1E, p. 153-157.

Stasiuk, M.V., Russell, J.K. and Hickson, C.J., 1996. Distribution, nature, and origins of the 2400 BP eruption products of Mount Meager, British Columbia; linkages between magma chemistry and eruption behaviour. Bulletin - Geological Survey of Canada. Geological Survey of Canada, Ottawa, ON, Canada, 27 pp.

Stevenson, L.S., 1947. Pumice from Halymore, Bridge River, British Columbia. American Mineralogist 32: 547-552.

Stevenson, R.J., Dingwell, D.B., Webb, S.L. and Bagdassarov, N.S., 1995. The equivalence of enthalpy and shear stress relaxation in rhyolitic obsidians and quantification of the liquid-glass transition in volcanic processes. Journal of Volcanology and Geothermal Research, 68: 297-306.

Stewart, M.L., Russell, J.K. and Hickson, C.J. 2001. Discrimination of hot versus cold avalanche deposits: implications for hazards assessment at Mount Meager, British Columbia. Geological Survey of Canada, Current Research 2001-A18, 15p.

Stewart, M.L., Russell, J.K. and Hickson, C.J. 2002. Revised stratigraphy of the Pebble Creek Formation, British Columbia: evidence for interplay between volcanism and mountainous terrain. Geological Survey of Canada, Current Research 2002-E3, 7p.

Stoopes, G.R. and Sheridan, M.F., 1992. Giant debris avalanches from the Colima volcanic complex, Mexico; implications for long-runout landslides (>100 km) and hazard assessment. Geology, 20(4): 299-302.

Swanson, D.A. and Holcomb, R.T., 1990. Regularities in the growth of the Mt. St. Helens dacite dome 1980-86. In: Lava Flows and Domes: Emplacement Mechanisms and Hazard Implications. J.H. Fink (ed.). Springer, Berlin, p3-24.

Thouret J.C., Lavigne, F., Kelfoun, K. and Bronto, S. 2000. Toward a revised hazard assessment at Merapi Volcano, central Java. Journal of Volcanology and Geothermal Research. 100:1-4 479-502.

Ui, T. 1983. Volcanic dry avalanche deposits – identification and comparison with nonvolcanic debris stream deposits. Journal of Volcanology and Geothermal Research, 18: 135-150.

Ui, T., Matsuwo, N., Sumita, M., and Fujinawa, A., 1999. Generation of block and ash flows during the 1990-1995 eruption of Unzen Volcano, Japan. Journal of Volcanology and Geothermal Research, 89: 123-127.

Valentine, G.A. and Fisher, R.V., 1993. Glowing avalanches: new research on volcanic density currents. Science, 259: 1130-1131.

Voight, B. and Davis, M.J., 2000. Emplacement temperatures of the November 22, 1994 nuée ardente deposits, Merapi Volcano, Java. Journal of Volcanology and Geothermal Resaerch, 100: 371-377.

Voight, B., Janda, R.J., Glicken, H. and Douglass, P.M., 1983. Nature and mechanics of the

Mount St. Helens rockslide-avalanche of 18 May, 1980. Geotechnique, 33: 243-273.

Walker, G.P.L., 1969. The breaking of magma. Geological Magazine, 106:2 166-173.

Webb, S.L. and Dingwell, D.B., 1990. Non-Newtonian rheology of igneous melts at high stresses and strain rates: experimental results for rhyolite, andesite, basalt and nephelinite. Journal of Geophysical Research, 95:B10 15,695-15,701.

Westgate, J.A. and Dreimanis, A., 1967. Volcanic ash layers of recent age at Banff National Park, Alberta, Canada. Canadian Journal of Earth Science, 4:155-161.

Wilson, C.J.N., 1980. The role of fluidization in the emplacement of pyroclastic flows: an experimental approach. Journal of Volcanology and Geothermal Research, 8: 231-249.

Wood, C.A. and Kienle, J., 1990. Volcanoes of North America, United States and Canada. Cambridge University Press, New York, 347p.

Woods, A.W., 2000. The dynamics of hazardous volcanic flows. Philosophical Transactions of the Royal Society of London, 358: 1705-1724.

Youd, T.L., Wilson, R.C. and Schuster, R.L., 1981. Stability of blockage in North Fork Toutle River. in: P.W. Lipman and D.R. Mullineux (eds.), The 1980 eruptions of Mount St. Helens, Washington. USGS Professional Paper 1250, p821-828.

Appendix I

Geochemical Data

Sample Preparation

A minimum of softball size rock samples were collected in the field during the 2000 and 2001 field seasons. Only juvenile blocks were sampled for chemical analysis. Where possible, matrix, xenoliths and weathering were discarded from the samples. Sample numbers correspond to field stations shown as a layer on the digital field map accompanying this thesis.

In the University of British Columbia laboratories, samples were split in a hydraulic splitter to fragments less than 10cm in diameter. These fragments were crushed to approximately 2cm in a Chipmunk crusher, discarding finer material. The 2cm fragments were hand-picked and cleaned with compressed air to avoid contamination from the crusher, weathering etc.. Samples were divided into three piles: 1. sample for chemistry, 2. duplicate for storage as 2cm fragments, 3. residual material for storage.

Chemical samples were further crushed in a Tungsten ring mill to <250 microns. Milling was limited to under 100s to minimize oxidation. These powders were dried, shaken in a paint shaker and split. Approximately 30g of each powder was sent to McGill University for X-Ray fluorescence analysis.

The analytical error was calculated by the standard deviation of three splits of the same rock powder. This is based on the assumption that powders are homogeneous in composition. Heterogeneities in samples derive from the presence of phenocrysts which are typically >10 times the size of the powdered rock. An estimate of geologic variance was calculated by the standard deviation of analyses of multiple fragments taken from the same initial rock sample. This variance is interpreted to result primarily from crystal sorting processes which can affect the analyzed composition. (All error is given as relative wt%)

Whole Rock Geochemistry (Major Elements: wt%)

Lava Flow

Sample	SiO2	TiO2	Al2O3	Fe2O3	MgO	CaO	Na2O	K2O	P2O5	Total	LOI
MS-00-130A	68.80	0.435	15.58	3.08	1.24	3.08	4.74	2.66	0.149	99.8	0.30
MS-00-130B	68.63	0.444	15.38	3.14	1.29	3.00	4.59	2.65	0.152	99.3	0.88
MS-00-136B	68.82	0.446	15.49	3.13	1.26	3.06	4.69	2.66	0.156	99.7	0.18
MS-00-134	68.88	0.443	15.41	3.03	1.27	2.96	4.63	2.63	0.129	99.4	0.52
MS-00-117	68.92	0.442	15.47	3.10	1.25	3.03	4.72	2.67	0.148	99.8	0.16
MS-00-143	68.92	0.442	15.62	3.15	1.27	3.10	4.70	2.67	0.148	100.0	0.22
MS-00-131	68.95	0.437	15.44	3.04	1.24	3.00	4.70	2.65	0.148	99.6	0.33
MS-00-122	68.70	0.449	15.70	3.19	1.35	3.22	4.61	2.63	0.147	100.0	0.21
MS-00-119A	68.64	0.457	15.65	3.27	1.38	3.22	4.83	2.58	0.153	100.2	0.13

Block and Ash Avalanche

Sample	SiO2	TiO2	Al2O3	Fe2O3	MgO	CaO	Na2O	K2O	P2O5	Total	LOI
MS-01-005B	68.47	0.440	15.36	3.17	1.27	3.04	4.68	2.65	0.149	99.2	0.92
MS-00-105C	68.60	0.443	15.50	3.14	1.29	3.11	4.60	2.65	0.149	99.5	0.67
MS-00-104A	68.76	0.435	15.43	3.10	1.24	3.01	4.61	2.70	0.144	99.4	0.57
MS-00-104B	68.24	0.431	15.41	3.07	1.25	3.00	4.64	2.60	0.148	98.8	1.14
MS-00-103C	68.57	0.424	15.41	3.02	1.24	3.00	4.69	2.66	0.145	99.2	0.70
MS-00-148L	66.50	0.502	15.92	3.64	1.65	3.70	4.59	2.40	0.167	99.1	0.76
MS-00-148H	65.77	0.528	16.55	3.92	1.97	4.21	4.52	2.19	0.172	99.8	0.41
MS-00-148E	68.78	0.429	15.49	3.08	1.27	3.04	4.65	2.62	0.148	99.5	0.69
MS-00-148C	65.41	0.549	16.42	4.01	1.88	4.22	4.58	2.25	0.184	99.5	0.57
MS-00-087A	68.64	0.453	15.52	3.14	1.28	3.09	4.67	2.67	0.154	99.6	0.34
MS-00-081A	66.67	0.490	15.89	3.57	1.60	3.66	4.56	2.42	0.167	99.0	0.97
MS-00-081B	65.05	0.557	16.57	4.08	1.96	4.38	4.49	2.20	0.186	99.5	0.75
MS-00-081C	68.21	0.458	15.62	3.29	1.36	3.24	4.57	2.57	0.153	99.5	0.71

Pumiceous Pyroclastic Flow

Sample	SiO2	TiO2	Al2O3	Fe2O3	MgO	CaO	Na2O	K2O	P2O5	Total	LOI
MS-01-006C	68.34	0.472	15.59	3.32	1.32	3.14	4.59	2.49	0.158	99.4	0.85
MS-01-006A	68.13	0.449	15.32	3.19	1.28	3.00	4.64	2.61	0.151	98.7	1.35
MS-01-006B-I	64.95	0.553	16.22	4.03	1.78	4.05	4.59	2.21	0.189	98.6	1.52
MS-01-006B-II	61.62	0.658	17.34	4.91	2.56	5.50	4.46	1.73	0.220	99.0	0.97
MS-00-102B	66.50	0.472	15.54	3.37	1.48	3.37	4.52	2.51	0.162	97.9	2.00
MS-00-101F	66.07	0.511	16.17	3.76	1.78	3.96	4.57	2.30	0.171	99.3	0.60
MS-00-101C	67.90	0.425	15.24	3.06	1.24	2.96	4.87	2.61	0.146	98.5	1.50

Pyroclastic Fall

Sample	SiO2	TiO2	Al2O3	Fe2O3	MgO	CaO	Na2O	K2O	P2O5	Total	LOI
MS-00-160C	66.70	0.509	15.87	3.61	1.47	3.49	5.29	2.43	0.166	99.5	0.71
MS-00-160B	67.29	0.501	15.89	3.52	1.42	3.47	4.63	2.49	0.164	99.4	0.74
MS-00-160A	67.47	0.486	15.83	3.44	1.37	3.36	4.71	2.52	0.162	99.3	0.77
MS-00-159	66.40	0.558	15.81	3.85	1.53	3.56	4.75	2.37	0.188	99.0	0.89
MS-00-157	66.73	0.512	15.50	3.57	1.41	3.26	4.66	2.47	0.173	98.3	1.43
MS-00-156	67.00	0.506	15.53	3.52	1.38	3.26	4.65	2.48	0.172	98.5	1.42
MS-00-155C	67.22	0.520	15.42	3.61	1.42	3.22	4.70	2.50	0.176	98.8	1.39
MS-00-155B	67.23	0.513	15.42	3.57	1.41	3.17	4.62	2.50	0.173	98.6	1.37
MS-00-155A	67.25	0.522	15.44	3.64	1.42	3.22	4.63	2.49	0.172	98.8	1.37

Relative Error (%)

Variance	SiO2	TiO2	Al2O3	Fe2O3	MgO	CaO	Na2O	K2O	P2O5	Total	LOI
Analytical	0.02	0.91	0.07	0.96	0.41	0.90	0.94	0.23	1.21	0.10	0.84
Geologic	0.36	1.35	0.37	1.24	1.47	0.72	0.57	0.61	1.21	0.25	1.52

Whole Rock Geochemistry (Trace Elements: ppm)

Lava Flow

Sample	BaO	Ce	Cr2O3	Sc
MS-00-130A	725	34	19	11
MS-00-130B	721	40	26	<d/l
MS-00-136B	745	34	24	13
MS-00-134	759	28	24	12
MS-00-117	753	38	24	<d/l
MS-00-143	738	28	21	<d/l
MS-00-131	790	33	<d/l	11
MS-00-122	732	31	22	<d/l
MS-00-119A	677	41	18	<d/l

Block and Ash Avalanche

Sample	BaO	Ce	Cr2O3	Sc
MS-01-005B	743	25	17	15
MS-00-105C	756	30	19	13
MS-00-104A	759	36	19	<d/l
MS-00-104B	753	32	21	<d/l
MS-00-103C	745	28	22	<d/l
MS-00-148L	705	32	24	<d/l
MS-00-148H	649	29	36	11
MS-00-148E	741	31	19	<d/l
MS-00-148C	657	41	27	14
MS-00-087A	741	28	19	<d/l
MS-00-081A	709	31	26	16
MS-00-081B	654	31	31	10
MS-00-081C	738	33	20	<d/l

Pumiceous Pyroclastic Flow

Sample	BaO	Ce	Cr2O3	Sc
MS-01-006C	716	29	17	<d/l
MS-01-006A	763	35	22	14
MS-01-006B-I	664	29	28	10
MS-01-006B-II	589	41	36	12
MS-00-102B	709	33	24	11
MS-00-101F	712	28	24	16
MS-00-101C	783	41	21	18

Pyroclastic Fall

Sample	BaO	Ce	Cr2O3	Sc
MS-00-160C	688	30	<d/l	10
MS-00-160B	701	22	16	<d/l
MS-00-160A	702	33	23	<d/l
MS-00-159	710	30	23	<d/l
MS-00-157	769	32	21	10
MS-00-156	733	33	21	10
MS-00-155C	767	33	<d/l	11
MS-00-155B	763	44	19	<d/l
MS-00-155A	730	25	<d/l	<d/l

Relative Error

Variance	BaO	Ce	Cr2O3	Sc
Analytical	2.78	38.2	<d/l	<d/l
Geologic	2.77	2.31	<d/l	<d/l

Glass Geochemistry (wt% oxides)

Thin sections were cut from samples for each geochemistry analysis. Selected sections were polished for microbeam analysis. The data presented here are analyses from thin sections of block and ash avalanche sample MS-00-148A. Matrix and inclusion glass compositions were analyzed with a Cameca SX50 electron microprobe (EMP). Acid etching used for reflected light optics allowed accurate placement of the beam to avoid microphenocrysts and vesicles. Due to the volatility of alkali elements in felsic glasses, the beam current was reduced to 5nA, and a 25x15 micron rastered beam was used in accordance with suggestions by Sprae and Rae (1995). Counting times were limited to 210 seconds through careful selection of elements. Analytical variance is calculated by taking the standard deviation of analyses taken within a small area of glass (200 microns). Geologic variance is calculated by taking the standard deviation of multiple measurements from the same sample, but distributed throughout a thin section. (values given in wt% oxides, error as relative wt%).

Data	Notes	SiO2	TiO2	Al2O3	Fe2O3	MgO	CaO	Na2O	K2O	Total
A1-1	Inclusion	74.1	0.333	13.7	1.509	0.352	1.55	4.57	3.24	99.3
A1-2	Inclusion	73.7	0.288	13.1	1.542	0.368	1.18	4.19	3.51	97.9
A2-1	Inclusion	75.1	0.322	12.4	1.621	0.340	0.81	4.60	3.55	98.7
A2-2	Inclusion	75.3	0.325	12.6	1.477	0.324	0.86	4.40	3.51	98.8
A2-3	Inclusion	75.0	0.351	12.7	1.585	0.288	0.82	4.27	3.60	98.5
A4-1	Inclusion	74.3	0.281	12.6	1.114	0.238	1.19	4.11	3.41	97.2
A4-2	Inclusion	74.9	0.292	13.1	1.229	0.237	1.23	4.39	3.43	98.8
A4-3	Inclusion	74.0	0.275	14.0	1.117	0.272	1.61	4.29	3.35	98.9
A4-4	Inclusion	75.6	0.275	12.9	1.292	0.336	1.03	4.25	3.46	99.1
A4-5	Inclusion	75.5	0.269	12.7	1.297	0.265	1.15	4.36	3.61	99.2
A4-6	Inclusion	75.0	0.229	12.7	1.211	0.260	0.92	4.33	3.56	98.3
A4-7	Inclusion	74.9	0.301	13.2	1.360	0.288	0.96	4.11	3.53	98.6
A4-8	Inclusion	75.2	0.284	13.1	1.364	0.251	0.97	4.33	3.48	98.9
A5-1	Inclusion	75.5	0.256	13.0	1.148	0.251	1.09	4.42	3.39	99.0
A5-2	Inclusion	76.0	0.249	13.1	1.203	0.272	0.95	4.52	3.51	99.9
A5-3	Inclusion	75.8	0.273	13.3	1.145	0.272	0.85	4.42	3.61	99.6
A5-4	Inclusion	76.4	0.316	13.3	1.155	0.201	0.95	4.53	3.68	100.5
A5-5	Inclusion	75.1	0.282	13.2	1.150	0.237	0.95	4.44	3.59	98.9
C1-1	Inclusion	77.2	0.464	11.2	1.199	0.144	0.44	3.50	4.75	98.9
C1-2	Inclusion	73.7	0.205	12.6	1.527	0.374	0.99	3.68	4.54	97.7
C1-3	Inclusion	75.4	0.354	11.9	1.463	0.333	0.98	3.43	4.29	98.1
extA1-1	Matrix	76.0	0.306	13.4	0.959	0.166	1.06	4.42	3.61	99.8
extA1-2	Matrix	74.6	0.335	13.1	1.766	0.333	1.31	4.29	3.46	99.2
extA2-1	Matrix	75.1	0.311	13.3	1.188	0.218	1.20	4.31	3.56	99.1
extA2-2	Matrix	75.6	0.278	12.5	1.163	0.200	0.95	4.37	3.58	98.7
extA4-1	Matrix	75.9	0.320	12.9	1.010	0.239	1.20	4.49	3.44	99.5
extA4-2	Matrix	76.2	0.292	13.3	0.932	0.226	1.05	4.40	3.49	99.9
extA5-1	Matrix	74.8	0.283	13.0	1.286	0.298	1.15	4.47	3.55	98.9
extA5-2	Matrix	75.3	0.278	13.4	1.307	0.204	1.09	4.53	3.62	99.7
extA6-1	Matrix	75.6	0.291	13.1	1.078	0.212	1.26	4.41	3.58	99.5
extA6-2	Matrix	74.7	0.290	13.1	1.409	0.450	1.44	4.36	3.39	99.1
gA1-1	Matrix	75.7	0.313	13.1	1.052	0.332	1.25	4.44	3.47	99.7
gA1-2	Inclusion	74.7	0.275	12.8	1.488	0.312	1.21	4.30	3.54	98.6
gA1-3	Inclusion	73.4	0.291	13.2	1.388	0.343	1.26	4.35	3.43	97.7
gA1-4	Inclusion	73.9	0.334	13.6	1.352	0.287	1.46	4.30	3.33	98.6
gA1-5	Inclusion	74.2	0.330	13.3	1.398	0.348	1.31	4.55	3.43	98.9
gA1-6	Matrix	75.0	0.343	13.3	0.860	0.262	1.22	4.43	3.51	98.9
gA3-1	Inclusion	74.8	0.289	13.4	1.502	0.244	1.16	4.53	3.57	99.5
gA5-1	Matrix	75.2	0.261	13.1	1.236	0.232	1.16	4.37	3.41	99.0
gA5-2	Matrix	74.8	0.295	13.5	1.614	0.263	1.02	4.42	3.42	99.3
gA5-3	Inclusion	72.8	0.250	13.9	1.228	0.239	1.82	4.51	3.06	97.8
gA5-4	Inclusion	75.5	0.318	12.9	1.301	0.248	0.97	4.60	3.57	99.5
gA5-5	Inclusion	75.4	0.277	12.9	1.133	0.258	0.90	4.38	3.58	98.9
Analaytical Variance		0.4	8.910999	0.8	4.239161	16.25828	12.46	1.35	2.16	
Geologic Variance		0.7	7.558308	1.9	23.67928	29.25798	14.88	1.49	2.08	

Appendix II

Clast Count Data

Clast count data (wt %)

Volcaniclastic rocks comprise a variety of clast types deriving from a dominant volcanic source (juvenile clasts), lesser volcanic sources (accessory clasts) and materials unrelated to the primary volcanic magmas (exotic clasts). The abundance of these varieties and changes in the abundances can have implications for understanding the processes attending a volcanic event. Data included here are abundances of pumice clasts types found in a primary pyroclastic fall deposit. Juvenile clast types are white pumice clasts that predominate the Plinian eruption event. Accessory clasts include grey, grey and white banded pumice and welded pumice breccia clasts. Exotic clasts include granitoid, and Plinth Assemblage dacite clasts.

The data included here derive from a single section taken through a primary pyroclastic fall deposit. This deposit is structureless, and virtually homogeneous in grain size. A fresh face was dug 15cm into the outcrop where pegs were driven in at 20cm intervals. 40cm size bags filled with pumice from these intervals, being careful to sample all material dug out. These samples were returned to the lab at UBC, dried, sieved to keep fragments larger than 2cm, and sorted by hand according to clasts types. These separates were then weighed by digital balance. One representative sample was sorted and weighed three times to calculate the analytical error for this technique. Geologic error was calculated by sorting and weighing three samples at the same stratigraphic elevation in the outcrop. Note the exotic clasts are much more dense than the pumiceous juvenile and accessory clasts, and thus are volumetrically less abundant than the data indicates.

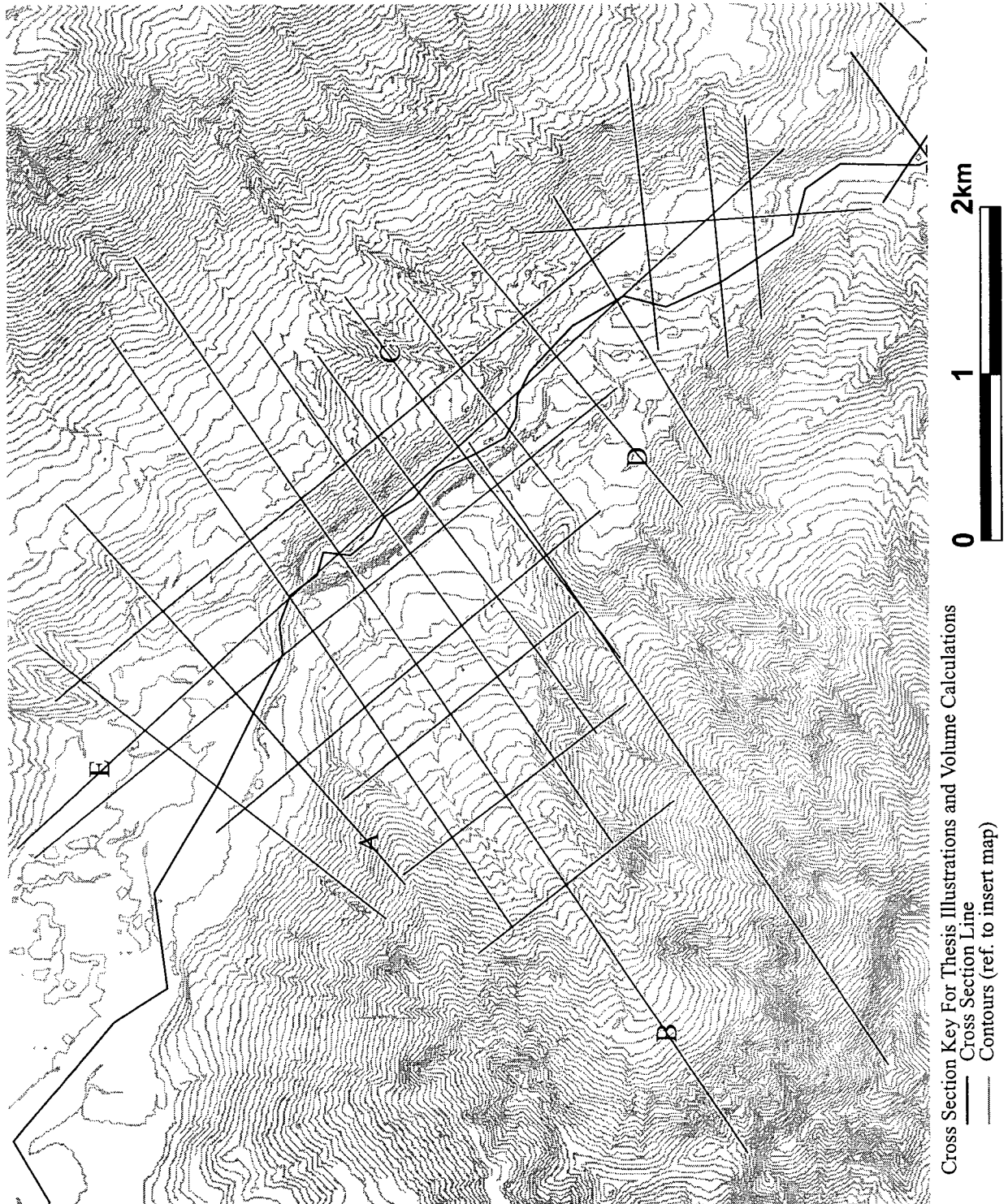| Interval	(m)	Juvenile	Accessory	Exotic
From	To	wt%	wt%	wt%
300	320	75.7	20	4.3
280	300	74.8	18.9	6.3
260	280	82.6	11	6.5
240	260	75.3	19.8	4.9
220	240	78.7	17.5	3.8
200	220	69.6	24.7	5.7
180	200	72.8	23.2	4
160	180	63.8	32	4.1
140	160	44	44.8	11.1
120	140	65.6	26	8.4
100	120	63.8	21.2	15
80	100	83.1	7	9.9
60	80	97.2	2	0.8
40	60	97.9	0.6	1.5
20	40	97.4	1.3	1.4
0	20	98	0.3	1.7

Appendix III
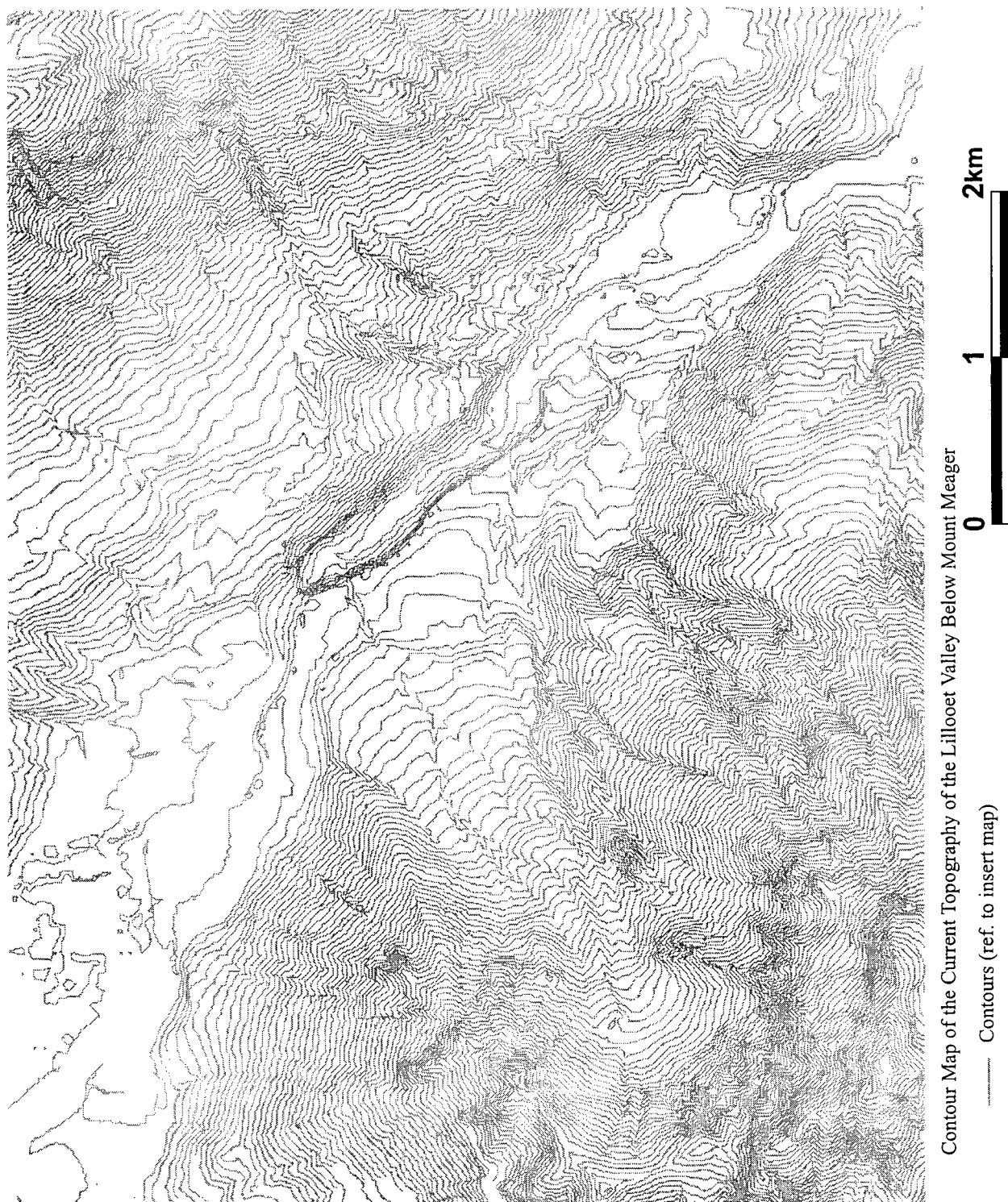
Cross-Section Key and Volume Maps
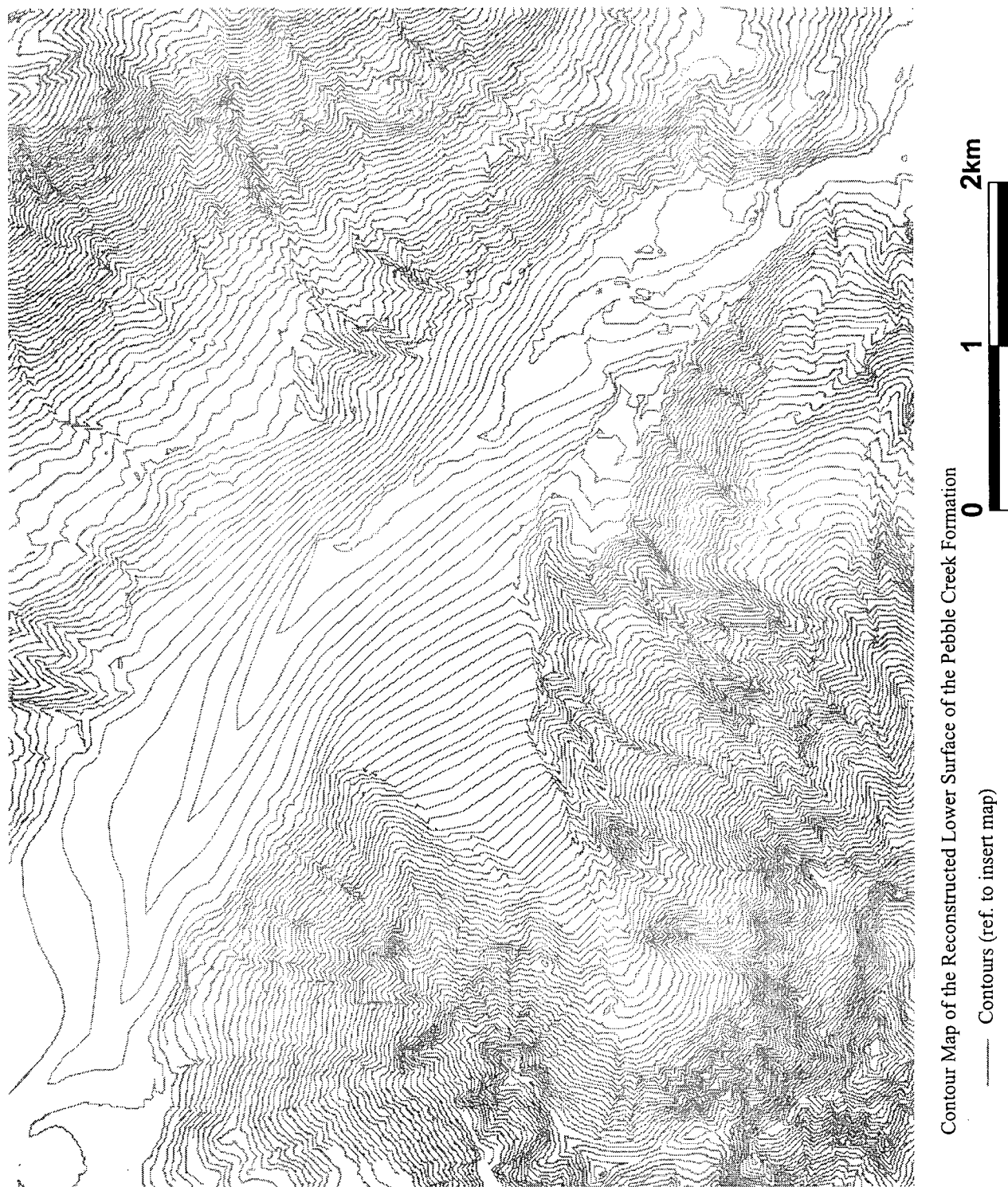
Cross Section Key

Digital map compilation for this thesis was done entirely from georeferenced TIFF images of the paper field maps using ARCView GIS version 3.1. Cross sections illustrated in this thesis were calculated from TRIM digital elevation data donated by the Government of British Columbia. Appendix III-I is a key map of the cross sections used for these illustrations, as well as used for reconstruction of the lower upper and current erosional surfaces of the Pebble Creek Formation deposits.
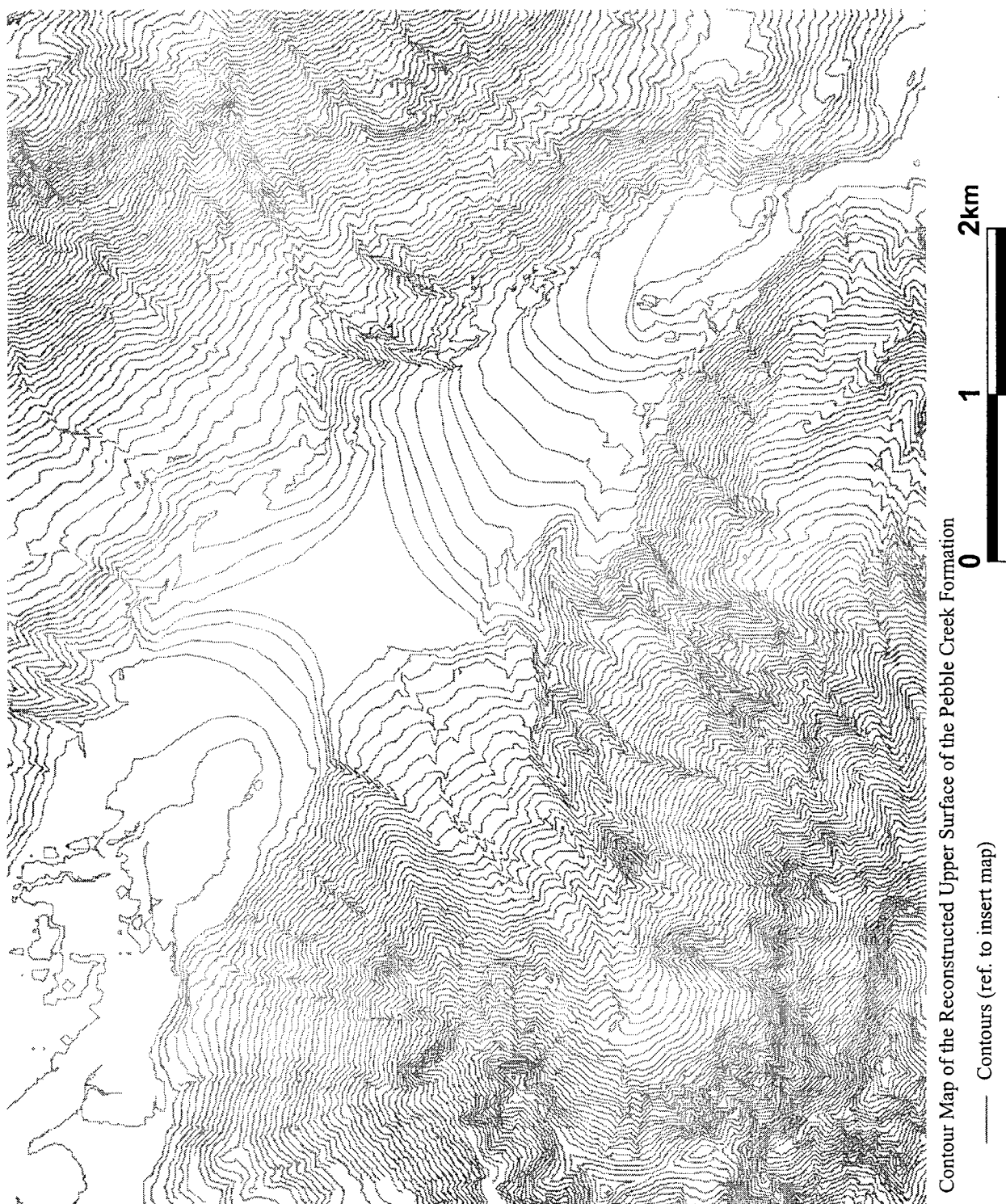
Appendix III-II illustrates the primary TRIM data based on the current topographic surface in the Lillooet valley below Mount Meager. Stratigraphic sections provided the primary constraint on the reconstruction of the 3D volumes of the Pebble Creek formation deposits. Where sections were unavailable, slopes outside of the area of the deposits were projected to reconstruct the lower, predepositional surface, illustrated in Appendix III-III. The upper surface was reconstructed based on the upper surfaces and interpreted erosional surface of the current topography (Appendix III-IV).

Reconstructions were done using the same initial basemap. Thus, any changes in the dimensions of the basemap represented the changes in surfaces due to the Pebble Creek Formation volumes. 3D triangulated TIN models were constructed using the altered TRIM data. The ARCView function "Area/Volume Statistics" calculates exact volumes below the elevation model using the dimensions of the 3D prisms of the TIN data. A volume was calculated for each reconstruction, and the differences taken as the volumes of the respective units the reconstructions were based on.

Cross Section Key For Thesis Illustrations and Volume Calculations
— Cross Section Line
— Contours (ref. to insert map)

Contour Map of the Current Topography of the Lillooet Valley Below Mount Meager

——— Contours (ref. to insert map)

Contour Map of the Reconstructed Lower Surface of the Pebble Creek Formation

—— Contours (ref. to insert map)

Contour Map of the Reconstructed Upper Surface of the Pebble Creek Formation

—— Contours (ref. to insert map)

Appendix IV

Lake Volume Data

Lake Volumes

The current elevation surface upriver of Keyhole Falls is used to represent the lower bed surface of the paleo-Salal Lake which built up behind the pyroclastic dam. Using the ARCView "Area/Volume Statistics" function (see Appendix III), volumes between a designated elevation and this lower bed surface were calculated. These volumes are representative of the lake water volumes for the given elevations of the lake.

Elevation (m.a.s.l.)	Dam Height (m)	Volume (10^6 m^3)	Peak Discharge (10^3 m^3/s)
800	120	1382.10	27.24
790	110	1139.60	24.28
780	100	911.40	21.31
770	90	711.85	18.44
760	80	530.28	15.57
750	70	387.83	12.97
740	60	260.11	10.34
730	50	176.93	8.19
725	45	134.74	7.01
720	40	105.17	6.04
715	35	78.97	5.08
710	30	58.40	4.22
705	25	38.52	3.30
700	20	21.95	2.39
695	15	14.95	1.81
690	10	9.00	1.25
685	5	4.04	0.68
680	0	0	0